The Dense Plasma Focus: A Versatile Dense Pinch for Diverse Applications

Mahadevan Krishnan, *Member, IEEE*

(Invited Paper)

***Abstract*—The dense plasma focus (DPF) is a Z-pinch that has been studied for 50 years. Within ten years of its discovery by Fillipov and Fillipova in Russia and Mather in the USA, this dense pinch was scaled up to 2-MA currents and neutron outputs of $\sim 10^{12}$/pulse. More remarkable is the fact that most of the relevant physics and scaling laws were elucidated within this first decade. The subsequent period has seen this type of pinch used as a teaching tool, developed as a portable neutron source for security applications, as a soft X-ray source for lithography, and as an energetic ion source for nanofabrication applications. This review builds upon several prior reviews. From the plasma physics standpoint, DPF physics is examined in light of fast Z-pinches to examine the similarities. More cross-fertilization between the two communities is suggested as a means to improve both types of pinches. From the applications standpoint, the many uses of DPFs are summarized to demonstrate the versatility of these pinches. Their ease of assembly and relatively low voltage operation have allowed DPFs to be disseminated worldwide as fusion testbeds (unlike their fast Z-pinch counterparts). Smaller or less economically developed nations have made valuable contributions to our understanding of the physics, as evidenced by the rich lode of publications that have advanced the field.**

***Index Terms*—Fusion, neutron source, plasma focus (PF).**

I. Introduction

THE PLASMA focus (PF) was independently discovered by Fillipov, Fillipova, and Vinogradov [1] and Mather [2] in the early 1960s. Remarkably, by 1975 or so, record neutron yields and a fairly comprehensive understanding of scaling laws (if not the detailed microscopic plasma physics) of these dense Z-pinches had been published by groups in several countries (USA, France, Italy, Germany, Russia). This review article has benefitted from valuable exchanges and conversations with several people who are gratefully acknowledged at the end of this paper. The ideas expressed here are based on these exchanges and on several detailed prior review articles on the subject [3]–[10].

The review article of Haines on Z-pinches [10] is notable as it discusses physics that is common to both the dense PF (DPF) and the so-called fast Z-pinches that are driven by high-voltage Marx generators. There might be benefits to greater cross-fertilization between these two hitherto separated research communities. For example, DPF machines scaled up to $\sim$MJ levels have used simple insulator structures that have not benefitted from decades of development of highly sophisticated vacuum insulators for high-current Z-pinches. While the vacuum designs might not apply to the gas-filled DPF devices, the DPF designs might adopt the field grading techniques that have served fast Z-pinches well. On the other hand, DPFs have explored neutron production in far greater detail than have Z-pinches, since the latter has been dominated by the study of X-ray production from higher atomic number loads. Precious few D_2 (and perhaps no DT) experiments have been performed on high-current Z-pinches. Hence, there might be value in comparing DPF physics with Z-pinch physics as plans advance for $>$ 15-MA D_2 pinches on machines such as Z [11]–[13]. Recent work [14] offers such suggestions.

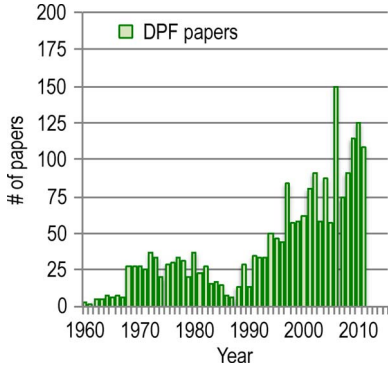

Fig. 1. Histogram plot of papers published on DPFs (and plasma guns) from 1960 to 2011 [15].

Fig. 1 shows a histogram plot of papers published on DPFs (and plasma guns) since 1960.

Fig. 2 shows a histogram plot of papers published on Z-pinches during the same period.

The peaks of Z-pinch or DPF papers in 1997, 2002, 2006, and 2009 correspond to dense Z-pinch conference proceedings. An interesting result is a significant decrease in Z-pinch papers from 2006, whereas this is not the case for the PF. The number of papers on DPFs was higher than the number of Z-pinch articles during the past few years. However, over the 50-year period, the total number of papers published is roughly the same: $\approx$2100 on DPFs and $\approx$2400 on Z-pinches. DPF research

Manuscript received May 11, 2012; revised August 17, 2012 and September 14, 2012; accepted September 17, 2012. Date of publication November 12, 2012; date of current version December 7, 2012.

The author is with Alameda Applied Sciences Corporation, San Leandro, CA 94577 USA.

Color versions of one or more of the figures in this paper are available online at http://ieeexplore.ieee.org.

Digital Object Identifier 10.1109/TPS.2012.2222676

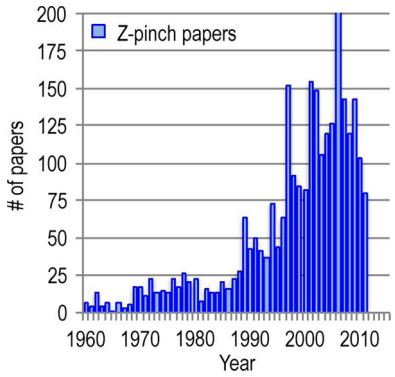

Fig. 2. Histogram plot of papers published on Z-pinches from 1960 to 2011 [15].

TABLE I
PARTIAL LISTING OF DPF FACILITIES WORLDWIDE

Facility or Organization	Name, type	Stored energy kJ	Discharge current kA	Ref.
Kurchatov Institute, Russia	PF-3, Fillipov	2800	3000	16
Frascati, Italy	Mather	1000	2800	17
Institue of Plasma Research, Germany	POSEIDON, Mather	500	1500	18
Institute of Plasma Physics and Laser Microfusion, Poland	PF-1000 Mather	400	1600	19
Institute of Nuclear Physics, Poland	PF-360 Mather	180	1850	20
Institute of Experimental Physics, Russia	Filippov	120	1200	21
Lawrenceville Plasma Physics, USA	Focus Fusion 1, Mather	114	2000	22
Teheran Polytechnic, Iran	DENA, Fillipov	90	2800	23
Institute for Plasma physics, Germany	Julich II, Mather	23	800	24
Nanyang Technological University, Singapore	NX2, Mather	2.4	300	25
Alameda Applied Sciences Corporation, USA	DPF-3, Mather	2	300	26
Alameda Applied Sciences Corporation, USA	DPF-2, Mather	0.09	70	27

made rapid strides from 1970 to 1985 when $>$ 100-kJ DPFs were constructed and studied at Los Alamos (700-kJ DPF), Limeil, Frascati, Stuttgart (DPF-78 and Poseidon), Düsseldorf (SPEED), Swierk (PF-360), and KIAE Moscow.

Table I shows a partial listing of DPF facilities worldwide. Dozens of facilities that fall into the range of stored energy and current have been omitted from this list. A glance at the peak currents and stored energy values shows that the ratio $I_{\rm peak}/E_{\rm stored}$ varies by orders of magnitude. The notion of scaling neutron outputs with stored energy is not well motivated as different designs lead to wildly varying coupling efficiency between the driver and the pinch. At least, the discharge current is related to plasma density in the pinch and so is a better scaling parameter. For higher energy DPFs, the pinch current is a more appropriate scaling parameter. (More on this will be discussed later.)

By the mid-1970s, most of the salient PF phenomena had been observed and described with well-founded models, at least at the macroscopic level. Despite the large number of papers listed in Figs. 1 and 2, many aspects of DPF (and indeed fast Z-pinch) research were not published in peer-reviewed journals, due to classification restrictions. Fortunately, a rich store of information may be found in several issues of the proceedings of PLASMA PHYSICS AND CONTROLLED NUCLEAR FUSION RESEARCH [30], [31]. [1, 2] Some early work at Los Alamos National Laboratory (LANL) remains unpublished to this day. An LANL internal report [32] describes how K. Ware, J. Mather, and others operated in 1974 the DPF 6-1/2 up to the full voltage of 60 kV at 720 kJ to produce 2.0×10^{12} neutrons at 3.2 MA of current. The experiments in Limeil, France, demonstrated 6×10^{11} neutrons/pulse with 340 kJ stored [34]. In Frascati, Italy, 5×10^{11} neutrons/pulse were measured, as described in [35]. In Stuttgart, Germany, 2.5×10^{11} neutrons were measured, as described in [36].

The many articles published during this productive period for Z-pinch research show that most aspects of the problem were studied and elucidated by the pioneers. Another important facet of DPF development is that DPF facilities are found in dozens of countries, particularly in small as well as less developed nations. This was made possible by the pioneering efforts of Prof. S. Lee, whose 1984 proposal to various international agencies was accepted by the United Nations University (UNU). With additional support from the International Center for Theoretical Physics (ICTP), Prof. S. Lee managed to build several small DPF devices at a cost of about $5000 each. Eight candidates from six countries (Egypt, India, Indonesia, Nigeria, Pakistan, and Sierra Leone) were selected and eventually awarded UNU fellowships. Today, that remarkable initiative by Prof. S. Lee has grown to a network of 44 institutions in 24 Asian and African countries, which is called the Asian African Association for Plasma Training. The 3-kJ UNU/ICTP Plasma Focus Facility is still a key facility in several laboratories in several countries, either in its original or modified/upgraded form, including Malaysia, Singapore, Egypt, India, Pakistan, Bulgaria, Iran, Syria, USA, and Zimbabwe. The device is also the archetype of the so-called Type-1 (single capacitor hence high inductance) PF. This versatile testbed is described in [37]. That paper contains rules of thumb for designing a PF based upon the Lee model code. These rules have been used for the design of many PF devices, including those in Asia, Africa, Middle East, Latin America, Europe, and the USA.

The three phases of a DPF pulse are shown in Fig. 3. The physics of such an event is difficult to accurately model. The breakdown transforms cold gas into a thin plasma sheath that lifts off the insulator surface (inverse pinch phase) and drives a shock axially to the end of the anode, where the sheath radially turns and is driven to the axis by the rapidly increasing $\mathbf{J} \times \mathbf{B}$ force. MHD modeling can capture the coaxial run-down phase

[1] See for example: On the mechanism of neutron production from the dense plasma focus (CN-24/G-5). Then, within this link, click on "past fusion energy conferences" and select STIPUB192_VOL2.pdf.

[2] See for example: Experiments on plasma focus dynamics, neutron production, and ion emission (IAEA-CN-38/G-1-2). Then, within this link, click on "past fusion energy conferences" and select STIPUB563_VOL2.pdf.

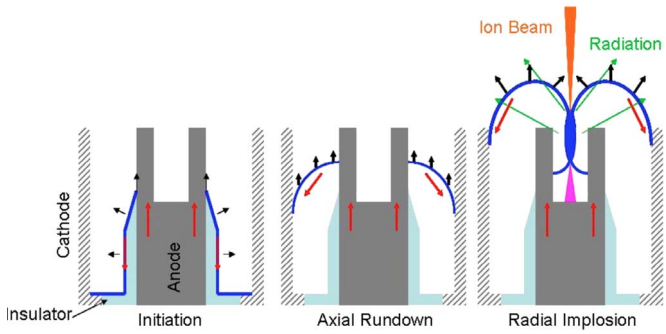

Fig. 3. Three phases of a typical DPF current pulse: initiation via flashover of the insulator, axial run-down phase, and radial implosion to form beams and dense pinch.

after the inverse pinch phase and a part of the radial implosion, but when the radial implosion reaches the final pinch phase, instabilities drive beam formation in the plasma. Finite Larmor radius effects, anomalous resistivity, and strong electric fields are present, so that the MHD solution must be complemented by particle in cell (PIC)-type simulations, to build a more comprehensive picture of the evolution of the pinch.

Even today's sophisticated numerical models (such as GORGON, ALEGRA, and PIC codes) cannot provide an ab initio picture of such pinches. However, these tools allow us to delve more deeply into the pinch phase and help delineate the dominant plasma physics at work as one scales up to $>$ 15-MA currents or $>$ 10-MJ stored energy.

With optimized capacitance, voltage, gas pressure, and electrode dimensions, all DPFs produce roughly the same plasma densities and temperatures in the focus region, the only substantive difference being in the focal spot volume and the duration of the dense spot. Why do plasma foci of deuterium seem to produce roughly the same temperature and density despite huge differences in current? Lee and Serban introduced the concept of a drive parameter in 1996 [38], [39]. The drive (also called speed) parameter is a direct measure of the speed of the electromagnetically driven current sheet. The square of this parameter is the energy density per unit mass. Lee and Serban noted the constancy of this drive parameter across a wide range of PF devices. The constancy of the drive parameter is therefore equivalent to the constancy of energy densities in the PF system, first in the axial phase and then, by extension of the dynamical equations and shock wave properties, in the radial phase. Thus, nearly identical phenomena are available in small DPFs as are observed in megajoule class devices. This energy density similarity allows a small country with limited resources to make useful contributions to our understanding of the subtle physics of nuclear fusion, whereas duplication of high-voltage Marx-bank-driven fast Z-pinch machines would be prohibitively expensive. The decade of the 1970s saw rapid progress in DPF scaling from the kilojoule to megajoule level. The decade of the 1980s saw (owing to the pioneering efforts of Prof. S. Lee) a veritable mushrooming of DPF facilities worldwide. The international nature of the subsequent research and publications that stemmed from it are a testament to the unique role that DPFs has played in spreading interest in fusion worldwide. The decade of the 1990s and beyond saw growth in practical applications of DPFs, for X-ray lithography, neutron-based explosives and special nuclear materials detection, materials research, and medical applications.

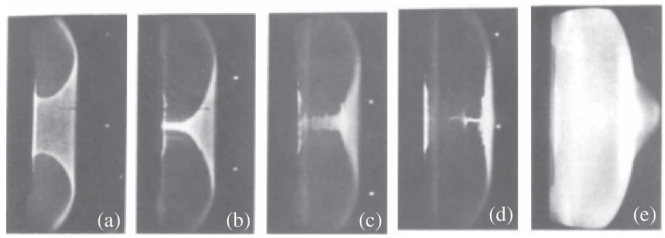

Fig. 4. (a) Radial compression. (b)–(d) Pinch formation. (e) Bubble ionization and axial shock wave into cold gas (from [3]).

This paper is organized as follows: Section II summarizes key aspects of prior reviews. Section III reviews DPF physics, followed by Section IV with a summary of many DPF variants developed for practical applications. Section V looks at DPFs and fast Z-pinches to highlight the benefits of cross-fertilization of future research, particularly as we look ahead to $>$ 10-MJ scaling of the physics. Section VI looks at future prospects.

II. Prior Reviews

An early review paper is by Bernard *et al.* in 1977 [3]. Fig. 4 (from [3]) shows images of the radial motion of the plasma sheath in a DPF.

The pinch phase is captured in –(d) lasting about 50 ns. Bernard *et al.* [3] presented holographic interferometry and Thomson scattering data to defend their arguments regarding the role of two different ion spectra in neutron production.

Highlights of this paper include:

- Report of neutron yield of up to 1×10^{12} neutrons of 2.5 MeV with 3×10^{6} neutrons/J [40].
- From the result of Cloth and Conrads [40] in (d,d), Bernard *et al.* extrapolates to 10^{14} neutrons of 14 MeV with $(2-4) \times 10^{8}$ neutrons/J if (d, t) mixture is used instead of (d,d).
- The scaling of neutron output with I^4 is mentioned, and it is pointed out that the limits of DPF fusion neutron production at lower and higher currents had not been fully explored. The review article by Soto [7] takes the concept of energy density similarity in plasma foci [38], [39] to extreme limits of 1 J of stored energy in a DPF, as discussed later.
- The early paper by Bernard *et al.* presents a comprehensive picture of most of the salient physics of DPFs as neutron sources. Holographic interferometry and Thomson scattering are used to track the spatial and temporal origin of neutrons. The debate as to what causes neutron production is addressed by cogent arguments that begin by criticizing the incorrect use of the term "thermonuclear fusion" as even the nonbeam component of the ion spectrum in a DPF is non-Maxwellian and reflects an ion distribution that is widely distributed in energy, direction, and number of particles. Yet, despite this admonition in 1977 based on measured and calculated ion spectra, the DPF community has continued to use the inappropriate concept of "thermonuclear fusion" for decades.

- Suprathermal density fluctuations inferred from radiation measurements point to the existence of anomalous resistivity in such plasmas, although the precise nature of the electrostatic waves and instabilities that drive this resistivity were not clearly delineated at that time. It was recognized that runaway electrons scattering off electrostatic waves could drive anomalous resistivity, but of the many possibilities (Bunemann modes, ion-acoustic turbulence, etc.), no clear picture was available at that time. However, to this day, there still exists no satisfactory explanation (supported by measurements) of such anomalous resistivity in DPFs or Z-pinches in general.
- Scaling of DPFs to $>$ 50-MJ/multi-MA levels is addressed in the context of current density limitations. The idea of injecting (puffing) gas into a hollow anode while using the static fill gas merely to shunt the current from the capacitor bank to the final radial implosion was introduced in this paper. Capacitive versus inductive storage options are reviewed. This paper discusses the notion of energy transfer efficiency from the driver bank to the inductance of the moving current sheet but does not put it on a rigorous footing. Trunk [41] and Lee [42] provided better insights into this issue, as described later.
- The review paper by Bernard *et al.* also describes the Julich II DPF that was specifically built to test the practicality of running a DPF neutron source repetitively. The Julich II capacitor bank stored 23 kJ and was designed to operate at 2 Hz at full power. About 10 kW of power were present in the hollow anode under these conditions, so the Julich II researchers used tungsten inserts to use evaporative material as the only way to carry off the heat load, although they also implemented water cooling for the anode. The DPF Julich II yielded an average neutron output of 6×10^9/pulse, which was maintained up to a repetition rate of two shots per second. The neutron output of each single shot within a run was recorded together with other parameters, such as working pressure, time between adjacent shots, temperatures, and spark gap performance. To put this result in some perspective, the output rate was 1.2×10^{10} neutrons/s (d,d), which would extrapolate to $\approx 10^{12}$ neutrons/s (d,t).
- This paper ends by discussing a 20-MJ DPF device from which $> 10^{17}$ neutrons/pulse would be produced if the known scaling laws would hold at this energy level. Then, at a repetition rate of 1 shot/s and at the distance of closest approach, 10^{15} neutrons/cm$^2 \cdot$ s would be available, so that bulk neutron damage effects could be studied within a reasonable time (days to months). A conceptual study of both the energy source and the discharge chamber showed that technological problems at this energy level were quite daunting, but tentative solutions were identified for all such problems.

In the 36 years since this paper, none of the ideas expressed in it has been challenged or significantly embellished, but other aspects of DPFs have been presented by newer work. One notable exception would be Lee's [8] more recent examination of the coupling of the driver to the dynamic impedance of the moving sheet and its implications for scaling to $\gg$ MJ levels. The work of Lee and Saw [8], [42]–[44] is reviewed in a later section.

Any review of DPFs would not be complete without mention of an unpublished report of the Australian Atomic Energy Commission in January 1976 by J. Tendys with the innocuous title "Dense Plasma Focus—A literature review." The breadth and depth of understanding of most of the salient physics in DPFs by the work of Tendys [9] is best captured by paraphrasing his conclusions as follows.

The DPF dynamics are driven by a current sheath produced by the breakdown across the insulator and driven along the electrodes to the muzzle of the gun by the $\mathbf{J} \times \mathbf{B}$ force. A shock that ionizes and heats the gas to a few electron volts, while driving most of the gas to the wall, is established in front of the sheath. The luminous shock front appears to have radial striations, at least at the early stages of the discharge, so that the front is not azimuthally symmetric. At the muzzle, a part of the ionized gas collapses to the axis to form a 1–2-mm-diameter pinch having a density and temperature greater than 10^{19} cm^{-3} and 1 keV, respectively. Only 5% to 10% of the gas swept up by the shock front during the collapse reaches the axis, with the rest axially driven away from the electrode out of the focus region. The shock ahead of the collapsing front can cause heating to several hundred electron volts, whereas the reflected shock at the axis, together with the magnetic compression, can raise this temperature to around 2 keV. Some tens of nanoseconds after the collapse, the pinch starts to break up due to $m = 0$ and $m = 1$ instabilities. At this time, the plasma column appears to diffuse outward, a pulse of high-energy X-rays (up to several hundred kiloelectronvolts) is emitted, and the neutron pulse starts. The X-ray spectrum is approximately thermal for energies less than 5 keV and has the form $E^{-3.5}$ at energies greater than 25 keV. The thermal portion of the emission corresponds to temperatures in the range from 0.4 keV to greater than 4 keV. The temperature of the ions is around 1 keV and, often, is higher than the electron temperature. During the neutron emission, the density falls to less than 6×10^{18} cm^{-3}. The magnetic field is compressed to values greater than 100 T. The neutron emission is most likely made up of two components: one from a thermal ion population and the other from a high-velocity ion beam accelerated in a magnetic neutral line configuration.

Tendys concludes that it is important for scaling to higher energies that a more thorough understanding be gained of the breakdown process at the insulator, so that it may be designed to eliminate secondary breakdown (flashover) before the pinch. He asserts that while the scaling law found has the neutron output increasing as I^4, this obscures the fact that many shots have no neutron output at all because of secondary breakdown. He suggests that a better understanding of the neutron output mechanism might reveal why many shots have a much lower output than average. A theory for the scaling laws requires an understanding of the electron and ion heating and acceleration mechanisms. He concludes that detailed time-resolved, and probably space-resolved, spectra would be required to find out what the differences are between a good focus and a poor one.

This paraphrasing of Tendys' remarkably useful "literature review" sums up our understanding of dense pinches even to this day. His suggestion that we try to understand what differentiates a good focus from a poor one is at the core of a recent publication by Bures and Krishnan [14] that is addressed later in this review.

When one compares the evolution of DPF papers with those related to fast Z-pinches, the differences are striking. Our understanding of the early phase and subsequent dynamics of fast Z-pinches from wire arrays has undergone major changes: the naïve picture of current equally divided among the wires that move toward the axis to assemble as the pinch has undergone a radical revision over the past 20 years [45]–[47]. Gas puff pinches have changed in design as we have evolved from the early thin-shell nozzles to snowplow-stabilized distributed gas loads, including central jets whose mass dominates the X-ray emission [48]–[52]. By contrast, today's DPFs follow the prescriptions laid out in reviews such as those by Bernard *et al.* [3] and Tendys [9] in the early 1970s with hardly any changes. It is true that there are subtleties such as addition of weak axial magnetic fields or tapering of the anode, but a tapered anode was first described by Ware [53] in his work at LANL with Mather and others in 1974.

The review article by Gribkov [6] summarizes progress made in Russia and Poland and also presents many applications of DPFs. A wide range of DPF devices is described from PF-1000, PF-6 (IPPLM), PF-10 (ITEP), and ING-102, ING-103, with stored energy from 100 J to 1 MJ and currents from 150 kA to 3 MA, with quarter periods from 400 ns to 7 μs. A medium-energy transportable device (2–7 kJ) can generate up to 10^9 of 2.5-MeV neutrons with (d,d) fill or up to 10^{11} neutrons/pulse of 14-MeV neutrons with (d,t) reactions. These DPFs have sealed chambers, are compact (1 m^3 and $<$ 400 kg), and have comparatively low cost. One newer version is also portable, weighing only 15 kg, and emits 10^7 neutrons/pulse with DT mixtures. Gribkov points out that DPF neutron sources are well suited for irradiation tests of wall materials for future controlled fusion reactors such as international thermonuclear experimental reactor (ITER). Gribkov describes an ongoing round-robin test series using neutron sources provided by five countries to test samples provided by Forschungszentrum, Germany. The challenges for controlled fusion are many, not the least of which is the materials problem. In the giddy early days of nuclear fission, industry mavens made bombastic claims, the most egregious of which was that the electricity from fission would be so inexpensive that they might have to give it away. History has taught us the folly of such an overly optimistic view of a new technology, fraught as it is with safety concerns and the legacy of several disasters that have highlighted the hidden costs. It would be prudent for fusion advocates to take a more cautious stance and recognize that as long as we generate energy via neutrons, there will be materials and radioactivity problems to tackle. One such is the possibility that after just one year of operation, a fusion plant might be forced to replace the first wall due to embrittlement and activation by neutron irradiation. With $\sim$30 tons of radioactive material to dispose of (perhaps annually), that would hardly qualify fusion as clean technology. At present, the fission reactors that are used for material irradiation studies do not provide adequate flux, and the neutron spectrum does not match that of the DT fusion reaction, hence the motivation for the International Fusion Materials Irradiation Facility (IFMIF). The IFMIF is to be developed by Europe, Japan, USA, and Russia under the umbrella of the International Atomic Energy Agency. The construction of a fusion demonstration reactor, i.e., DEMOnstration power plant (DEMO), for demonstrating competitive electrical power generation will be the next important program milestone after ITER. The timely availability of a sound materials database has become an indispensable element in international fusion road maps. The primary mission of the IFMIF is to generate a materials irradiation database for the design, construction, licensing, and safe operation of DEMO. Estimates of the cost of the IFMIF vary from a low of $\sim$\$1B to higher values. One key area of concern for fusion reactors is the first wall. The irradiation environment is particularly severe in this region, and unless we have demonstrated that the wall material will survive the high neutron doses expected, regulatory approval cannot be guaranteed for these reactors. For most structural materials, high flux irradiation with $>$ 20 displacements per atom per full power year (dpa/fpy) followed by post irradiation examination is the norm [54]. IFMIF is required to achieve a total facility availability of 70% and will be operated in two phases: the half-intensity and full-intensity phases. The three-year first phase will be used to screen several candidate structural materials and to obtain calibration rules that would allow better use of the existing irradiation database obtained from fission reactors and from other methods. In the second phase, the IFMIF will operate as a production facility with emphasis on high availability. This phase is expected to last for at least 20 years. Assuming I^4 scaling, a DPF operated at 13 MA and at a rep-rate of 1 Hz could emit $\approx 1 \times 10^{18}$ neutrons/s. At a distance of 40 cm from such a quasi-isotropic source, the flux would be $\approx 7 \times 10^{17}$ neutrons/$m^2 \cdot$ s. This is equivalent to 1.5 MW/m^2. The IFMIF neutron flux specification is 2 MW/m^2 into a 0.5-L volume. A 13–15-MA rep-rated DPF facility could be built and operated for a fraction of the $\sim$\$1B cost estimated for the IFMIF accelerator. Admittedly, the DPF would not deliver the doses required for full-scale materials damage studies, but even at a quarter-scale or lower, a less expensive facility would complement the larger accelerator testbed for DEMO.

The review paper by Haines on Z-pinches [10] is relevant to DPFs as well as to fast Z-pinches. Haines revisited the problem of ion viscosity that had earlier been studied by Potter [55], [56], which plays an important role in ion heating in all Z-pinches, and also discussed the microinstabilities that might be the source of the fast ion and electron beams in a DPF pinch. Haines also pointed out the need for momentum balance when generating an ion beam and showed how coronal ion orbits outside the pinch core (around $m = 0$ necks) might provide this balance.

III. DPF Physics

The physics of DPFs has been described in hundreds of papers. In this review, a few have been selected to present various measurements made in DPFs, their physical interpretations, and

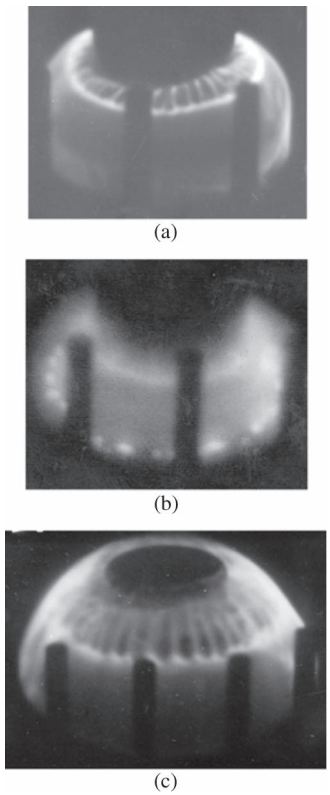

Fig. 5. Image converter camera frames in the high-pressure regime (2.5 mbar). (a) Exposure time: 5 ns, taken at 200 ns from the start of current. (b) Exposure time: 100 ns, taken at 250 ns from the start of current. (c) Exposure time: 5 ns, taken at 750 ns from the start of current. The inner electrode diameter is 40 mm [57].

numerical and analytical models. The logical flow begins at the insulator and progresses along the DPF to the final pinch phase.

A. Measurements

The first phase of a DPF is the insulator breakdown phase. An article by Milanese and Moroso [57] shows optical framing camera images of the breakdown phase for a small DPF called PACO at 250 kA at two pressures, i.e., a high pressure of 2.5 mbar and a lower pressure of 1.5 mbar. Figs. 5 and 6 show these images.

The author showed that the filamentary structure of the sheath at higher pressure is detrimental to neutron production, whereas the uniform breakdown at lower pressure produces a better pinch with higher neutron output. This is an early verification of the notion that the DPF implosion sensitively depends on the initial breakdown conditions along the insulator.

In 1986, Kies [58] presented a detailed study of discharge initiation and sheath formation in high-current (several megaamperes) dynamical pinches. The 300-kV PF SPEED 2 allowed the study of the discharge behavior over a wide range of power (10–100 GW). Kies estimated an upper limit of energy density into the sheath ($\sim$100 J/cm^2) that decreases with increasing insulator radius. He considered several techniques to increase this energy density, among which was the idea of depositing copper particulates over the surface. The metal distribution

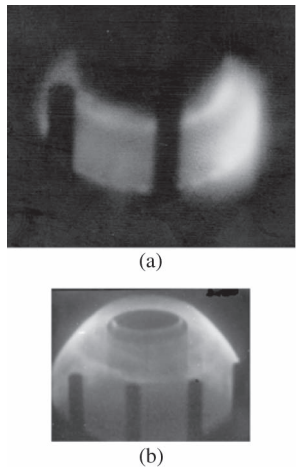

Fig. 6. Image converter camera frames in the optimum-pressure regime (1.5 mbar). (a) Exposure time: 100 ns, at 200 ns from the start of current. (b) Exposure time: 5 ns, at 800 ns from the start of current. The inner electrode diameter is 40 mm [56].

across the insulator surface evidently improved breakdown and allowed higher energy over larger insulator surface areas. This is the first reported study of the breakdown phase of insulators in DPFs. Kies presented a model for breakdown and estimated the time interval needed from the application of the voltage pulse to the formation of the shock/sheath and subsequent acceleration. We will return to this breakdown phase when discussing models in Section V.

Kwek *et al.* [59] presented detailed Schlieren images of the current sheath in the coaxial run-down phase. Their studies showed the significance of the current sheath structure in the run-down phase on the neutron production in the PF. Different filling pressures show structural changes in the sheath as revealed by their Schlieren images. Their results indicated that ionization processes during the propagation of the sheath in the run-down phase play an important role in determining the optimum-pressure regime. In most successful PF devices, the optimum operating pressures seemed to be centered around 10 mbar regardless of the energy of the devices. They also observed that the speed of propagation of the sheath in the run-down phase was seldom greater than 10 cm/μs (100 km/s). This optimum value of axial velocity was later connected to the so-called drive parameter by Lee and Serban [38], [39].

Moving further along the implosion to the radial pinch stage, detailed measurements of ion spectra (Thomson scattering), density (holographic interferometry), and neutron anisotropy over a wide range of DPF currents were published in 1974 by Bernard *et al.* [60]. From the turbulent scattering spectrum, they concluded that nonthermal processes must be responsible for the neutron output. Another important feature mentioned in this paper is that the neutron production strongly depends on electrode polarity. For the same filling pressure of 3 torr, the ionization wave is slower (only 2×10^7 cm/s) when the inner electrode is negative versus $\sim 10^8$ cm/s when it is positive. The mechanism by which the ionizing deuterons are accelerated is clearly dependent on the electrode polarity. To see how the radial velocity might drive the ion spectrum, consider an electric field E_z whose source term is $v_r \times B_\theta$. Consider a current

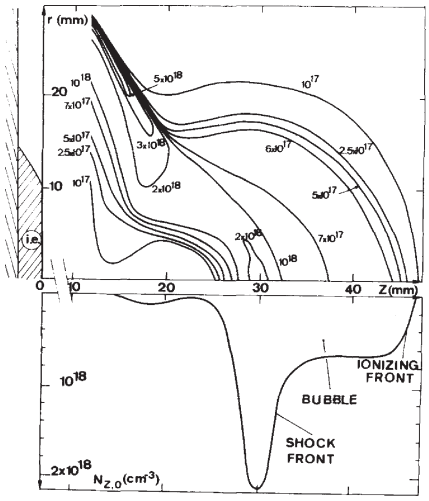

Fig. 7. Density map and on-axis profile at the time of the maximum of the neutron pulse [60].

of 250–500 kA at a radius of 1 mm. The magnetic field is 50–100 T. For a radial velocity of 2×10^5 m/s, the value $E_z = 1{-}2 \times 10^7$ V/m. Over a typical $\sim$1-mm scale for $m = 0$ necks, the net electric potential across the gap is 10–20 kV, which is not sufficient to give a hard enough ion spectrum to drive nonthermal fusion. Bernard *et al.* considered the ionization wave launched by the incoming deuterons and concluded that a velocity of 2×10^5 m/s would imply no deuterons > 10 keV. However, with a positive polarity, the velocity is $5\times$ faster; hence, the potential is 50–100 kV. An ion distribution with mean energy around 50–100 keV would have a higher cross section for (d,d) fusion. Ruden [61] also described the polarity-dependent effect of gyroviscosity on the flow-shear-stabilized Rayleigh–Taylor instability and how that applies to the PF.

For the main pinch phase, several papers have been published on measurements of density in the pinch with spatial and temporal resolution. The early paper by Bernard *et al.* [60] presented density maps taken using holographic interferograms. One such density map taken at the time of peak neutron emission is shown in Fig. 7.

Fig. 7 shows a distinct spike in density located about 30 mm from the anode face with a bubble beyond it. The ionizing front demarcates the region between the undisturbed cold gas and the imploded plasma. The lower density region upstream of the spike could support strong electric fields that accelerate ions into the spike and bubble to drive fusion.

A more recent paper by Kubes *et al.* [62] presented more sophisticated measurements of plasma density in high-current DPFs that complement the earlier data by Bernard *et al.* In the paper by Kubes *et al.*, a pinch generated in the PF-1000 device working in deuterium at 1 MA was measured with an interferometer and scintillation detectors. The 527-nm wavelength probe laser was split into 16 beams with a time delay in the range of 0–220 ns. This diagnostic tool makes possible the imaging of the evolution of the axial and radial distributions of plasma density in the pinch at stagnation and their comparison with the evolution of hard X-ray (HXR) and neutron production. The evolution of the dense structure is described with respect to its importance in fusion processes.

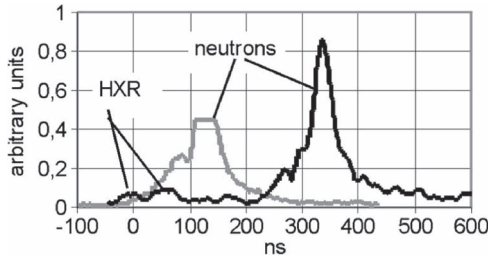

Fig. 8. p-i-n diode HXR signals and signals from scintillation detectors (gray) side-on at a distance of 1.7 m and (black) downstream at a distance of 7 m [62].

The signals of HXRs captured by a p-i-n diode and neutrons captured with scintillation detectors are shown in Fig. 8. The scintillation detector placed at a 7-m distance from the center of the pinch column downstream (black) detected both HXRs and neutrons. The side-on detector at a distance of 1.6 m was filtered with 4 mm of lead (to absorb HXRs). HXRs and neutrons were emitted in two pulses. The first HXR pulse started at a time of -30 ns (see Fig. 8), reached a maximum at 0 ns, and was over by 30 ns. The second HXR started at 40 ns, reached maximum at 70 ns, and died out by 100 ns. Neutron signals were processed by the time-of-flight (TOF) method. The first neutron pulse was much smaller than the second. Both practically started at the same time as the HXRs, and their full-width at half-maximum (FWHM) was 50 ns. A dominant portion (70%) of neutrons in the first peak was produced over a 50-ns interval. The maximum neutron signal recorded at 7 m downstream occurred 30 ns before the upstream maximum. The peak neutron energy downstream was 2.7 MeV, and the peak energy upstream was 2.25 MeV. Therefore, neutron-producing deuterons moved mostly downstream with an axial energy component of about 50 keV. These characteristics determined the dominant beam-target mechanism of neutron production. Recall our earlier estimate of a cross-field voltage of 50 kV in necks, which is consistent with the 50-keV energy implied by these measurements.

Fig. 9 shows iso-density contours from the interferograms taken at times -30, 0, and $+30$ ns, as indicated in Fig. 8. Kubes *et al.* [62] concluded that HXRs and neutrons were emitted in two pulses with an FWHM of 30 ns. The second pulse was more intense with a downstream peak energy of about 2.7 MeV. The beam-target mechanism of neutron generation was caused by deuterons moving downstream with an energy of about 50 keV. The plasma density during stagnation was not uniform either in the radial or axial directions. Upon the implosion of the current sheath, a dense structure with a radius of 20 mm is formed, whose maximum density at the center has reached $2{-}4 \times 10^{18}$ cm^{-3} and decreases with time. The number of deuterons in the dense spike was estimated to be $\sim 5 \times 10^{19}$ and constant. The lower density void between the anode face and dense spike is the region of deuteron acceleration, whereas the dense spike is the target for fusion.

Another paper that provides evidence for the beam-target mechanism of neutron production is by Beg *et al.* [63]. That paper described neutron emission from a 3-kJ Mather-type PF. The dependence of neutron output and anisotropy with a change in anode length was investigated. Anode lengths of high and

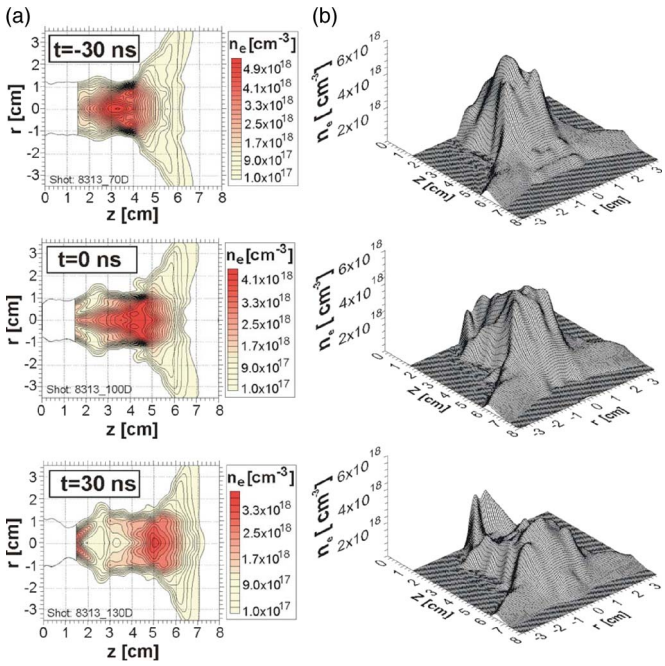

Fig. 9. Iso-density contours from the interferograms at times −30, 0, and 30 ns, as shown in Fig. 8 [62].

low fluence anisotropy as well as for high neutron yield were identified. Observation of large fluence anisotropy suggested the presence of a beam–plasma interaction as the dominant neutron production mechanism.

Several other papers describe measurements in DPFs. Kies *et al.* [64] described measurements of the formation of micro-pinches in the SPEED2 focus when high-Z gases ($Z >$ 18) are used but more stable columns with lower-Z gases.

Gribkov *et al.* published two detailed papers [65], [66] that describe an experimental study of the PF-1000 facility. The pinch plasma has a diameter of about 1 cm with a length of about 10 cm. Temperature was estimated to be in the range of 1.2–1.4 keV. Plasma density was estimated to be $0.7-0.9 \times 10^{19}$ cm^{-3}. Confinement time of the pinch was stated to about 150 ns, which is several times longer than the ideal MHD growth times of plasma. These authors suggest further improvement of the PF-1000 facility by changing the electrode geometry. They suggested a reduction in anode length. Then, the driver–load matching conditions would demand a further increase in the initial pressure of working gas (see Lee and Serban [38]) that, in turn, might improve the final "target" characteristics together with the neutron production efficiency. In a second paper [66], Gribkov *et al.* showed that a geometry change in both the chamber and the collector might also result in the improvement of the runaway ion beam characteristics. They offered the intriguing suggestion that the best configuration of a DPF anode might not be a cylinder. Al-Hawat [67] showed measurements of the axial velocity of the current sheet using magnetic probes and compared these measurements to a snowplow model. The paper by Aliaga-Rossel and Choi [68] is singled out for its exposition of the role of radiative cooling on the sheath dynamics. Detailed Schlieren measurements allowed them to show how a Kr-doped D_2 PF collapses to a higher density due to radiative thinning of the current sheet. The presence of a higher-Z component in the admixture leads to a higher ionization and radiation loss, both at low temperature during the radial compression phase and at higher temperature during the pinch phase. The increase in losses effectively reduces the shock to piston separation during the compression and, thus, leads to the thinner plasma sheath observed. This paper is also the first to report the existence of two phases of neutron emission in a relatively low energy focus. They identify the first neutron burst as due to thermal physics in a dense hot plasma, followed by (about 100 ns later) a beam-target mechanism at work in a more diffuse cooler plasma.

Krompholz *et al.* [69] presented detailed measurements of neutron, ion, and electron spectra in a 1-kJ focus from which they reported an unusually high neutron output of 2.8×10^8 neutrons/shot at a maximum current of only 220 kA. They claimed that neutron emission originates from a ∼100–400-keV deuteron beam within a $\sim 40^\circ$ cone angle along the z-axis of the focus geometry. The ion energy was directly determined by combined magnetic and TOF analysis. The 40° cone angle was deduced using a beam-target model and the neutron energy spectra, which provide the center of mass velocity of the reacting ions. The z-axis deuteron spectrum was fit to a power law: $e^{(-E/Eo)}$ with $E_o \sim 50$ keV. This paper was published in 1976 and (similar to that by Bernard *et al.*) represents a remarkably prescient harbinger of later interpretations of beam-target fusion and nonthermal ions in plasma foci.

Czekaja *et al.* [70] presented the first detailed measurements of magnetic field in a ∼1-MA focus using Faraday rotation (laser polarimetry). Assuming an axisymmetric magnetic field distribution, they used Abel inversion procedures to generate maps of magnetic field (current distribution) from single focus discharges. Qi *et al.* [71] later presented laser polarimetry measurements of magnetic field in a 300-kA focus.

Klir *et al.* [72], in a recent article, have examined the role of thermonuclear versus beam-target fusion in ∼MA pinches and shown that even at ∼1 MA, the PF-1000 focus' neutron output is dominated by beam-target fusion. They examined the causes for this and suggested that the recently suggested MAG-LIF concept [13] has promise for thermal fusion. (More on that will be discussed later.)

Krauz *et al.* [73] showed measurements of current distribution in a 1-MA focus plasma using magnetic probes. In this paper, details were presented of the dynamics of the plasma current sheath and current distribution in the PF-3 facility, which is one of the largest PF machines in the world. The experiments were done at bank energy of 290 kJ and discharge current of 1–2 MA. The current sheath parameters were measured with absolutely calibrated magnetic probes installed at different distances from the system axis and at different heights above the anode plane. They discussed the formation of closed current loops due to the development of shunting breakdowns in the insulator region. The maximum residual plasma density at which the electrode gap remains magnetically self-insulated was estimated.

Steinmetz *et al.* [74] used a neutron pinhole camera to map the neutron emission of the Frascati 1-MJ plasma focus over an energy range of 250–500 kJ, using a six-channel detector array. Single-shot neutron streak images, space- and time-resolved,

were obtained with an axial resolution of 2 cm and a time resolution of about 5 ns. Results showed that over 70% of the neutrons (i.e., more than 10^{11} neutrons per shot at 490 kJ) were emitted from a coaxial cylindrical volume about 4 cm long and less than 4 cm in diameter at the anode tip. Neither axial nor radial motion of this main source was observed throughout the emission lasting 200 ns FWHM.

Finally, Roshan *et al.* [75] described measurements of intense high-energy deuteron beams in a ~2-kJ focus and correlation of these beams with neutron yield.

There are many more papers in the literature that describe measurements in plasma foci. Only a few have been singled out here to provide the reader with flavor to such extent that detailed measurements have been made using optical techniques or TOF neutron spectroscopy, and that have proven effective. Dozens of references are to be found in the papers cited here for related work by others.

B. Models and Physical Interpretations

The gross dynamics of DPFs has been interpreted since the early days, as evidenced by the papers of Bernard *et al.* [3], [60], Trunk [41], and several others. Jager and Herold [76] described a generalized beam-target model, i.e., the "Gyrating Particle Model," during the dynamic phases of the PF POSEIDON (280 kJ, 60 kV, Mather type) to explain the fast accelerated deuterons gyrating in pinch structures. The results of this new model are compared with spectrally and spatially resolved measurements of fusion protons and accelerated deuterons, to give evidence of the validity of this generalized beam-target model for both phases. The number and the distribution function of accelerated deuterons, consistent with observed fusion yield, are presented. Schmidt *et al.* [77] also described this model. Sestero *et al.* [78] addressed the challenge to account for the large number of neutrons produced per shot in plasma foci, as well as for the long duration of the neutron emission phase, unless one assumes that the fast ions, which are presumably produced in the collapsing phase, are confined for a substantial length of time within the focus region before being lost to the electrodes. The authors suggested that such a confinement may be provided by the mirror properties of the quasi-force-free helical configurations that were predicted by Taylor [79] to be the likely endpoint for highly sheared dissipative pinch discharges. The authors suggested that in plasma foci, particularly of the Filippov type, evidence has accumulated in favor of the existence of long-lasting (≈100 ns) helical plasma–magnetic structures that seem to simultaneously occur with the second neutron burst.

Kies *et al.* and Milanese *et al.* [80], [81] provided two other examples of good measurements and interpretations. What all these papers recognized was the need for a more detailed examination of the pinch phase, to better understand the instabilities that drive ion (and electron) beam formation and fusion in such pinches.

The basic equations of magnetoplasmadynamics are essentially nonlinear, and the problem is at least 2-D. This demands numerical codes. The difficulties arising from this were satisfactorily solved for the first time by Roberts and Potter [82] who theoretically described the focus discharge up to the pinch phase. Their results were compared with the experiments by Morgan *et al.* [83] and showed fair agreement with the plasma data. The Ph.D. thesis paper by Potter is a classic [55], which describes a 2-D numerical calculation that captures the gross dynamics of a Mather-type DPF. Potter compared his predictions of neutron yield with experiments and showed that the DPF pinch was in an intermediate regime between a collisional fluid-like (MHD) plasma and a hybrid kinetic fluid. The ion Hall parameter $\omega\tau < 10$. The ion–ion collision time was estimated as ~20 ns, which is comparable to the macroscopic pinch lifetime; hence, he correctly concluded that the ions cannot acquire a Maxwellian distribution. We shall return to this point later, but first, the work of Lee is mentioned with regard to modeling the dynamics using a simple 1-D macro written for execution using Microsoft Excel.

A recent paper is a summary of Lee's five-phase model for description of any DPF that he has recently extended to a six-phase model by including anomalous resistivity [84]. The Lee model is deceptively simple, runs as a macro in Microsoft Excel, and provides the DPF researcher with a handy tool to evaluate various electrode designs without recourse to more time-consuming numerical models. The Lee model code couples plasma and current sheath dynamics, thermodynamics, and radiation with electric circuit equations to simulate the dynamics of the PF. Lee simulates any Mather-type PF device by fitting the computed current waveform to a measured current waveform using four model parameters, i.e., f_m, f_c, f_{mr}, and f_{cr}; the former two account for nonperfect mass swept up and current drive due to all physical and machine processes in the axial phase and, likewise, the latter two for the radial phases. The model code has in the past included five phases, namely, an axial phase treated as snowplow-like, a radial inward shock phase using a slug model, a radial reflected shock phase with the reflected shock radially moving outward until it hits the radially incoming current sheath "piston," followed by a slow compression radiative pinch phase with the radiative loss of energy coupled into the compression of the pinch. A final phase with large column axial expansion is modeled to complete the current waveform evolution , Refs. 6–14[84]. This recent paper evolves the Lee model to the case of DPFs that have relatively large driver inductance. As an example of its utility, Lee *et al.* [84] showed the measured current of 125 kA from a 400-J DPF fitted to his model, a higher current of 350 kA from the NX2 DPF at Singapore fitted to the model and a similar fit but from the 1.8-MA PF-1000 DPF. The remarkable agreement between measured and fitted currents in each case speaks for itself. Lee has made two valuable contributions to DPF research: a) his pioneering efforts to disseminate DPF testbeds worldwide have stimulated innovative research in all corners of the globe, making the DPF a unique fusion testbed that is accessible to the most humble of nations, and b) his development of the so-called Lee macro that he has generously made available to all via a web link [85], which he constantly updates.

The measurements surveyed in the previous section show that the three phases of the DPF are well characterized including during the neutron emission that occurs in two steps in some cases. Nevertheless, the diagnostics used, although

sophisticated, are limited in spatial and temporal resolution to $\sim$1 mm and $\sim$5 ns scales. However, microscopic phenomena in such pinches might occur on $\sim$0.1 mm and $<$ 1 ns timescales. Coleman *et al.* [48] presented evidence for 0.1-mm filaments in a dense Z-pinch that was driven by 3.5-MA currents. For a typical radial velocity of 4×10^7 cm/s, the transit time across a 0.1-mm filament is 0.25 ns. Interchange instabilities such as the $m = 0$ mode having the shortest wavelength (k^{-1}) should grow at a rate $\omega = (v_r^2(k/r))^{0.5}$. For a pinch radius of 0.5 mm and equal ion and electron temperatures, the growth time is $\sim$1 ns. It is obvious that better spatial and temporal resolution measurements are necessary to enhance our understanding of the microinstabilities in dense pinches.

Haines [86] provides a detailed description of the kinetics in dense Z-pinches. Haines pointed out that if the drift velocity of the current-carrying electrons exceeds a threshold for generating microinstabilities (lower hybrid or ion-acoustic instabilities), this leads to anomalous resistivity. Haines also examined the formation of ion beams in $m = 0$ necks, showed why the beams are emitted only in one direction, and posed an important question: how is the momentum of the ion beam conserved? Haines teaches that in the necked region, as the (Bennett) line density drops, a runaway electron current and microturbulence will occur. The plasma in this region will be heated by this anomalous resistance and radially expand. This expansion will lead to a redistribution of current in a time of order 50 ps, and a reversal of axial electric field E_z is possible. At larger radii, dB_θ/dt is large and negative and, therefore, so is dE_z/dr. The ion acceleration that could occur will be in one direction near the axis and in the opposite at larger radii, thereby allowing axial momentum to be conserved. Beg *et al.* [87] discuss the acceleration of electron beams in the low-density regions between $m = 0$ necks by large $v_r \times B_\theta$ electric fields, as estimated earlier. In a related paper, Auluck [88] discusses momentum balance in the current sheath as it implodes. If he assumes that the current-carrying layer is of lower density than the shock driven in front of it, he shows that momentum balance could be satisfied if there is a net rotation in the current-carrying layer. The angular momentum of deuterons in this current layer would be transferred by mixing to the dense nonrotating ions in the pinch as the sheath is decelerated, leading to a broadening of the ion and, hence, neutron spectrum. Due to the cylindrical geometry of the imploding sheath, such a net rotation of ions would imply an azimuthal current J_θ because the electrons would rotate at slightly higher velocity (the centrifugal correction to their velocity being formally small compared with that for the deuterons) [89]. Such a J_θ current density would generate a self-consistent axial magnetic field B_z. Krishnan and Prasad [90] pointed out that in a rotating cylindrical plasma, it may be shown that the inward force $J_\theta \times B_z$ balances the outward centrifugal force $\rho v_\theta^2/r$. Hence, if Auluck is correct in his supposition, the magnetic field in a dense pinch might have a helical structure and ions might spiral around the axis with a few being axially emitted. Similar phenomena have been proposed for the origin of plasma jets from accretion disks in young stellar objects [91]. Unless measurements are made to show the presence of axial magnetic fields in dense pinches, such suppositions must remain speculative.

Bernstein and Hai [92] postulated that the high-energy deuterons are generated by an acceleration mechanism in which the ion velocities are randomly oriented because of curved motion in the magnetic field of the pinch. In a later (1972) paper, Bernstein and Comisar [93] provide a thorough analysis of ion acceleration mechanisms in plasma foci. First, they examined the two then-prevailing models for neutron production: a) the so-called moving boiler (a translating Maxwellian ion distribution) and b) a monoenergetic group of accelerated deuterons that collide with stationary ions. They showed that neither of these models is consistent with the large body of experimental results from plasma foci. These measurements from many laboratories had shown that the d,d neutrons emitted outward along the axis (0°) have energy of $\sim$250–450 keV greater than the neutrons emitted in the radial direction (90°). Some neutrons had energy exceeding 3.4 MeV. The FWHM of the neutron energy spectra was 300–450 keV. These neutron spectra and fluence distributions were clearly at odds with a simplistic moving boiler model and were also quite inconsistent with an arbitrarily assumed on-axis directed ion beam that collided with stationary cold plasma regions. Their cross-field acceleration model leads to a power law distribution for the deuterons as E_o^{-3}, which was shown to be consistent with electron energy spectra inferred from HXR measurements. Given that the HXR and neutron emission were coincident in time, they felt justified in choosing a power law for ions that was the same as that for the electrons. They compute the ion velocity distribution functions using a cross-field model that gave realistic angular distributions. They noted that accelerated deuterons move mostly at an appreciable angle to the axis rather than parallel and that lower energy ions tend to stay off-axis with the highest energy ions flowing parallel to the axis. This is a significant observation as it implies that energy spectra measured from the escaping ions in plasma foci do not reveal the true ion distribution function as they sample only the escapees. Another notable conclusion drawn by these authors is that since the d,d neutrons are produced by ions in the 50–600-keV range, one should be careful about extrapolating to d,t outputs. Whereas the cross section for d,t fusion increases by 200$\times$ in the 50–150-keV range, it decreases to only 10$\times$ at 600 keV. Hence, a d,t pinch should have ions mostly in the 50–150-keV range. (We will return to this point later in Section VI when we discuss future prospects.)

In 1985, Yamada *et al.* [94] measured the energy spectrum and the angular distribution of high-energy deuterons produced by a PF device, both in low- and high-pressure regimes, and found 5×10^{14} fast deuterons (0.3–3 MeV) at a beam current of 8 kA at low pressure (1.5 torr). Ion pinhole images confirmed a plasma diode formed just above the anode surface that accelerated the deuterons to high energies. A beam-target model showed that it was *not* the fast deuterons ($>$ 330 keV) but the slow deuterons ($\sim$74 keV) that contributed to the total neutron yield. These results are consistent with the earlier notions of Bernstein and Comisar [93].

In the last few decades, significant efforts have been led by various research laboratories [40], [95]–[97] to investigate the velocity distribution of deuterons producing neutrons, and different models have been deduced, e.g., the crossed-field acceleration model [93], converging ion model [96], etc., but

to date, the entire mechanism of the ion acceleration has not been fully understood, and investigations are ongoing to reveal causes and effects of the anisotropy [98]–[101].

Deeney [102], [103] and Choi *et al.* [104] presented nanosecond resolution studies of hotspots in Z-pinches and DPFs and revealed features of relativistic electron beams generated in such pinches. Other notable hotspot studies include the work by Favre *et al.* [105], [106]. Favre *et al.* used a combination of multiple pinholes and slit-wire X-ray photography to measure the characteristic size and temperature of the hotspots, over a range of pressure and gas mixing ratios in a 3.8-kJ focus. Filtered p-i-n diodes and a beam-target detector were used to investigate the time evolution of the hotspots. Typical size for the hottest emitting region, at temperatures between 200 and 400 eV, was found to be around 150 μm, with a typical duration of the high-temperature phase on the order of 10 ns. The temperature in the final phase of the time evolution of the hotspots reached values that were nearly twice those of the plasma column where they are formed. Characteristic size of the hotspots was about half that of the initial plasma column.

Another paper that delves into DPF neutron production physics is by Aliaga-Rossel and Choi [68], as mentioned earlier. These authors were among the first to dope D_2 DPFs with noble gases in a systematic manner. The measurements of the neutron signals obtained in this experiment on DPF-78, a 60-kV 28-kJ PF showed that the neutron emission was composed of two identifiable pulses or periods with a spatial anisotropy that depended on the level of doping as well as the doping gas. These experiments were well planned in terms of parametric variations. An admixture of gases with an equivalent mass density of 5 mbar of D_2 was employed throughout the experiment. The Kr admixture produced the greatest increase in neutron yield, followed by Ar and then Ne. Their time-resolved measurements of neutron and HXR pulses as well as side-on versus end-on measurements in the presence of dopants allowed them to conjecture as to the origin of the two distinct periods of neutron emission in such DPFs. The first period of emission starts during the final phase of the radial compression of the plasma column and before the formation of the hot plasma pinch column. The most likely origin of neutron production is claimed to be the radial acceleration of ions from a Fermi mechanism, in which gyrating ions gain energy by bouncing off the incoming sheath, as had been proposed by Deutch and Kies earlier [107]. It was calculated that an ion can gain energy from thermal to 100 keV in four bounces from the sheath, for a sheath velocity of 300 km/s. The peak neutron production during this first period would occur when these energetic ions interact with the dense plasma in the pinch column that is subsequently formed. For krypton-doped discharges, the plasma sheath was observed to be thinner than in neon-doped discharges, resulting in better compression and a much tighter pinch. The best neutron yield from krypton-doped discharge could be explained by a much more efficient Fermi acceleration process and one or two more bounces of the ions from the creation of a tighter pinch. The presence of a higher-Z component in the admixture would lead to a higher ionization and radiation loss, both at a low temperature during the radial compression phase and at a high temperature during the pinch phase. The increased losses would reduce the shock to piston separation during compression and lead to the thinner plasma sheath observed. After the formation of the dense pinch, the much higher level of radiation losses would cool the pinch column quickly, leading to the rapid fall of the neutron signal in the side-on direction.

Further discussion of the role of instabilities in DPFs (or any dense Z-pinches) and how the ion spectrum generated in such plasmas scales with current or stored energy is deferred to a later section, where we compare neutron outputs from DPFs and fast Z-pinches and discuss scaling to $>$ 30-MA currents. The following section presents a brief summary of variants on the DPF that have been developed for diverse applications.

IV. DPF Variants

A. DPF Soft X-Ray Sources

Kato and Be [108] described the use of a DPF as a soft X-ray source for X-ray lithography. They found that by diluting noble gases (Ne, Ar, Kr) with H_2, the soft X-ray output was higher than with pure noble gas fills. While they do not provide a hypothesis for why the hydrogen impurity increased the output, they note that the fraction of hydrogen to rare gas by mass was roughly constant (4% for Ne and 7% for Ar and Kr). Kato and Be estimated the total soft X-ray output from a Ne pinch by assuming isotropic emission into 4π as 112 J from a 2.8-kJ stored energy. This wall plug efficiency of 3.7% was remarkable and represented a maximum for Ne from DPFs. At that time, to provide perspective, imploding gas jet pinches had shown efficiency of $< 1\%$, whereas electron beam bombardment sources (vacuum tubes) showed $10^{-4}\%$ efficiency. This work marks a key milestone for DPF applications that, up to that time, had been dominated by the study of neutrons in the context of fusion.

In the early 1990s, the work by Kato and Be motivated the development of a higher rep-rate DPF Ne soft X-ray source in the USA. Prasad *et al.* [109] demonstrated a 20-Hz source that operated at 300-kA peak currents with 25-J/pulse Ne outputs.

The work by Prasad *et al.* was followed by the work of Petr *et al.* [110] who described an all-solid-state PF pulse power system that could operate at up to 80 Hz with 260-kA peak current. That work focused on neon K-shell radiation for lithography, and the source ran for 800 000 shots at 27 Hz with a 12-J $\pm 40\%$ output (at $\sim$1-keV soft X-ray energy). The soft X-ray power from the Petr source was about 300 W.

The 25-J/20-Hz result [109] is a soft X-ray power of 500 W. Such a 500-W "light bulb" at 1.2 nm remains a world record, and the source was developed for integration with a stepper for proximity focusing X-ray lithography. In the early 1990s, the expectation (hope) was that below 0.25-μm feature size X-ray lithography would replace optical projection lithography for future generations of chip manufacture that would follow Moore's law. History proved otherwise as the UV lithography industry came up with several innovations (chemically amplified resists, phase contrast masks, and shorter wavelength excimer UV sources) that pushed existing and mature projection lithography toward finer and finer feature sizes, continually barring entry

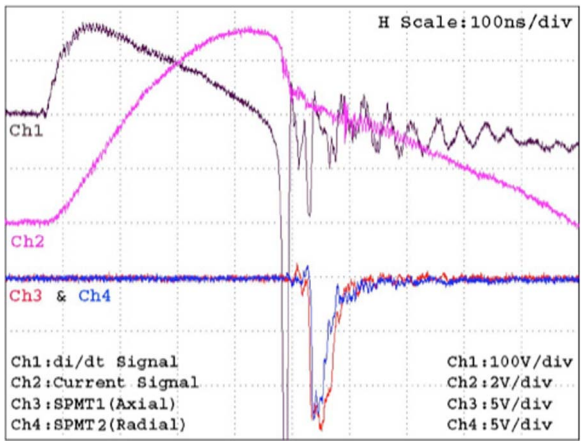

Fig. 10. Current derivative (dI/dt), current, and scintillator–photomultiplier signals at 3.5 mbar H_2 filling gas pressure [113].

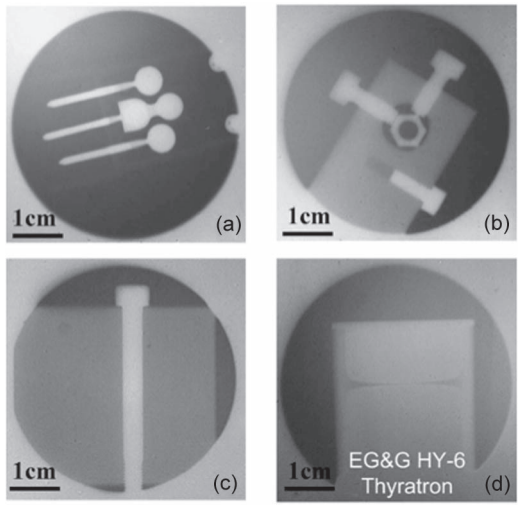

Fig. 11. HXR radiographs obtained using Pb-insert in anode. Number of exposures: (a) three, (b) four, (c) four, and (d) five [113].

to X-rays. Meanwhile, extreme ultraviolet lithography (EUV) came of age, and X-ray lithography was a discarded technology, despite ~$1B in development investment by the US government and the private sector (primarily IBM). Eventually, Intel invested in EUV lithography and EUV projection lithography is now the next frontier for Moore's law.

In 2000, Beg *et al.* [111] published a study on Ne and Ar emission from a small DPF that stored 2 kJ and ran at 200 kA. In N_2 and Ne, the plasma imploded to form a uniform cylindrical column, whereas for Ar, the plasma consisted of a number of hotspots. A maximum X-ray yield of 16.6 J and pulse length of 10–15 ns were obtained in neon. The temperature estimated from spectroscopic observations was about 300–400 eV at an electron density of $3-5 \times 10^{20}$ cm^{-3} in neon. The motivation of Beg *et al.* was to use the DPF soft X-ray source as a backlighter to obtain shadowgraph images of other pinches.

In 2004, Wong *et al.* at NTU/Singapore [112] completed optimization of their 3-kJ NX2 DPF (similar in scale to the DPF by Kato and Be in 1986) and pushed the wall plug efficiency to 5.6%, by measuring a total Ne output of 140 J into 4π. These results were obtained with operation at 1 Hz. Operation in argon showed that optimized SXR ($\lambda \sim 0.4$ nm) yield was up to 1.3 J/shot. While operating with neon under optimized conditions with a water-cooled anode in repetitive mode, the NX2 device was used as an SXR source to imprint a test lithograph on a highly sensitive chemically amplified resist SU-8. Test structures showing the effect of a stepper with aspect ratio 3 : 1 on a 10-μm-thick SU-8 resist film were obtained.

The DPF has been also used as an HXR source. Fig. 10 from Verma *et al.* [113] shows typical current, dI/dt, and scintillator–photomultiplier traces from a shot that had a current of 70 kA at a stored energy of 170 J from a compact (0.02 m^3, 25 kg) DPF that has been successfully demonstrated as a portable radiographic source for nondestructive imaging applications. Fig. 11 shows radiographs taken from Verma *et al.* [113] using this source. The submillimeter resolution in the radiographs revealed that the radiation source is of small size that enhances the imaging resolution. Moreover, since the radiographs were obtained by multiple exposures without blurring of the image, this indicated that the position of the radiation source on axis did not wander more than ~0.1 mm from shot to shot.

B. DPF for Nanofabrication

An early paper by Gribkov *et al.* [114] describes the use of the NX2 DPF configured as an Ar X-ray source (~0.4-nm wavelength) for micromachining. A notable feature of this work is the use of a gas admixture of Ar and Kr to enhance the Ar K-shell yield. The Ar X-ray output around 0.4 nm was $<$ 0.4 J/pulse with pure Ar or Ar:D_2 mixtures. The pinch was also characterized by hotspots. With the Kr admixture, the pinch was tighter and brighter. The authors speculate that as the current sheet radially moves inward, the lower mass (strictly speaking, lower mass/charge ratio) Ar ions would move ahead of the higher mass/charge ratio Kr ions and arrive at the axis first. Zel'dovich and Raizer discussed this in their invaluable textbook [115]. The slower moving Kr ions in the shock would (via radiative cooling) make the sheet thinner and compress the Ar plasma to a tighter pinch on axis.

In 2007, Bhuyan *et al.* of Catolica University in Chile [116] investigated high-energy ion beam irradiation on Si (100) substrates at room temperature using a low-energy PF device operating in methane gas. The unexposed and ion-exposed substrates were characterized by X-ray diffraction, scanning electron microscopy (SEM), photo-thermal beam deflection, energy-dispersive X-ray analysis, and atomic force microscopy (AFM). The interaction of the pulsed focus generated ion beams with characteristic energy in the 60–450-keV range with the Si surface results in the formation of a surface layer of hexagonal silicon carbide. The SEM and AFM analyses indicated clear step bunching on the silicon carbide surface with an average step height of 50 nm and a terrace width of 800 nm.

The Catolica group later reported [117] on the production of different types of submicrometer-sized carbon composite coatings, using high-energy carbon ion beam irradiation of solid targets. The carbon ion beams of characteristic charge state C^{4+} and C^{5+} and energy in the 50–600-keV range were produced in a 1.8-kJ 160-kA PF device operating in methane

gas and with a hollow anode. The interaction of the high-energy carbon ion beams with different substrates, including silicon (100) and titanium, resulted in the formation of surface coatings with different characteristic morphology and composition. In the case of a silicon substrate, a step-bunched surface layer of hexagonal SiC or an amorphous carbon layer is formed, depending on the focus anode material. In the case of titanium, gradient layers of TiC with embedded carbon nanostructures were observed. Detailed characterizations of the different surface coatings were conducted using SEM, EDX, XRD, AFM, AES, and Raman spectroscopy. The natural angular anisotropy of the focus ion beams allowed investigation of the effect of ion beam characteristic energy and flux on the resulting coatings. The authors discuss an empirical model of fast ion-induced deposition, which attributes the process to a combination of ion beam implantation and transient physical vapor deposition due to a plasma bubble ejected from the anode as a result of high-energy electron beam bombardment.

Recently, Rawat of NTU [118] has written a comprehensive review article on the use of DPFs for nanofabrication. The DPF device with an extraction aperture was used as an intense pulsed ion source to investigate the effects of ion irradiation on pulsed laser deposition (PLD)-grown FePt thin films of two different thickness of about 67 and 100 nm. By adjusting the operation parameters of ion irradiation using the UNU/ICTP DPF device, the FePt thin films, particularly in nanoparticle form, could be successfully grown using energetic PF H^+ ion irradiation. Another useful result was that the annealing temperature for phase transition of FePt thin films from low Ku fcc phase to high Ku fct phase was reduced by PF ion irradiation to 400 °C from the conventionally required 600 °C. It was postulated that ion irradiation lowers the activation energy for diffusion by inducing vacancies or interstitial point defects and, hence, lowers the annealing temperature for phase transition. Rawat showed that the hard magnetic properties were significantly enhanced by single shot PF ion irradiation at a lower postdeposition annealing temperature of 400 °C, resulting in lesser grain growth or agglomeration of nanoparticles with reduced exchange coupling effect, which is a highly desirable trait for the application of these nanoparticles in ultrahigh-density data storage. This observation is consistent with other experiments conducted using so-called energetic condensation [119], [120]. The basic idea is that energetic ions deposit energy into several atomic layers beneath the surface. The rapid quenching of the ions in these layers creates a highly nonequilibrium state of the lattice that is "shaken up," and multiple shallow defects and vacancies are created. As this disturbed state relaxes to equilibrium, low-defect or defect-free crystal growth is possible even with grossly mismatched elements. Krishnan *et al.* [120] have shown how energetic condensation of Nb ions from a cathodic arc plasma drives single-crystal growth of Nb (100) at relatively low annealing temperatures on MgO, a surface whose lattice mismatch with the Nb (100) lattice is rather large. However, such subplantation physics requires relatively low energy ions (< 1 keV). The DPF emits far more energetic ions that would deeply penetrate into the substrate and cause deep defects that are not easily annealed at lower temperatures. Another advantage of energetic ion irradiation using the DPF device is that it can reduce the phase transition temperature to hard magnetic phase in a single shot ion exposure with ion pulse duration on the order of about a hundred to a few hundred nanoseconds. The use of transient pulsed energetic ions from the DPF, as opposed to that of long exposure time irradiation from continuous ion sources, provides a fast and effective way to lower the phase transition temperature with significantly enhanced hard magnetic properties with lower particle size.

The NX2 PF device, operating in sub-kilojoule range, was successfully used to synthesize CoPt nanoparticle thin films with small particle size and narrow size distribution using two different operating modes: 1) different hydrogen filling gas pressures while keeping the substrate–anode top distance and the number of PF deposition shots fixed at 25 cm and 25 shots, respectively, and 2) using different numbers of PF deposition shots at a fixed substrate–anode distance of 25 cm at filling hydrogen gas pressure of 6 mbar. Morphological features such as nanostructure formation and their shapes and sizes showed a strong dependence on the filling gas pressure and the number of PF deposition shots. A recipe to synthesize well-separated and narrow-size-distributed CoPt nanoparticles was obtained by tuning the filling gas pressure and the number of PF deposition shots. The deposition rate at a deposition distance of 25 cm and at an optimized gas pressure of 6 mbar was estimated to be about 17.8 Å/shot, which is more than 30 times higher than that of conventional PLD, which is reported to be about 0.50 Å/shot. The findings of Rawat are remarkable as the DPF produces not only ions but also shocks and blast waves and a plasma jet moving at high velocity toward a sample. For certain applications, these extraneous energy sources might be deleterious, but for synthesis of hard magnetic thin films (as used in storage media), the DPF appears to show promise as a high deposition rate coating device.

C. DPF Particle Beam Sources

An early paper by Stygar [121] describes the formation and properties of ion beams in a DPF. The ion and electron spectral data for four DPF shots are shown in Fig. 12 for a deuterium fill gas pressure of 3 torr and a bank voltage of 24 kV (11.5-kJ stored and ~500-kA peak current). The neutron yields for these four shots were within 10% of 2.2×10^9.

A notable feature of these spectra is that the ions are nonthermal and have energy that extends out to ~250 keV. This allows them to drive beam-target fusion and produce $\sim 10^9$ neutrons/pulse that would be quite impossible in a thermal plasma at a typical pinch temperature of ~1 keV. The second is that both electrons and ions (moving in opposite directions) show similar power laws, suggesting a common mechanism at work. Stygar showed a graph of measured beam current versus discharge current for a D_2 fill pressure of 3 torr (see Fig. 13).

An estimate of the total number of electrons in the fast peak observed on the Faraday cup at 12.5 kJ is on the order of 2×10^{15}. The mean ion beam fluence over a 15-cm-diameter plate 20 cm away from the focus was estimated to be $6 \pm 2 \times 10^{14}$ cm^{-2}. The ratio N^+/N^e was $\sim 50 \pm 30$, which was consistent with $(M^+/M^e)^{1/2}$, which is predicted by a model for a uniform-current-density diode accelerator [122].

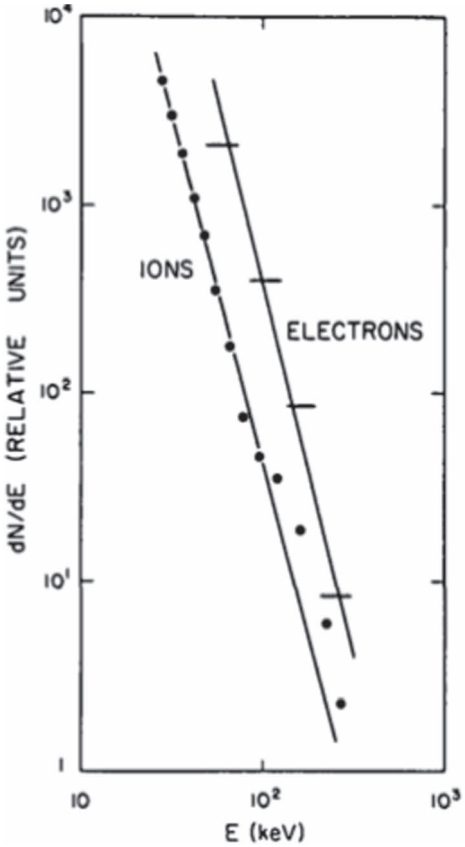

Fig. 12. Simultaneously recorded ion and electron energy spectra. Straight lines are power law fits to the ion and electron spectra, where exponents are −3.5 and −3.8, respectively [121].

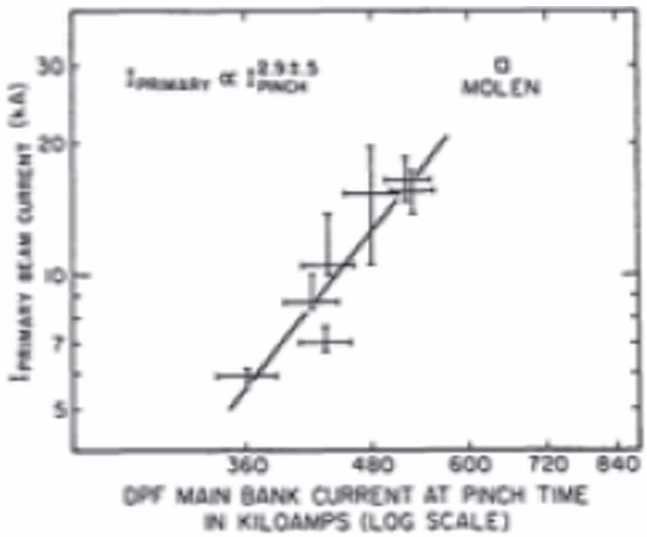

Fig. 13. Observed scaling of peak electron beam current with main DPF current. Filling pressure was 3-torr deuterium [121].

The electrons and ions are accelerated at the same time by the same transient electric field. To provide some perspective on a beam current of ∼20 kA from a 600-kA main bank current, suppose that the main bank was repetitively fired at 10 Hz. If the electron beam pulsewidth is ∼50 ns, the average beam current would be 10 mA. With modern pulsed power technology such as linear transformer drivers, it is possible to operate a 10-Hz circuit at 600 kA. Then, a 10-mA electron beam source seems attractive for applications. However, the spectrum of the beam is broad (see Fig. 12). If the beam had to be filtered to extract a narrow band of energy, the useful current would be much lower. Modern RF or induction accelerators would be far more efficient and portable than a 600-kA DPF device. The same arguments would hold for ion beams as well. The niche that such beam sources would occupy would be for those applications that benefit from the narrow pulsewidths. One such application is for special nuclear material (or explosives) detection using a fast-neutron pulse, as described in the following section.

The Catolica group in Chile [123] measured the basic properties, charge states, energy spectrum, and flux of ion beams generated in a low-energy methane PF. The dominant charge states of carbon ions were measured to be C^{4+} and C^{5+}, with maximum flux on-axis on the order of 2×10^{22} ions $m^{-2} \cdot s$, when operating with 0.35 torr of methane. The dominant charge states of the carbon ions were argued to be consistent with a model in which ion acceleration takes place before the high-density high-temperature phase of the focus discharge. The measured ion beam parameters pointed to potential applications in materials science.

The Catolica group also discovered [124] a curious anisotropy in ion emission from their focus. The angular distribution of hydrogen and carbon ions showed a highly anisotropic character. The flux of hydrogen ions was found to be maximum on the focus axis, whereas the flux of carbon species was maximum off axis with a dip on axis. Maximum ion emission was confined within a cone half-angle of 15°. The authors suggested that finite ion Larmor radius plays an important role in the anisotropic emission of the different kinds of ions from the focus pinch region.

Recently, Tang *et al.* [125] have proposed to develop a multistage DPF as a high-gradient particle beam accelerator. The concept suggested is to place DPFs in a linear sequence so that the ion beam generated in one pinch propagates to the next and is further accelerated by the second pinch and so on. This is analogous to laser plasma accelerators (LPAs) [126] wherein segments of capillary discharges would be used to boost injected electrons at one end to ≫ GeV energy at the other. The LPA concept has been demonstrated to the gigaelectronvolt level, and plans are underway to extend it to 100 GeV in the next few years. The LPA offers much higher field gradient (∼1 GeV/cm) than does the DPF (∼0.2 MeV/cm), but the charge bunch in a DPF would be much higher.

D. Neutron Sources

The DPF literature is replete with descriptions of Mather- and Fillipov-type foci. Rather than repeat published information that is found in several references, this paper presents a few more unusual variants for completeness. It was recognized early on that typical DPF electrode designs could not be scaled to the high currents required for breakeven fusion: a highly optimistic 10 MA as predicted by Imshennick *et al.* [127] or a more realistic 30 MA as predicted by Vikhrev and Korolev [128]. The presence of solid material in close proximity to a burning fusion reactor would be impractical, to say the least. Lee *et al.* invented

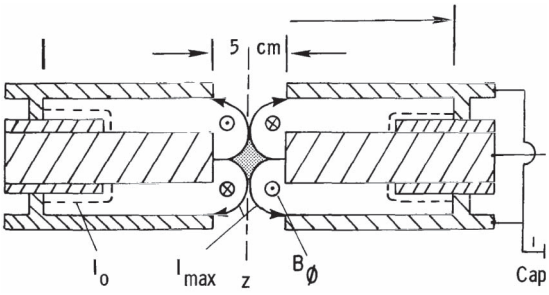

Fig. 14. Cross-section view of hypocycloidal pinch [129].

the hypocycloidal pinch, which might offer a way around this conundrum [129].

Fig. 14 shows a cross-section view of the concept. The basic idea is to use disk electrodes that allow the run-down phase to radially converge inward and form a pinch that is free-standing in a large open space between the disks, thereby decoupling the hot plasma from the nearby electrodes. The efficacy of this approach would depend upon how large a "hole" one could make in the disk and still produce a hot dense pinch on axis. Another feature of the hypocycloidal pinch is its lifetime that was shown to be much longer than the typical ~50-ns duration of Mather-type pinches. The extended confinement of the plasma in the hypocycloidal pinch seems to result from the interaction of two foci in the magnetic neutral plane formed by the cusp configuration of the current sheets in the center hole, which is a unique feature of this configuration. One should also note that the simultaneous arrival of the upper and lower current sheets on the axis of the center hole is necessary to form the symmetric cusp configuration of the current sheets.

The second set of unusual DPF variants discussed is from the groups in Chile and Singapore. The aim of the work at Chilean Nuclear Energy Department (CCHEN) has been to characterize the physics of dense plasma foci and to carry out the design and construction of smaller devices, in terms of both input energy and size, capable of providing dense hot plasmas. Scaling laws have been applied to design and construct PF devices with storage energy in a region never explored before (tens of joules and less than 1 J). In particular, all the devices, from the largest to the smallest, maintain the same value of ion density, magnetic field, plasma sheath velocity, Alfven speed, and specific energy per particle. Therefore, fusion reactions are even possible in ultraminiature devices (driven by generators of 0.1 J for example), as they are in the larger devices (driven by generators of 1 MJ). However, the stability of the plasma pinch depends upon the size and energy of the device. This remarkable scaling of DPF physics down to the 1-J level is described in several papers from 2002 to the present. While the concept of constancy of drive parameter and equivalent concept of constancy of energy density for all plasma foci were introduced and extensively discussed in the period starting 1996 by Lee *et al.* [38], [39] including in gases other than deuterium, Soto *et al.* made a further contribution in 2005 by demonstrating the extension of those constancies down to the nanofocus at the ~1-J level [130]–[137]. Several of these papers from the CCHEN group describe the lower energy limits. This scaling of DPFs is not only interesting for scientific reasons but could have implications for practical applications. However, a note of caution must be sounded here. While it may be true that energy density scaling seems to hold as one makes DPFs smaller, the problem is that the fusion process is a parametric process, with a threshold of energy to efficiently drive beam-target fusion. The electric field in a DPF (if it scales as vxB) would be a constant for a fixed $v \sim 250$ km/s and roughly equal B $\sim$ 40 T in a self-similarly scaled pinch; 200 kA in a 1-mm pinch or 10 kA in a 0.05-mm radius pinch. Thus, the electric field (~ 250 km/s $\times$ 40 T $\approx 1 \times 10^7$ V/m) would be the same in the two pinches. However, the miniature 10-kA pinch might be only ~0.3 mm in length (smaller anode). Hence, the net ion acceleration potential might be only ~4 kV in the 10-kA pinch. This mean energy of 4 keV would be far less efficient at driving beam-target fusion, since the cross section at 4 keV is $\approx 10^5$ times lower than it is at 60 keV (the mean energy in the 200-kA pinch). In other words, the fact that energy density is constant as one reduces stored energy does not guarantee that the I^4 scaling will persist at lower energy (current). Indeed, thermal physics might drive fusion in the 10-kA miniature DPF, but with a scaling coefficient that is much weaker than that for the higher current machines.

The NTU group has also published several papers on scaling DPFs to lower energy and higher rep-rates [138]–[142]. A Mather focus operating at 140 kA from 1800 J was reported by Favre *et al.* [143].

Several papers describe innovations aimed at improving the reproducibility of neutron emission from DPFs. One such is by Zakaullah [144]. This paper describes the study of neutron emission in a low-energy PF with β-source-assisted breakdown. A mesh-type β-source of Ni-63 was used to preionize the gas near the insulator sleeve of two low-energy (1.15 and 0.58 kJ) Mather-type PF devices. The neutron emission was found to be increased by up to 25%. The results of this experiment suggested that preionization may be helpful in designing a device as a sealed neutron source for different field applications.

Enhanced and reproducible neutron emission from a PF with preionization around the insulator sleeve induced by depleted uranium (U-238) was reported in 2006 by Ahmad *et al.* [145]. The maximum average neutron yield was 2.5×10^8 at 3.5 mbar without preionization, which increased up to 3.85×10^8 with preionization. It was claimed that the preionization enhances neutron yield by about $(50 \pm 5)\%$, broadens the neutron emission pressure range, and improves shot-to-shot reproducibility of PF operation for neutron emission. Fig. 15 (reproduced from [145]) shows ten successive shots fired with and without preionization.

The reproducibility of neutron yield is improved with preionization. The improved ionization at breakdown of the insulator might create a more uniform current sheet in the coaxial section that, in turn, leads to a better and more reproducible pinch. The word reproducible in this regard can be misleading. One does not mean uniform. Since it is known that the neutron output is driven by beam-target phenomena that are themselves the result of instabilities in the pinch, how then can a more uniform sheet improve an unstable final condition? It is possible that the pinch goes unstable in any case, but that the dense plasma target regions where fusion occurs are more reproducible when

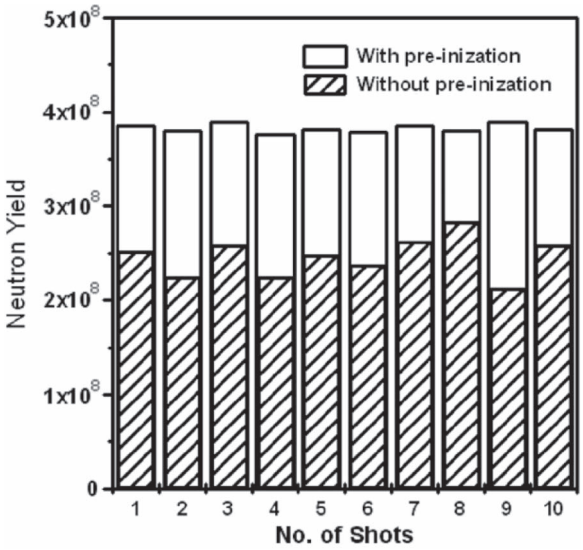

Fig. 15. Shot-to-shot variation of neutron yield at optimum pressure for 23-kV charging voltage with and without preionization [145].

there is preionization. Ahmad *et al.* showed evidence that the active volume with preionization is indeed larger than without, confirming this hypothesis.

Nardi *et al.* [146] were among the first to use knife-edges or field distorting elements around the base of the insulator sleeve of a DPF to enhance its neutron output. Such enhancements would be helpful in lower voltage DPFs that might otherwise suffer from nonuniform breakdown across the insulator.

Lu *et al.* [147] described the use of a knife-edge at the base of the insulator sleeve to enhance breakdown and improve neutron output and reliability. When the insulator length was varied to optimize the output, the knife-edge protected shorter insulator sleeves from restrikes. The knife-edge is thought to produce a more uniform liftoff sheet that leaves behind a better vacuum and, hence, prevents restrikes of the insulator.

An early demonstration of a rep-rated DPF neutron source was published by Verma *et al.* [148]. They reported enhancement in time-averaged neutron yield by an order of magnitude using the fast miniature PF FMPF-2 in repetitive mode. The FMPF-2 device (2.4 μF, 56 nH, 13.8 kV, T1/4 $\sim$ 575 ns) operates at up to 10 Hz in the quasi-continuous mode. Using pure deuterium as the fueling gas, a time-averaged neutron output of $(6.2 \pm 4) \times 10^5$ neutrons/s at 1-Hz operation was enhanced to $(6.5 \pm 0.6) \times 10^6$ neutrons/s at 10-Hz operation for burst lengths of 30 consecutive shots. The stored energy of this DPF was 230 J (to deliver about 80 kA of peak discharge current at 13.8-kV charging voltage).

Krishnan *et al.* [149] and Bures *et al.* [150] described a transformer architecture built at AASC/California to drive a rep-rated DPF. The motivation for a transformer architecture is that DPFs are driven by current rather than voltage, within limits. The voltage need be only high enough to charge the moving inductor in the coaxial region (the dL/dt dynamic impedance) plus any ohmic dissipation in the circuit. The coaxial inductance is the magnetic storage for the pinch that derives a fraction of its energy from this store. A 20-nH coaxial inductance with a $\sim$1 μs (sinusoidal) risetime gives a dynamical impedance dL/dt of $\sim$20 mΩ. Charging this to 100 kA requires only $\sim$2 kV. It is obvious that a driver that delivers 100 kA with $\sim$2 kV to the vacuum interface would suffice to charge the DPF. The much higher voltage generated by the pinch is local to the pinch. Along a closed loop that includes the pinch, for a flux-conserving system, the quantity $d(LI)/dt = 0$; hence, the voltage LdI/dt (due to the pinch) is balanced by IdL/dt along the closed loop. The magnitude of the term IdL/dt can be 50 kV or higher, although the charge voltage in the coaxial section might be as low as 2 kV in the above example. This dynamic "emf" is the driving term for the ion spectrum that is non-Maxwellian and has a tail that might extend beyond 100 keV and more efficiently drive fusion. If the bank impedance is similar to the coaxial impedance, a peak voltage of $\sim$4 kV is necessary in the bank. What this means is that a 6 : 1 step-down transformer could be used to convert a 24-kV/12-kA primary loop current into a 4-kV/72-kA secondary current that drives a small DPF. The advantage of such an architecture is that the stored energy is low for the given current, and a single Thyratron switch may be used in the primary loop. The Thyratron is capable of $\sim$1-kHz rep-rates; hence, the eventual rep-rate of the DPF is limited only by thermal management considerations. Another advantage of the transformer is that the secondary inductance and (more importantly) resistance are both reduced from their primary side values by the square of the turns ratio. For the 6 : 1 step-down design, this reduction is a factor of 36 : 1. The transformer-driven architecture reduces the stored energy for a given current into the DPF. For example, the AASC DPF stores 93 J at 24 kV and delivers 71 kA to a DPF load. At 100 Hz, the wall plug power drawn by such a driver would be 9300 W. If 30% of this power is deposited into the anode, the anode cooling circuit must handle about 280 W. Such a heat load is handled by a simple coil at the base of the anode that circulates chilled distilled water.

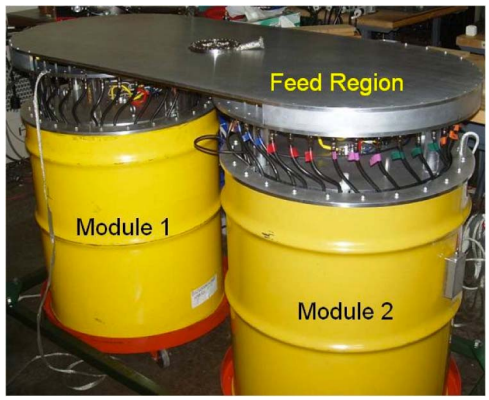

Fig. 16. Photograph of DPF-2 prototype fast-neutron source. Two Thyratron switched modules are shown. The DPF head is replaced by a short circuit to calibrate the cathode Rogowski coil [150].

By contrast, a direct capacitor-driven DPF that also drives 70 kA was published by Verma *et al.* [151], which stores 200 J but is more compact (25 kg) than the AASC source.

Fig. 16 shows a photograph of the prototype fast pulsed neutron source built using these principles.

The driver consists of two identical modules, each of which stores 46 J (at 24 kV) in a primary capacitor bank. The two

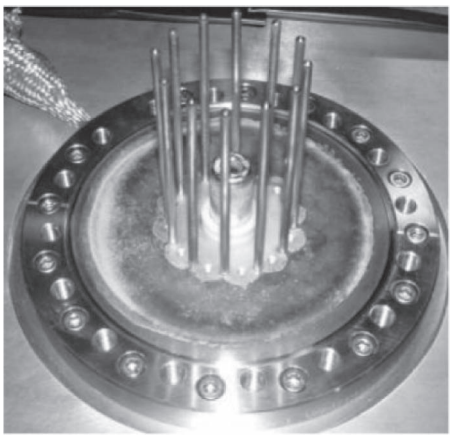

Fig. 17. Photograph of DPF head. Anode is 15-mm diameter × 20-mm long. Cathode rods are on a 40-mm-diameter circle [150].

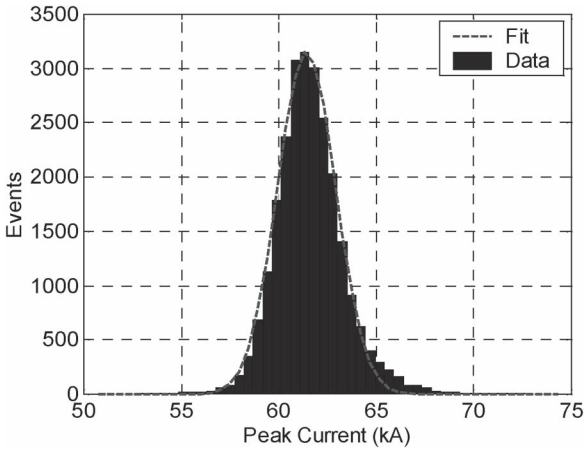

Fig. 18. Histogram of peak currents for all the shots in experiment 035a, plotted in 50 bins [155].

modules discharge ≈12 kA through a Thyratron switch (L3 Communications L-4945 Hydrogen Thyratron) into the primary loop of a 6 : 1 step-down finemet core transformer. The secondary loop generates a 4-kV/72-kA power pulse into the dynamic DPF load. The DPF head emits $\approx 5 \times 10^5$ neutrons/pulse (d,d). This system may be operated at up to 100 Hz, to give 5×10^7 neutrons/s (DD) or 5×10^9 neutrons/s (d,t). The DPF head (see Fig. 17) consists of a 15-mm-diameter × 20-mm-hollow stainless steel anode, with a set of 12 coaxial cathode rods arranged in a circle of 40-mm diameter.

Bures *et al.* [152] showed that when the D_2 fill was diluted by addition of noble gases (2%, 4%, and 8% Ar and Kr were added to D_2), the neutron output was increased by a factor of 3–4. One possible explanation is that the higher-Z gas radiatively cools the sheath and makes the pinch denser so beam-target fusion is more efficient. Recall the paper by Aliaga-Rossel and Choi [68] and that by Kato and Be [108] in this regard. This conjecture remains to be tested by measurements or numerical simulations. Verma *et al.* also investigated high-Z admixtures with beneficial results [153].

A considerable body of work exists on repetitive operation of DPFs as neutron sources. An early paper by Burns *et al.* [154] describes an ultraclean DPF of the Mather type operated at 220 kA from a 1.4-kJ bank with both D_2 and $D_2 : T_2$ mixtures. Over 600 consecutive shots were fired (but over a period of months) without purging the gas. The neutron outputs measured were $\approx 3 \times 10^9$ neutrons/pulse (d,t).

The vast majority of experiments conducted on dense pinches (DPFs or fast Z-pinches) has tended to present data and analyses that were based on tens to hundreds of shots. On the largest machines such as Z (20 MA) [11], one is often forced to contend with an experiment that allows less than ten shots to study a particular phenomenon. On the other hand, nonlinear or stochastic plasma phenomena exhibit strong parametric variations from shot to shot. Hence, a test campaign that accumulates thousands rather than tens or hundreds of shots would enable statistically significant analyses to be performed.

The transformer-driven 70-kA DPF built at AASC offers just such a testbed. Bures *et al.* [155] described rep-rated neutron outputs from this DPF. Data were presented from runs of 25 000 shots each. The short-circuit inductance of the pulse power is 17 nH with a 5-mΩ resistance. The SS304 anode had an active length of 20 mm with a 15-mm diameter. The SS304 cathode was composed of 12 3-mm-diameter rods centered on a radius of 40 mm. An alumina insulator with an active length of 10 mm was used to isolate the anode from the cathode in vacuum. Before a series of experiments, the vacuum spool was pumped to less than 10^{-6} torr. Once this base vacuum pressure was reached, D_2 gas was added to the chamber until the desired pressure was reached. Fill pressure was controlled to better than 1% using a capacitance monometer with a 20-torr range. PF operation was controlled by a laptop computer and a timing generator. Rogowski coil output signals were digitized at 2 ns/pt. The ^{3}He neutron detector data were digitized at 4 μs/pt. Typically, a few experiments were required to condition the electrodes and the insulator. During these conditioning shots, typically 1000 shots per experiment at 1 Hz, the deuterium pressure dropped from the fill pressure to a value as much as 25% lower. The system was considered conditioned when the pressure after a run was within 2% of the initial fill pressure. The deuterium gas seemed to be dissolved into the anode and other SS304 structures in the chamber. Experiments conducted with inert gases after long deuterium runs have measured neutron yields ranging from 10% to 50% of the pure deuterium yield. The neutron yield drops to background levels after about 600 shots in inert gases, confirming this dissolution and reemission of D_2 from the anode. A similar pressure drop is observed when deuterium operation is resumed as the electrodes reabsorb the deuterium. No effort was made to cool the anode. Thus, the temperature of the anode increases until a steady-state value is reached at a fixed repetition rate. The typical steady-state value for 1-Hz operation was ∼200 °C. The vacuum spool was externally cooled using fans and its temperature remained below 40 °C. Operation at 1 Hz was found to be stable without electrode cooling.

A 25 000 shot experiment was selected to show typical behavior. Fig. 18 shows the histogram of the peak currents in the experiment called 035a.

The average of the peak currents was 61.6 ± 1.8 kA with a peak in the distribution in the 61-kA bin with a width of 0.5 kA. I^4 scaling suggests an 11.6% standard deviation in neutron output is expected from the 2.9% deviation in the peak current.

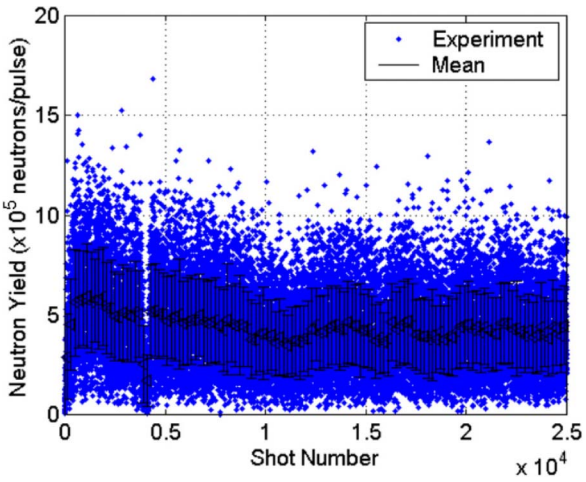

Fig. 19. Neutron yield of experiment 035a as the experiment progressed. The triangles represent the mean of 200 shot groups with the error bars representing the standard deviation of the group [155].

Fig. 19 shows the neutron yield of experiment 035a as the experiment progressed. The triangles represent the mean of 200 shot groups with the error bars representing the standard deviation of the group. A typical standard deviation was 50%. A noticeable reduction in neutron yield was observed at 4000 shots. The reason for the reduction is not clear at this time. The neutron yield trend shows a decrease in mean yield up to 10 000 shots. The mean yield could be well represented by a constant after 10 000 shots given the standard deviation of the mean. Fig. 19 shows that the neutron yield variation is far greater than the 11.6% predicted from the variation in peak current. However, this assumes that peak current is the only important parameter in determining the neutron yield.

The accepted scaling relationship between current and neutron yield does not consider other factors, but it does address the mean behavior of the source. The proportionality constant in the scaling relation changes for different anode geometries and different gas mixtures. It has been shown that doping the deuterium with inert gas [152] increasing the repetition rate of the source [155]and altering the electrode geometry from a right cylinder to a conical geometry [152] can increase the neutron yield of a given PF. If one considers that neutron production is mainly from energetic ions interacting with the dense plasma region or surrounding gas, the problem is more complex than a simple relationship with the current. Given the significant change in DD fusion cross section with ion energy, which grows by nearly four orders of magnitude from 10 keV to 1 MeV, the ion energy spectrum is an important consideration. (More on this will be discussed in the next section.)

The rep-rated DPF-2 was used to demonstrate a novel concept for detection of special nuclear materials or high explosives. Krishnan *et al.* [156] described tests in which (surrogate) iron targets were placed at different distances from the point neutron source.

Fig. 20 (from [156]) shows the test configuration that was used.

Detectors such as Stilbene and $LaBr_3$ were used to capture inelastically induced 847-keV gammas from the iron target. Shielding of the source and detectors eliminated most (but not all) of the source neutrons from the detectors. Gated detection, pulse shape analysis, and TOF discrimination enabled separation of gamma and neutron signatures and localization of the target. Fig. 21 shows the $LaBr_3$ data plotted versus energy from a narrow time slice between 30 and 80 ns.

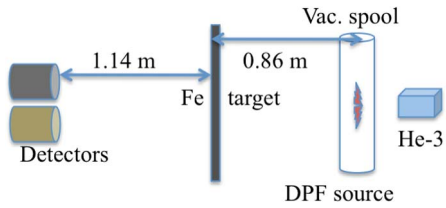

Fig. 20. Configuration for the test of the TOF detection concept [156].

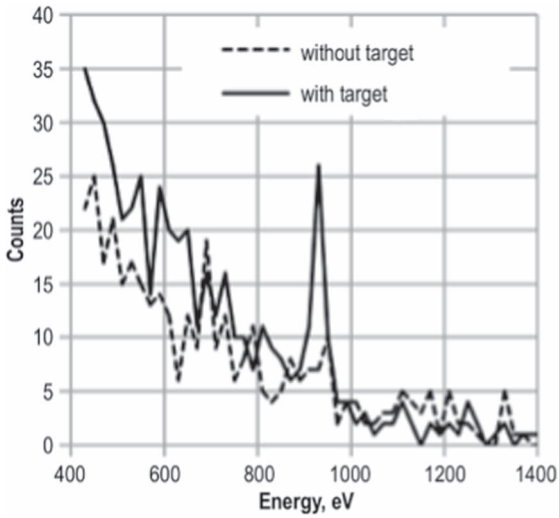

Fig. 21. Detected counts (LaBr3) versus energy (in a 30–80-ns time slice). (Solid line) With target. (Dashed line) Without target [156].

This slice covers the period when the iron target gammas reach the detector. The prominent peak around 850–900 keV clearly validates the TOF technique, as the source neutrons have not yet reached the detectors during this time slice. For example, an special nuclear materials target would emit prompt neutrons and gammas when probed by source neutrons, whereas an high explosives (HE) target would emit characteristic gammas from its constituent elements when excited by source neutrons.

For the HE detection problem, the DPF would be run in a mixture of D_2 and T_2 gas to generate 14.1-MeV DT neutrons. The speed of the DD neutrons is 2.17 cm/ns, whereas the 14.1-MeV neutrons travel at 5.17 cm/ns. The typical pulsewidth of the source is 20 ns (FWHM) so that range gating can achieve a spatial resolution of ~40 cm (DD) or 100 cm (DT). A simple Monte Carlo simulation was run to obtain an idea as to how such a detection scenario might work. Fig. 22 shows the Monte Carlo configuration.

The isotropic neutron source has a 100 cm $\times$ 100 cm $\times$ 2.5 cm detector array placed 1.0 m from and "edge-on" to the source, to minimize neutron interactions with the detectors. The target for this simulation was a 30-cm-diameter $\times$ 10-cm-thick Fe target located 3.0 m from the source as shown. The simulation used five DPF pulses with 2×10^6 neutrons/pulse, in a pulsewidth of 20 ns, with a neutron spectrum of 2.45 $\pm$ 0.1 MeV. The $\pm$0.1-MeV spread is due to the beam-target

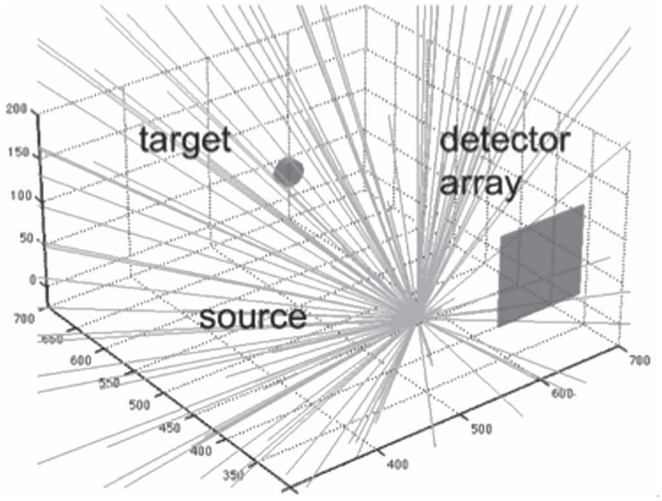

Fig. 22. Configuration used for Monte Carlo simulation of a field test of the detection concept. Neutron source isotropically emits; target is at 3 m from the source; detector array is "edge-on" to the source to minimize source neutron background signal [156].

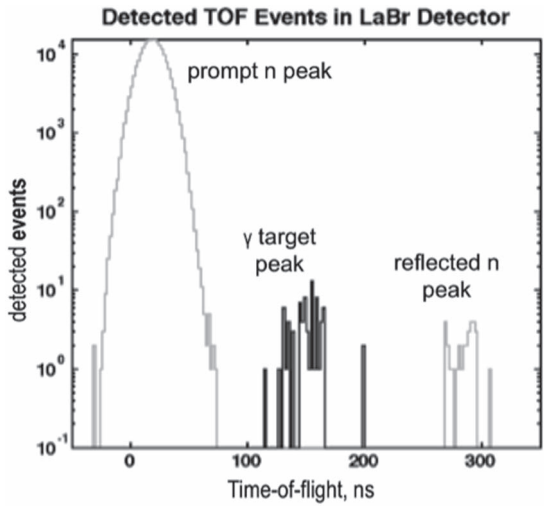

Fig. 23. Results of Monte Carlo simulation. Prompt neutron peak is followed by gamma return signal from target. Reflected neutrons from target arrive much later and are well separated from target gamma peak [156].

mechanism discussed earlier, which gives $+0.1$ MeV in the forward direction and -0.1 MeV in the backward direction. The results are plotted in Fig. 23.

The high count rate of 10^4 events near the start is due to the intense burst of source neutrons flashing the detectors at early times. The flight time of neutrons to the target 3 m away is 138 ns, and the inelastic gammas take 10 ns to return to the detectors. Fig. 23 shows about ten gamma counts in the 130–160-ns band. Still later (around 280 ns), there is a peak due to source neutrons that are reflected by the target back to the detectors. The gammas generated by the vacuum spool around the neutron source, as well as by the iron cores below the source, are buried within the initial peak that is labeled in Fig. 23 as the prompt neutron peak. It should be noted that the $\sim$10 good gamma counts in this case required only five pulses of the neutron source, i.e., a total neutron output of 10^7 neutrons. If the source is operated at 100 Hz and the interrogation runs for 10 s, the total gamma count would be $\sim$2000. This simple Monte Carlo model has not included clutter from nearby objects and realistic detector response; hence, the signal/background ratio has not been evaluated for a practical scenario. Nevertheless, a gamma count rate of $\sim$2000 in just 10 s, which corresponds to a total neutron output of 2×10^9 neutrons, is encouraging. The dose to the interrogated target would be < 1 mrem.

Another concept put forward for the use of a DPF for nuclear or HE detection is based on elastic scattering of neutrons, as proposed by Brooks *et al.* in 1998 [157] and Gribkov and Miklaszewski in 2005 [158]. The basic idea is that fast neutrons when elastically backscattered by low-Z nuclei lose a significant fraction of their incident energy in the collision. If one uses a short neutron pulse and scatters it off an unknown collection of objects, the low-Z nuclei will preferentially backscatter the neutrons and slow them down. If a sufficiently fast detector (scintillator–photomultiplier) is placed along the backscatter direction and is well shielded from primary fast neutrons, it is possible to capture the delayed neutron signals and, from the time delay, determine the atomic number and concentration of the scattering nuclei. The idea is not new, but it is well known that fast-neutron scatter analysis requires long interrogation times due to the low intensity of commercially available sources and their operation in single counting mode.

In the experiment by Gribkov, the DPF was so intense $(10^9$ neutrons/pulse$)$ that the scintillator signal was an analog signal rather than single quantum counts. However, the scattered neutron signals were buried in the tail of the primary neutron signal (despite shielding) as the DPF is a quasi-isotropic emitter. Using wavelet techniques, they extracted the tiny backscattered signals from the tail of the primary signal and demonstrated the technique by using liter volume bottles of methanol (CH_3OH) containing C, H, and O as constituents. The main advantage of a DPF in this application is that one could make a very intense burst of DD neutrons and obtain information from a single flash or just a few pulses. For example, a cargo container might be interrogated using two DPF sources that are located at right angles to one another. By delaying the two pulses with respect to one another and using detectors located at different angles, analysis of backscattered signals could be used to localize high concentrations of low-Z nuclei in the container.

In the last part of this section, results from a higher current DPF-3 in operation at AASC (similar to NX2) are described to show statistical data from D_2 pinches at 240-kA currents. These data demonstrate that although the mean neutron output might follow well-discussed scaling laws such as I^4, when one gathers data at a fixed current over a large number of shots, the shot-to-shot variation departs from simple scaling laws based on macroscopic parameters such as current or voltage. The data and analysis presented of DPF-3 data are used to motivate the following section, in which scaling laws and design criteria are discussed.

Bures *et al.* [159] described a study of a 230-kA PF at a fixed pressure, charge voltage, and electrode geometry for 930 shots. The neutron yield at 230 kA was found to be 5.6×10^7 neutrons/pulse with a standard deviation of 55%. The highest yield shots exceeded 10^8 neutrons/pulse. Using

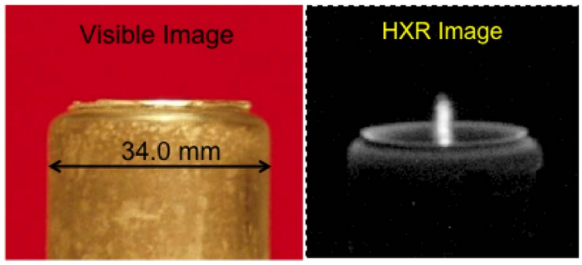

Fig. 24. Photograph of a 34-mm SS304 anode and HXR image from a 279-kA Ar pinch at 2.5 torr (25 shots in a row) [159].

terminal measurements of voltage and current, the time-varying inductance and the pinch voltage were derived. A linear relationship was found between the minimum in the time derivative of the current (dI/dt) and the pinch voltage. Increasing pinch voltage correlated with increasing neutron yield at the same peak current. Therefore, it is desirable to increase the (absolute) minimum in the dI/dt and thus the current "bite" to increase the neutron yield. The large deviation in the neutron yield cannot be explained using terminal measurements alone; hence, time- and spatially resolved diagnostics are needed to better understand how microscopic phenomena such as instabilities affect the shot-to-shot neutron variations.

Fig. 24 shows a photograph of the 34-mm SS304 anode and an HXR image from a 279-kA Ar pinch at 2.5 torr (25 shots in a row were required to produce the image on a Digital Imaging Plate).

The HXR image was taken through a 0.4-mm-thick Al vacuum window, whose low energy cutoff is around 8 keV. The HXR emission from the pinch is brighter than that from the anode rim, which indicates a high-current density runaway electron beam coursing through the pinch and diverging before it impacts the anode. The HXR emission from the half of the pinch that is buried inside the hollow anode is attenuated by the walls of the SS304 anode (5 mm). From this attenuation, we may estimate that the HXR emission is relatively weak above 60 keV. Fig. 25 shows measured traces of dI/dt (Rogowski coil in cathode base) and voltage (measured using a Northstar 80-MHz bandwidth high-voltage probe located just outside the vacuum). The red current trace is the integral of the measured dI/dt trace. For this shot, the peak current was only about 210 kA.

The dI/dt and voltage traces are scaled to arb. units to see them on the same scale as the integrated current. Ohm's law for the circuit may be used to calculate the dynamical inductance, assuming that the dissipative resistance is small. The inductance history is presented in Fig. 26.

With reference to Fig. 26, the transition from coaxial snowplow acceleration is assumed to occur at the time when the voltage trace changes direction and begins to increase, around 1050 ns in the figure. The coaxial inductance grows quasi-linearly to about 9 nH (consistent with a terminal axial speed of ~100 km/s), followed by a sharper increase during the radial pinch phase to about 25 nH. The 16-nH pinch inductance is consistent with a 14-mm-long column that has a radius of 0.13 mm. This is too small a pinch radius (see an HXR image of pinch in Fig. 24) and implies that either there might be anomalous

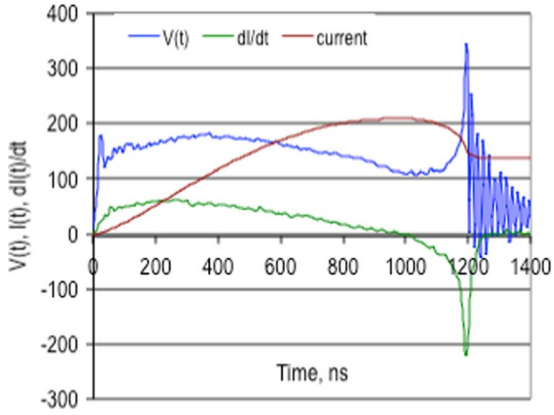

Fig. 25. Measured dI/dt and voltage traces (arb. units) from DPF-3 operating in 2-torr Ar at AASC.

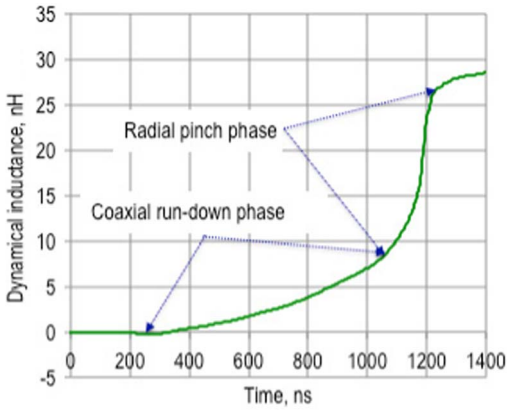

Fig. 26. Inductance versus time for DPF circuit calculated from measured dI/dt and $V(t)$ assuming negligible resistance.

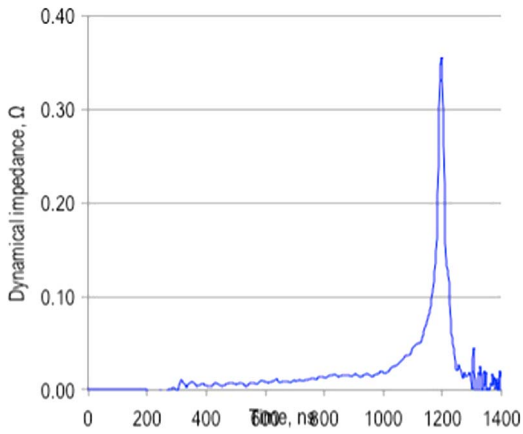

Fig. 27. Calculated effective dynamical impedance versus time.

resistivity that was not taken into account in the analysis or the pinch current might follow a more tortuous path around the axis, which would easily account for the 16-nH inductance of a larger radius pinch.

If one were to lump the anomalous resistance and dynamical impedance dL/dt into an effective dL'/dt, such an effective pinch impedance is plotted in Fig. 27.

For this particular shot, the impedance is 0.35 Ω at peak voltage (minimum in the dI/dt trace). Note that during the

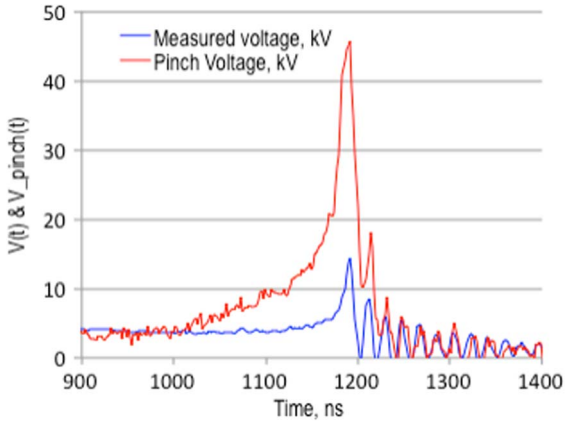

Fig. 28. (Blue) Measured and (red) calculated voltage traces for DPF-3 shot.

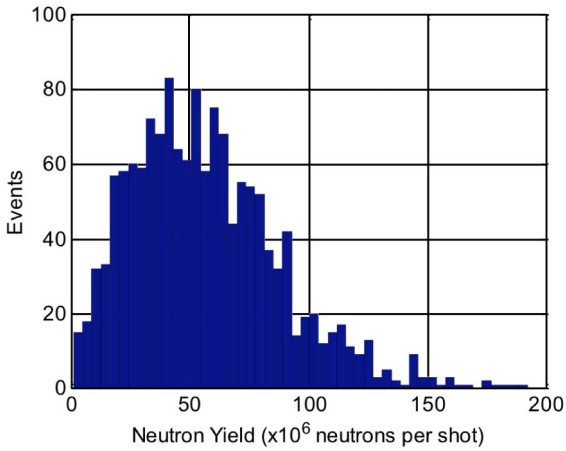

Fig. 29. Distribution of neutron yield (bars) in 50 equally spaced bins with a mean of 5.6×10^7 neutrons/pulse and a standard deviation of 55%. The peak in the neutron distribution is at 4.1×10^7 neutrons/pulse [159].

coaxial phase, the calculated impedance is 20 mΩ, consistent with the estimate made earlier and with that by Lee [8], [42].

Fig. 28 shows the measured voltage trace (blue) and the calculated pinch voltage trace (red) for this shot. The peak voltage at the pinch is 45 kV, whereas the bank charge voltage was only 10 kV for this shot. The pinch voltage FWHM is ~30 ns in this case, but a pure D_2 pinch would show a broader peak. The higher-Z Ar ions drive a thinner sheet due to radiative cooling, and hence, the impedance/voltage spike would be narrower than in D_2.

Similar analyses allowed estimation of the peak pinch voltage from D_2 shots using DPF-3, as reported by Bures *et al.* [159]. Fig. 29 shows a histogram plot of neutron outputs measured from DPF-3 over a sequence of $\approx$ 1500 shots at currents of $\approx$240 kA.

Table II (from [159]) summarizes the neutron measurements. The average current (peak) was 233 $\pm$ 4 kA for these shots. The data from tests 003c, 003d, and 003g were combined into a single data set to examine the neutron yield distribution. The mean of the distribution is 5.6×10^7 neutrons/pulse with a standard deviation of 55%. The yield distribution is asymmetric about the peak in the distribution with a tail extending toward higher neutron yield. Using the deviation in the peak current alone ($\sim$2%), the expected deviation in the neutron

TABLE II
(FROM [159]) MEAN NEUTRON YIELD AND MEAN PINCH VOLTAGE

Experiment	Number of Shots	Neutron Yield Mean $\pm$ 1σ ($\times 10^7$ neutrons/pulse)	Pinch Voltage Mean $\pm$ 1σ (kV)
002d	515	3.0±1.4	25±4
003c	425	5.6±2.9	27±4
003d	375	6.0±3.5	27±4
003g	130	6.3±3.4	26±4

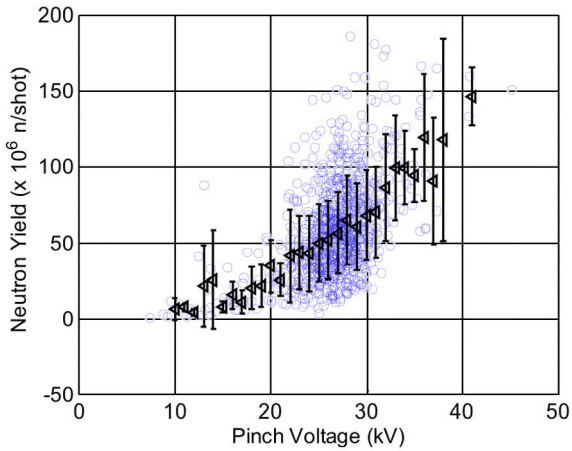

Fig. 30. (Blue circles) Neutron yield per shot versus pinch voltage calculated using dI/dt and $V(t)$ measured outside the vacuum. The black triangles represent the average neutron yield in 1-kV bins. Bins with less than 2 pts were not considered in the analysis. The error bars represent the 1σ standard deviation in each bin [159].

yield distribution would be $\sim$8% based upon I^4 scaling. The mean of the distribution agrees with I^4 scaling predictions by Lee (6.7×10^7); hence, there is clearly more physics that influences the shot-to-shot variation in neutron output for a fixed current. The mean pinch voltage was 27 $\pm$ 4 kV for these shots. Previously reported values for neutron yield variation (discussed earlier in this paper) were as low as $\pm$21% in DT at a similar current level [154].

The neutron yield is most correlated with pinch voltage (V_{pinch}) for a fixed peak current. The trend is shown in Fig. 30. The measurement threshold is 7.5×10^5 neutrons/shot in the configuration used in this experiment. To get a picture of the trend, the data were grouped into 1-kV bins in pinch voltage. The average of each voltage bin is shown as a black triangle in the figure. The error bars are the 1σ standard deviation in each 1-kV bin. The trend of the mean is increasing neutron yield with increasing pinch voltage.

The previous sections have presented a selected survey of the diverse aspects of DPFs. This paper began by describing the historical evolution of the understanding of DPF physics by summarizing measurements of the three phases of the DPF discharge. Applications of DPFs were also surveyed. Unlike its fast Z-pinch counterparts, the DPF has found many applications. Some of these applications demand rep-rated operation that has spurred innovation in pulsed power modulators and in DPF head design. The following section returns to a discussion of the physics of neutron production in DPFs, as prelude to an

assessment of scaling laws and a comparison of DPF pinches with fast Z-pinches.

V. Scaling Laws and Design Criteria

When discussing scaling laws for DPFs, there are many ways in which to address the problem. First, consider the problem as an electrical circuit, in which a capacitor along with a static inductance L_o drives a dynamical inductance that consists of two phases: the coaxial run-down phase followed by the radial implosion phase. The static inductance L_o plays a role during the coaxial phase. This was first discussed by Trunk in 1975 [41]. Trunk presented a numerical analysis of two DPFs built at the Stuttgart Plasma Institute. These devices were designed from the beginning in such a way as to permit variations of the power supply circuit and the discharge geometry. The two installations were called "MINIFOCUS" and "NESSI." The main characteristics of the focus discharge (formation of a shock wave with constant propagation velocity in the axial phase, rapid collapse to form a hot and dense pinch in the radial compression phase) had been already described in detail by Potter in 1971 [55], [56]. Potter recognized that the governing equations of the problem of coaxial acceleration and radial compression in a DPF are inherently nonlinear, and the problem is at least 2-D. This necessitates numerical methods of solution. Potter was able to theoretically describe the focus discharge up to the pinch phase. His results were compared with the experiments by Morgan *et al.* [83], who showed reasonable agreement with the plasma data.

The work of Trunk is interesting as it is the earliest attempt to establish design criteria for DPFs by analyzing two different devices (MINIFOCUS and NESSI) over a wide range of parameters and, by so doing, to extract some of the salient physics. For example, Trunk considered how variation of the static bank inductance L_o might affect the peak current. At that time, it was already well established by data that the neutron output roughly scaled as I^4 in Mather-type DPFs. Trunk conducted numerical studies of the two DPF devices at Stuttgart and examined the effect of varying the external inductance (outside the vacuum) on the current.

Consider what happens as the static inductance L_o is varied for a fixed $dL_{\rm coax}/dt$ impedance. The moving current sheet has inertia, i.e., it lifts off the insulator slowly and accelerates only after a certain delay after breakdown. If L_o is too low, the current rapidly rises before the sheet begins to move, the sheet is accelerated by a high value of current, and the high-impedance $dL_{\rm coax}/dz$ damps the current. The peak is reached before the sheet reaches the end of the anode, and the pinch phase is driven by a lower current than the peak current. In such cases, scaling neutron output with peak current would show an apparent change in the scaling exponent of neutron output with current that is but an artifact of improper driver design. On the other hand, if L_o is too large, the rate of rise of current is slow, and that allows the sheet to accelerate while keeping the current high (peak reached at the end of the anode), but the magnitude of that peak current is lower due to the higher value of L_o. There is obviously a value of L_0 relative to $L_{\rm coax}$ that keeps the current from dipping before the sheet has reached the end of the anode, while maximizing its value. For the specific case of the NESSI design, Trunk estimates that this value of L_0 is 20 nH, which is around 50%–70% of $L_{\rm coax}$.

However, Trunk did not take into account a constraint on these solutions that is imposed by a fixed value for the axial velocity during the run-down phase. The so-called drive parameter defined by Lee and Serban [38] suggests a value of $\sim$100 km/s for the peak axial velocity. The works of Lee [8], [42] and Lee and Saw [43], [44] have more recently provided a more comprehensive picture of the constrained nature of this problem and how the constraints help determine optimal circuit parameters.

Lee pointed out that once we set the axial speed as a constant around 100 km/s for an optimized DPF, it follows that the impedance due to the changing coaxial inductance $dL_{\rm coax}/dt$ is also a constant. Another way to see this is that if the sheet reaches a constant velocity along the coaxial tube, $dL_{\rm coax}/dt$ is equivalent (to within a scale factor) to $dL_{\rm coax}/dz$. For a velocity of 100 km/s and typical cathode and anode radii of 2 and 4 cm, respectively, the impedance dL/dt is $\approx$14 mΩ. Due to the logarithmic dependence of $L_{\rm coax}$ on cathode and anode radii, for all practical Mather-type DPFs, the coaxial impedance is on the order of 10 mΩ.

Lee considered the problem of scaling DPFs to very high currents (stored energy) so as to produce neutron outputs that might be useful for material damage studies of the first wall of a burning fusion reactor such as ITER or its more practical successor, i.e., DEMO. Lee provides a theoretical study of why earlier DPF experiments showed an apparent maximum or saturation of neutron production and how this could be overcome. Using his 1-D Microsoft Excel macro, he shows that if capacitor banks are just built larger, with more capacitance, with longer and longer pulses, DPF electrodes will also get longer. This, in turn, increases the coaxial inductance. Eventually, a multimegajoule bank would have such a low value of L_o that the current would peak before the sheet reaches the anode tip, and neutron output would be lower than predicted for the peak current. The dynamical inductance of the coaxial section (that is roughly a constant for all foci) makes it impossible to increase peak current beyond around 4 MA, even with huge capacitor banks of 45 MJ or more. Lee's proposed solution to this dilemma is to use capacitors operating at higher voltages. This can increase peak current without increasing pulse length. Lee suggests a change in scaling criterion to scaling with pinch current rather than peak current in such cases. A 300-kV Marx-bank-driven DPF was described in 1986 by Decker *et al.* [160].

The notion of optimal energy or power transfer from the driver to the load is more relevant to situations in which the radiated output is a large fraction of the electrical energy input: for example, in high-current Z-pinches that are optimized for Ne or Ar K-shell emission. In those cases, maximizing energy (or power transfer) from driver to imploding load is a useful exercise. However, for neutron production from plasma foci or fast radial Z-pinches, maximum power (or energy) is not as relevant an optimization parameter, as shown by Lee [8], [42]. Consider a $\sim$MJ focus that emits $\sim 10^{13}$ (d,d) neutrons. The total energy in the neutron burst is 4 J. The energy in neutrons is such a negligible fraction of the stored energy that it is irrelevant

how well the stored energy is coupled into the implosion in this case. As the neutron output increases further, such criteria might become more important. For most practical focus neutron sources in operation today, the more relevant consideration is not power or energy transfer from the driver to the load per se but the question of how to maximize the processes that drive fusion, either beam-target or thermal.

Next, consider the radial pinch phase. The radial phase rapidly occurs relative to the quarter-period of the bank. When the sheet reaches the anode tip, if the capacitor bank voltage has dipped to a low value, a large fraction of the electrostatic energy initially stored in the capacitors has been converted to magnetic energy in the external inductance L_o and coaxial inductance $L_{\rm coax}$. The radial implosion extracts some of this magnetic energy by reducing the current. However, because of the finite interval of the pinch, only a fraction of this "storage" inductance can be "seen" by the pinch. The energy extracted by the pinch is "local" to the pinch, i.e., the capacitor bank plays a negligible role during the pinch phase. To see this, consider that the timescale for the extraction of energy by the pinch is $\tau = L/\langle Z\rangle$, where $\langle Z\rangle$ is the net impedance of the dynamical pinch (the sum of its dL/dt and/or anomalous resistance). Given the lifetime of the pinch ($\sim$50–80 ns) and its typical impedance (due to pinch dL/dt and/or anomalous resistance) of $\sim 0.25-0.35\ \Omega$ (see Fig. 27), the inductance "seen" by the pinch is in the range of $\sim$12–35 nH. The pinch inductance itself is $\sim$5 nH/cm (for a compression ratio of $\sim 10:1$). A 3–5-cm-long pinch would create an inductance of $\sim$15–20 nH. This inductance is on the order of the inductance that the pinch can "see" during the finite pinch interval. Thus, the pinch can "see" only a small portion ($\sim$10–15 nH) of the inductance upstream of itself, along the coaxial electrodes. Most of the stored magnetic energy would be extracted by the pinch after it begins to expand outward at later times. An efficient driver would thus keep the coaxial inductance to values $\sim$20 nH or lower, depending, of course, on satisfying the criterion of accelerating the sheath to the Alfven speed of $\sim$100 km/s in the coaxial region. From the standpoint of the pinch, it would appear that any inductance outside the vacuum in a Mather DPF is wasteful inductance as it stores energy that cannot be tapped by the pinch. From the standpoint of efficient coupling between the driver and the coaxial section, the value of L_o should be neither too high nor too low, as shown by Lee. The systematic iterations considered by Lee and Saw [8], [42]–[44] put these considerations on a useful and practical footing for existing and possible future DPF sources up to the 25-MJ level.

The next optimization to consider is the ratio of $I_{\rm pinch}/I_{\rm peak}$. This question is subtle and dependent upon the microscale physics at play. Lee *et al.* [8], [42]–[44] used numerical experiments optimizing every case considered over a range of energy to obtain the scaling relationships, i.e.,

$$Y_n = 3.2\times 10^{11} I_p^{4.5}$$
$$Y_n = 1.8\times 10^{10} I_{\rm peak}^{3.8}.$$

All gross physical aspects of the interactions of the various components are included in the formulation of the code. For example, if the impedance $d(LI)/dt$ is high, that drives a high voltage along the pinch with an attendant hard ion spectrum that can efficiently drive fusion even in a relatively low temperature plasma. However, suppose that the high dL/dt arises from the formation of a tight pinch (high compression ratio), then $I_{\rm pinch}$ would be low, and the density of the target plasma (from the Bennett relation) would be low and, hence, could reduce the neutron output. On the other hand, if the pinch current is high (to support a high target plasma density), the voltage generated might be low, leading to a softer ion spectrum and reduced fusion. There could be an optimum pinch current that strikes a compromise between generating a hard ion spectrum and providing enough target areal mass to stop the fast ions and drive fusion. The optimum fraction is dependent upon the particular reaction of interest. DD versus DT fusion would require different optima as the cross sections are very different around 50–100 keV. This is why scaling of neutron output with $I_{\rm pinch}$ is better motivated than with $I_{\rm peak}$, particularly for high-current DPFs. However, even this scaling is to be tempered with the realization that for the same $I_{\rm pinch}$, one could get very different ion spectra, as those spectra would depend on the path taken by the implosion to reach $I_{\rm pinch}$. In other words, an implosion could reach the same $I_{\rm pinch}$ but generate very different voltages in the pinch (due to different dI/dt) and hence different ion spectra, leading to widely different neutron outputs. A recent paper by Bures and Krishnan [14] addresses this point and offers a revised scaling law for neutron production. (More on this will be discussed in the following section.)

We turn now to a brief discussion of scaling of these phenomena to high currents. The design of a DPF is constrained by physical criteria. The coaxial section must be designed so that the terminal speed of the sheet reaches around 100 km/s (the Alfven speed) for the given pressure, current, and anode radius (Lee and Serban [38]). The anode radius is constrained by practical considerations such as cooling (if rep-rated operation is desired) or material damage at high currents. The linear current density around the periphery of the anode is a limiting factor at $\gg$ MA currents. Pressure is also constrained by breakdown physics. It is no accident that most DPFs operate in the vicinity of 1–30 torr. Lower pressures would create volume breakdown (glow discharge) and prevent a coherent sheet from driving a shock. Too high a pressure creates filaments (spokes) in the gas that would leave unionized gas behind, leading to restrikes and poor pinches. A few attempts at active preionization (using alpha or beta particles) were mentioned earlier. In the future, perhaps better preionization might allow higher pressure operation of high-current DPFs. If the pressure is constrained to be in the range 1–100 torr, the optimum drive parameter (~ 90 kA/cm $\cdot$ torr$^{0.5}$ in Lee's units) sets the range of the anode radius for a given current. The anode radius (with a fixed gap between electrodes) sets the inductance/unit length of the coaxial section. An optimum drive bank inductance L_o would allow the current to peak when the sheet reaches the end of the anode, while ensuring that the velocity is $\sim$100 km/s, hence an optimum anode length. The coaxial impedance sets the drive voltage required, which uniquely determines the bank capacitance.

As an example of such parametric optimization, Lee and Saw [43], [44] argued that scaling up from a 1-MA capacitor bank

requires close to 19 MJ to reach a target D–D neutron yield of 10^{13} per pulse. However, their numerical experiments found that a modern bank with typical lower damping may achieve the same target D–D neutron yield at 8 MJ when operating at a typical voltage of 35 kV. The energy requirement is further reduced to 3 MJ by increasing the operational voltage to 90 kV. Because the effective beam energy is already high at 90 kV, there is little advantage in operating at voltages above 90 kV for the D–D neutron yield. By Lee's ansatz, the computed effective beam energy [42] for 90 kV is ~330 keV. Above 300 keV, the rise in the D–D fusion cross section is slow. Lee pointed out that there is little advantage to operating a DPF above 90 kV. For DT fusion, the situation is worse, as the D–T fusion cross section [161] has already peaked at 120 keV, in which case a bank voltage of 40 kV might suffice.

Decker *et al.* [162] were among the first to realize that the dynamical impedance of the moving current sheet in a PF constrains the driver to be a high-impedance driver to keep the current at its peak value as the sheet reaches the end of the anode. To allow a megaampere-level focus to be efficiently driven, they designed and built the SPEED2 driver that operated at up to 300 kV. Decker *et al.* showed that the higher voltage bank gave higher neutron output for the same stored energy, as expected from impedance considerations.

VI. Future Prospects

The history of the DPF began in the 1960s and showed rapid progress within a decade. Since then, DPF research has kept pace with other Z-pinch developments, although the fast Z-pinch has raced ahead in peak current. DPFs were scaled to the 2-MA level as early as 1974 [163], but since then, no further scaling has been reported. The Z accelerator at Sandia National Laboratory (SNL) [11] tests 100-ns implosions of wire arrays and gas puffs at the 20-MA level.

The oft-quoted I^4 scaling is derived here from basic considerations. First, consider a simple model of a uniform pinched plasma of mean deuteron density N and temperature T confined to a volume V for time t_c. The yield Y is estimated from

$$Y \alpha N^2 V (\sigma v)_{\rm av} t_c \tag{1}$$

$$t_c = r/v \tag{2}$$

where r is the final radius of the pinch, v is the thermal speed of ions in the collapsed thermalized plasma, and $(\sigma v)_{\rm av}$ $({\rm cm}^3/{\rm s})$ is the thermally averaged reaction rate. According to Lee [38], the final pinch radius r and the length of the plasma scale with the anode radius a of the PF for properly chosen length of the anode stub. From the snowplow model of pinch formation, we also have

$$\mu \frac{a^2}{\tau^2} = \mu \nu^2 \propto I^2 \tag{3}$$

where μ, which is the initial mass loading per unit length of the deuterium gas, is assumed proportional to the mass per unit length of pinched plasma at maximum compression, and τ is the time to reach peak current I. Assuming a fixed compression ratio, i.e., a/r, we obtain

$$Y \propto (Na^2)^2 (\sigma v)_{\rm av}/\nu \propto \mu^2 (\sigma \nu)_{\rm av}/\nu \tag{4}$$

$$Y \propto \mu^2 f\left(\frac{I}{\mu^{1/2}}\right) \propto \mu^2 f(\nu) \tag{5}$$

where

$$f(\nu) = (\sigma v)_{\rm av}/\nu. \tag{6}$$

In the energy range near 1 keV, typical of DPF pinches, the cross section increases, roughly speaking, with the fourth power of temperature T or the eighth power of speed v. Thus, in this range

$$Y \propto I^8/\mu^2. \tag{7}$$

The drive (also called speed) parameter defined by Lee and Serban [38] is directly a measure of the speed of electromagnetically driven current sheets. The square of this parameter is therefore energy density per unit mass. Lee and Serban [38] showed that almost all optimized DPFs over a wide energy (current) range have a relatively constant axial speed of ~100 km/s. Hence, for a fixed compression ratio and fixed D, μ^2 scales as I^4. Thus

$$Y \propto I^4. \tag{8}$$

For nonthermal ions, N^2 in (1) is replaced by the product $N_b^* N_p$ (where N_b is the beam ion density, and N_p is the plasma ion density), and the velocity-averaged cross section $\langle \sigma v \rangle_b$ will be different from that for the thermal plasma at 1 keV. The observed scaling of Y with I^4 even in nonthermal neutron production implies a certain functional dependence of the fast ion beam component on pinch current. For the nonthermal case, we may rewrite the equations as

$$Y \alpha N_b N_p V < \sigma v >_{\rm av}^b t_c \tag{9}$$

$$t_c = r/v \tag{10}$$

where $\langle \sigma v \rangle_{\rm av}^b$ has the superscript b to indicate that the velocity-averaged cross section in this case is for an energetic ion beam and not for a thermal ion plasma. The confinement time is still on the order of the pinch radius divided by the ion sound speed. We do not know how the runaway ion beam current is related to the main current. However, the main current is related to the plasma density via the Bennett relation (and pinch radius that scales as "b" for a fixed compression ratio). If the beam current is some fraction of the pinch current, it follows that the beam ion density also scales with plasma density but in an as yet unknown manner that depends upon the specifics of the instabilities that drive the ion beam formation. In the case of the runaway ion beams, their mean energy is around 50–100 keV in most of the lower current (< 1 MA) DPFs studied to date. Depending upon the spread around this mean, the velocity-averaged cross section $\langle \sigma v \rangle_{\rm av}^b$ will have different values but will

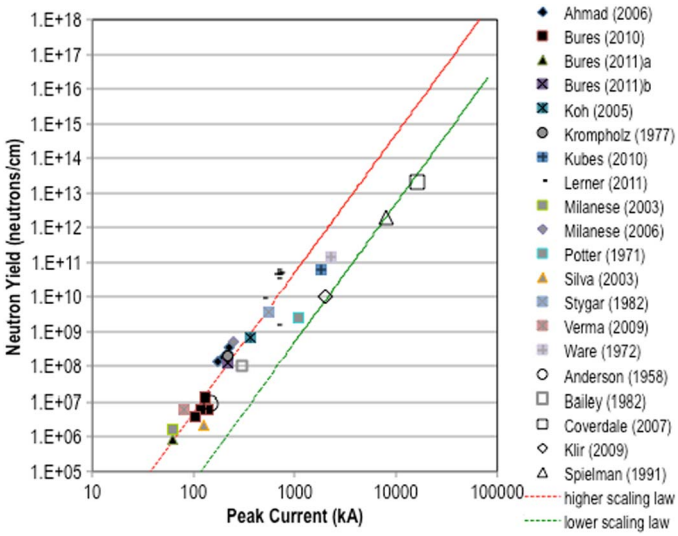

Fig. 31. Universal plot of neutron output/cm versus peak current for DPFs and fast Z-pinches [14].

not explicitly depend upon the plasma temperature, as was the case for a thermal bath. For this case, (9) reduces to

$$Y \propto \mu^2 \langle \sigma v \rangle_{\rm av}^b / \nu. \tag{11}$$

Given that $\langle \sigma v \rangle_{\rm av}^b$ is a number that depends upon the specific beam energy and spectral width and that, as before, we invoke the criterion that the ion sound speed is roughly constant ($\sim$1-keV cold pinch plasma), the yield scales as

$$Y \propto I^4. \tag{12}$$

Hence, the I^4 scaling is consistent with both a thermal plasma at $\sim$1 keV or a beam-target plasma in which the beam density (current) scales with pinch density (current). However, what is the numerical scale factor for the scaling law that gives absolute neutron outputs? Bures and Krishnan [14] have addressed this issue in a recent publication. They showed a universal plot of measured neutron output from DPFs and fast Z-pinches over a wide range of currents. Several others have presented similar plots, but these authors plot the neutron output/unit length, which allows better comparison of DPFs (that tend to make long pinches, i.e., $\sim$1–10 cm) with fast Z-pinches that tend to be restricted to lengths $<$ 2–3 cm. Fig. 31 shows such a plot.

The two straight lines are I^4 power laws. The data fall into two groups: The lower energy ($<$ 300-kA current) outputs lie on the higher of the two scaling lines, whereas the higher energy machines ($>$ 1-MA current) tend to rolloff on to the lower of the two lines. There is a factor of 100 difference between the two scaling lines and poses the question: Is the transition from higher to lower scaling a consequence of the higher current or is it due to nonoptimal design of the pinches? With reference to (12), the absolute yield may be written as

$$Y = \alpha I^4 \tag{13}$$

where the scale factor a is dependent upon the details of the plasma and beam physics in the pinch. Neutrons are produced in the reaction

$$\mathrm{D} + \mathrm{D} \rightarrow \mathrm{He}^3(0.82\ \mathrm{MeV}) + n(2.45\ \mathrm{MeV})\ \text{neutron branch}. \tag{14}$$

For a thermal pinch, the laboratory energy of the deuterons involved in this reaction amounts to only a few kilovolts; hence, the difference between the laboratory and center-of-mass energies given in parentheses is negligible. However, that is not the case for beam-target fusion. The branching ratio between the neutron branch and the proton branch

$$\mathrm{D} + \mathrm{D} \rightarrow \mathrm{H}^3(1.01\ \mathrm{MeV}) + \mathrm{H}(3.02\ \mathrm{MeV})\ \text{proton branch} \tag{15}$$

is about one half [164].

For deuteron energies below 13 keV, the total reaction cross section at laboratory energy E (keV) is

$$\sigma = \frac{182}{E} e^{\frac{-44.24}{\sqrt{E}}}\ \text{barns} \tag{16}$$

and for energies between 10 and 100 keV, it is

$$\sigma = \frac{288}{E} e^{\frac{-45.8}{\sqrt{E}}}\ \text{barns}. \tag{17}$$

The total reaction rate averaged over a Maxwellian spectrum at temperature T (keV) is

$$(\sigma v)_{\rm av} = \frac{2.33x10^{-14}}{T^{2/3}} e^{\frac{-18.76}{T^{1/3}}}\ \mathrm{cm}^3/\mathrm{s}. \tag{18}$$

The former cross sections may be used for any spectrum of deuterons that may be generated in the pinch, to estimate the reaction rate if the deuterons are thermalized at the temperature of the pinch. Given the deuteron density n and assuming thermalized deuterons, the neutron production rate per unit volume is

$$R = \frac{1}{4} n^2 (\sigma v)_{\rm av}. \tag{19}$$

Here, one factor of one half comes from the branching ratio, the other from the fact that the incident particles in the reaction are identical. Fig. 32 shows the neutron production rate as a function of temperature in a pinch with a radius of 3 mm, a length $L = 1$ cm, and a mean deuteron density of 10^{18} cm^{-3}. (These parameters are consistent with a Bennett pinch at 300-kA pinch current.) For a 100-ns pinch lifetime and 1–2 keV, Fig. 32 gives an estimate of 10^6–10^7 neutrons/cm. However, there are several published reports of neutron output from 220–300-kA Z-pinches that are in the range of 10^8–5×10^8 neutrons/cm [138], [159]. It is obvious that thermal fusion is not at play in such pinches.

Denoting the current carried by nonthermal deuterons by I_b, the neutron production rate in nonthermal processes between the accelerated deuterons and the much colder background deuterons of density n is

$$R_n = 0.5 n \sigma(\varepsilon^*) I_b \frac{L}{e} \tag{20}$$

where ε^* is the runaway ion beam mean energy, and e is 1.6×10^{-19} coulomb. Assuming that 10% of the pinch current is carried by the fast deuterons at 100 keV, this yields a rate of

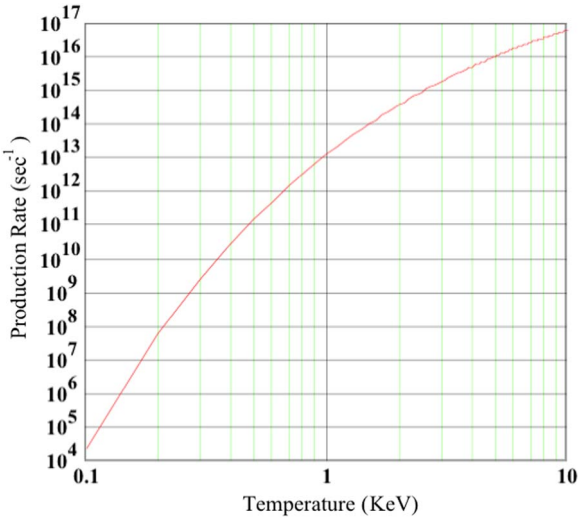

Fig. 32. Neutron production rate versus temperature in a thermal pinch.

3×10^{15}/s, which is much higher than the thermal production rate at T = 1 keV but comparable to that at T = 5 keV. A 50–100-ns pinch would radiate $1.5 \times 10^{8}-3 \times 10^{8}$ neutrons/cm, consistent with the measurements.

This assumption of 10% of the pinch current appearing as a beam current is consistent with measurements presented by Kubes *et al.* [62] and, much earlier, by Gullickson and Sahlin [163]. The work by Kubes *et al.* used sophisticated interferometric density measurements to reveal the existence of various phases in the neutron emission of the PF-1000 PF: an initial compression to a minimum diameter of about 15 mm, followed by a quiescent slightly expanded phase (25 mm in diameter), an instability phase, and finally, a decay of the dense plasma structures. Maximum densities were reported in the range of 10^{19} cm^{-3}. The double peaked structure of the neutron time history coincides with a) compression to a minimum diameter and b) late-time instabilities. The estimated fraction of thermonuclear neutron production—in contrast to the beam-target mechanism—amounted, in both neutron pulses analyzed, to less than 5%.

The origin of such a 30-kA runaway ion beam in a 300-kA pinch is the key to understanding why there is so much scatter in the data in Fig. 31 from [14]. For a fixed pinch current, the ion beam current might vary from shot to shot depending upon the details of how the $m = 0$ necks are formed and how the accelerated ions are scattered and slowed down by the inhomogeneous pinch before they leave the active volume. Then too, even if the ion beam current is fixed, the mean energy (spectrum) of those ions might vary depending upon the voltage generated by the $m = 0$ necks or other instabilities that drive the ion beam. Then, the cross section would vary and hence the reaction rate. With reference to Table II [159], the estimated pinch voltage variation was 27 ± 4 kV, which is a 15% variation in mean voltage. If the ion beam energy also varied by 15%, the cross section would vary by about 54% between 27 and 31 keV. This is surprisingly close to the ±55% variation in neutron output reported by Bures *et al.* [159]. On the other hand, the result is not inconsistent with the small (±2%) variation in peak current observed in those data. If the pinch voltage shows wider variation, the neutron output could be more variable. For example, between 30 and 100 keV, the (d,d) fusion cross section varies by a factor of 14. Such stochastic variation in beam-target neutron output is also the reason for the wide range of measured neutron outputs with peak current reported in [14].

Bures and Krishnan [14] have analyzed data from 12 000 shots to demonstrate this very point. The data from 12 000 pulses analyzed from eight different Z-pinches presented in that paper show that the neutron yield varies by as much as ±15 000% about the best fit value of the conventional I^4 scaling model. A revised scaling model derived from the reaction rate equation and a circuit model that includes the time derivative of the current dI/dt (normalized to its initial value) reduces the scatter in data from ±15 000% to ±100%. For the special case of very high normalized dI/dt, the standard deviation between the revised scaling prediction and measured neutron yields is reduced to just ±30%. Bures and Krishnan offer a revised scaling law, i.e.,

$$\frac{Y_n}{l_{\text{pinch}}} = \left(\beta \left| \frac{\frac{dI}{dt}\big|_{\min}}{\frac{dI}{dt}\big|_{\max}} \right| + \gamma \right) I_{\max}^{\delta}. \tag{21}$$

The neutron yield is Y_n; l_{pinch} is the pinch length; $I_{\max}$ is the peak current; $dI/dt|_{\min}$ is the minimum of the time derivative of the current; $dI/dt|_{\max}$ is the maximum of the time derivative of the current; and β, γ, and δ are fitting parameters. While derived from the reaction rate equation and circuit equation, the fitting parameters β, γ, and δ are adjusted to provide the best fit model to the experimental data.

Although the introduction of dI/dt_{ratio} in [14] improves the accuracy of the scaling model, a physical link between dI/dt_{ratio} and the microscopic processes inside the pinch awaits further analysis and measurements. It was previously shown that the pinch voltage correlated with the neutron yield on AASC's PF-3 device [159]. The basic physical picture is as follows: Higher dI/dt implies higher voltage across the pinch. The higher voltage is an integral of the electric field over the pinch volume. Higher voltage implies higher mean ion energy. If the ion distribution follows a power law (as mentioned earlier), the higher dI/dt pinches produce fast ions with higher mean energy. The higher dI/dt is also consistent with tighter pinches and hence higher density. The higher target density confines the hot ions better, and hence, more hot ions remain in the pinch volume to interact for longer with the static target ions, and more neutrons are produced. This is a plausible scenario for why [14] found such a remarkable improvement in the correlation of neutron yield with current when dI/dt was included in the scaling law. Bures and Krishnan provide intuition about why they chose this linear function of dI/dt as follows: It is observed that the peak current governs only the average (global) pinch plasma density via a Bennett equilibrium when the pinch temperature and radius are known. However, pinches (both from plasma foci and fast radial implosions) exhibit structure such as $m = 0$ necks and other instabilities. These dynamic structures cause dynamical changes to the pinch voltage (V_p) that are, in turn, related to the time derivative of the current dI/dt. The pinch voltage is the source term for the ion spectrum (either thermal or nonthermal) that determines the neutron

TABLE III
PARAMETERS FOR 300-kA AND 10-MA DPF DESIGNS (SEE TEXT)

		I (kA)	300	
rho (Torr)	a (cm)	B (T)	n (/cc)	Lpinch (nH)
10	1.1	20	1E+18	4.6
		I (kA)	10000	
rho (Torr)	a (cm)	B (T)	n (/cc)	Lpinch (nH)
100	10.0	50	9.0E+18	43

TABLE IV
PARAMETERS FOR 300-kA AND 10-MA DPF DESIGNS (SEE TEXT)

		I (kA)	300	
	Maxwellian	fast ions (50keV)	fast ions (100keV)	
rho (Torr)	i-i t_{th}, ns	i-i t_b, ns	i-i t_b, ns	$(w*t)_{ion}$
10	157	153	386	153
		I (kA)	10000	
100	17.3	21	51	42

output. They pick experimentally motivated power laws for the nonthermal ion energy distribution and show that the fusion rate is linearly proportional to the mean ion energy, which is, in turn, proportional to the mean pinch voltage. Hence, it seems reasonable that one should include a linear function of dI/dt in the scaling relationship as that is connected to the neutron production rate via the complex microphysics inside the pinch.

This begs the question: Why is the neutron output from the higher current pinches (DPFs or fast Z-pinches) tending toward the lower scaling line? One possible reason is that the higher current pinches have higher density and, hence, damp the fast ion spectrum to lower mean energy and, hence, reduce the reaction rates. However, another possibility is that the absolute pinch voltage might be so high in higher current pinches that fast ions escape the pinch altogether. For example, if a 10-MA pinch has an impedance of 0.3 Ω, the mean voltage might be as high as 3 MV, but that does not necessarily imply a hot ion spectrum centered around 3 MeV. To get an idea of the ion–ion thermalization and neutron production processes in DPFs, we consider two designs: a 300-kA DPF and a 10-MA DPF.

Table III summarizes a few useful numbers for the two designs.

The pressures selected were 5 torr for the 300-kA DPF and 100 torr for the 10-MA DPF. First, the Lee drive parameter (equivalent to an axial speed of 100 km/s) gives the anode radii as 1.5 and 10 cm, respectively. For a fixed compression ratio of 5 : 1, the B-fields are calculated as 23 and 80 T. From the Bennett condition, the pinch density is 1×10^{17} cm^{-3} for the 300-kA design and 9×10^{18} cm^{-3} for the 10-MA pinch. Here, we have assumed that the pinch current is 70% of the peak at 300 kA and 54% of the peak at 10 MA for reasons that will be obvious shortly. Recall that we had used the density of 10^{18} cm^{-3} and the radius of 3 mm earlier to estimate a thermal neutron production rate of 10^{13} s^{-1} in the 300-kA pinch. The beam-target rate was 3×10^{15} s^{-1}, based on 50-keV ions in the beam and a current of 30 kA. The assumed pinch radius of 3 mm implies a compression ratio (anode radius/pinch radius) of 5 : 1, consistent with our assumption. This ratio gives a pinch inductance of 4.4 nH for the 300-kA design. By the circuit analysis arguments presented earlier, an optimum coaxial inductance might be $\approx$6 nH with a driver inductance L_o of $\approx$4 nH. The ratio $I_{\rm pinch}/I_{\rm peak}$ (by flux conservation) would be $\approx$69%. This is why we used 70% of 300 kA as pinch current to estimate the density.

Using the same compression ratio for the 10-MA pinch, the inductance is 43 nH in that case. The optimum coaxial inductance (25-cm-long anode with a 10-cm gap) might be $\approx$30 nH, with external $L_o \approx 20$ nH. The ratio $I_{\rm pinch}/I_{\rm peak}$ would now be $\approx$54%. Hence, we used 50% of the 10 MA flowing in the pinch to deduce a density of 9×10^{18} cm^{-3}. This higher density makes the "thermal" neutron production rate roughly 100$\times$ higher for the 10-MA pinch [see (19)] than for the 300-kA pinch. We have assumed a 1-keV plasma temperature in either case. Next, we estimate ion–ion energy exchange collision times for the thermal (Maxwellian) plasma at 1 keV and for beam-target slowing down of ions at 50 and 100 keV. Table IV shows the results.

The Maxwellian thermalization time (ion–ion) in the 300-kA pinch is 157 ns, on the order of the pinch lifetime $\sim$50–100 ns. The ion–ion slowing down time for runaway 50/100-keV ions is similarly long. What this means is that the 300-kA pinch is not in thermal equilibrium, and the notion of an ion temperature is questionable. The ions are accelerated to 250–300 km/s as they arrive near the axis, which is a mean deuteron energy of 640–920 eV. However, the finite lifetime of the pinch prevents the ions from fully thermalizing and creating a Maxwellian energy distribution in this case. When instabilities create high electric fields near the axis, runaway ions are produced that suffer only a few energy exchanging collisions before they leave the pinch. The gyro radius of the ions is small, and the product $\omega * \tau$ is $\gg 1$, as noted in the last column of Table IV. This means that the ions are confined by the strong magnetic fields (except those close to the axis where they can escape) and hence execute gyro orbits that keep them in the pinch for longer than would be the case if they were simply flowing along the electric field. This confinement allows creation of a more isotropic ion velocity distribution and generation of (d,d) neutrons at various angles. The ions might scatter off electrostatic waves (micro-turbulence) and be organized into a power law spectrum more efficiently than by ion–ion collisions. The high values of $\omega * \tau$ imply that the ions will gyrate around the magnetic field, and only those that are near the axis where the field goes toward zero will escape the pinch. Beam-target fusion, therefore, proceeds at all angles around the axis, although the electric field might predominantly be along the axis. This is why there is a weak anisotropy ($< 2 : 1$) in the neutron emission observed by many.

For the 10-MA design, the Maxwellian thermalization time as well as the thermalization times for 50- and 100-keV ions are closer to the pinch lifetime. In this case, one expects a more thermal ion distribution and hence thermal processes to be more important. The 100-keV ions that are slowed down by ion–ion collisions on the 50-ns scale would become slower ions, whose slowing down timescales would be shorter and shorter, and hence, a cascading reduction in ion energy would result. Within the 100-ns lifetime, a typical 100-keV ion might be slowed down to the body of the Maxwellian ion distribution. This simple estimate provides a plausible explanation for why

Welch *et al.* [12] found that the thermal contribution to neutron output in the case of the 15-MA Z experiment with D_2 gas puffs was nearly half of the total neutron emission. By contrast, the large scale plasma simulations code calculations showed that for a lower current Z-pinch (150 kA), the neutron output was dominated by beam-target emission.

Regardless of whether the emission is thermal or beam-target, the big difference between the two scaling curves in Fig. 31 remains a puzzle. What is it about the high-current pinches (gas puffs or DPFs) that causes their output to fall onto the weaker curve? If we could make more detailed measurements of the ion spectra and, also, unravel the microscopic physics that governs those spectra, we might find ways in which to move from the lower curve toward the higher one. The factor of 100 between the two curves is tantalizing. Can the higher current pinch designs be changed to increase their yields?

It is clear that increasing the pinch voltage is desirable for higher neutron output, but only within limits. At sufficiently high voltage, the ion energy might sufficiently increase that the ions are no longer confined; the nonthermal fusion yield will decrease. If the mean ion energy scales with increasing voltage at a fixed current, this could lead to an increasing neutron rate until the ion energy exceeds the peak in the fusion cross section. In the case of DD reactions, the peak in the cross section is 2.4 MeV [161], whereas DT reactions have a peak cross section at 109 keV [161]. Measurements in a 1.8-MA PF by Kubes *et al.* show that regions of the pinch are diode-like, leading to ion acceleration and formation of a nonthermal spectrum [62]. We observe that the particle density in the pinch region increases with current [3], [19]. The magnetic field also increases with current. Both increasing particle density and magnetic field would reduce the ion's mean free path. It is not clear if the nonthermal acceleration mechanism can be sustained at the highest currents.

The other possibility is that the ions continue to accelerate to high energy allowing their mean free path (for scattering off other ions or waves) to exceed the pinch length. It is common to measure ion beams escaping the pinch region in small plasma foci. Experiments up to the 1-MA level suggest modest populations of $>$ 1-MeV ions [163]. Measurements should be made on the highest current machines to address if the fast ions are escaping the pinch or whether fast ions cannot be efficiently generated. The outcome of these measurements will determine how best to optimize the pinch for the nonthermal fusion and which fusion reaction is optimum. Fusion energy from D-T may not be practical from a nonthermal ion source with significant ion populations above 100 keV due to a reduction in fusion cross section above 109 keV [161].

The transition point from the high-yield trend line to the low-yield trend line in Fig. 31 is not known at this time under the optimum operating conditions. If the transition point is at currents such as $\sim$5 MA, net fusion gain via a simple gas puff Z-pinch may be impractical. Concepts such as MAGLIF [13] would be the only path forward for Z-pinch fusion. The potential payoff for exploring the transition is the ability to construct a higher data rate facility to study nonthermal effects in an inertially confined plasma. If the high scaling trend of the data in Fig. 31 and the revised scaling model can be realized at a few megaamperes, the present Z neutron yield on the lower scaling line can be realized at 5.5 MA on the higher scaling trend in Fig. 31. A 6-MA facility could fire several shots per day, increasing the data needed to improve models. Applications such as high-intensity pulse neutron sources could be realized in manageable facilities.

Equation (20) provides another way to look at the scaling behavior. For two currents I_2 and I_1, (20) may be rewritten as

$$\frac{R_2}{R_1} = \left(\frac{I_2}{I_1}\right)^2 \left(\frac{I_{b2}}{I_{b1}}\right) \left(\frac{r_1}{r_2}\right)^2 \left(\frac{\sigma_2}{\sigma_1}\right). \tag{22}$$

If the beam current is some fixed fraction of the pinch current, (21) shows that for I^4 scaling to hold

$$\frac{\sigma_2}{\sigma_1}\left(\frac{r_1}{r_2}\right)^2 \alpha \frac{I_2}{I_1}. \tag{23}$$

The ion beam energy depends upon the pinch voltage V_p that, in turn, depends upon dL_p/dt, which may be written as

$$V_p \alpha \frac{I_p}{r}\frac{d}{dt}(r). \tag{24}$$

Thus

$$\frac{V_2}{V_1} = \left(\frac{I_{p2}}{I_{p1}}\right)\frac{r_1}{r_2}. \tag{25}$$

How to relate the pinch voltage ratio to the ratio of cross sections in (21)? Several authors have measured (and postulated) ion spectra with a power law of the form ε^{-x}, where $2 < x < 4$. At 3-MA currents, Gullickson and Sahlin [163] and several others have shown that the tail of the ion distribution reaches out only to $\sim$1 MeV. This is consistent with a plasma impedance of 0.25 Ω and a pinch current of $\sim$1 MA that would create a pinch voltage of $\sim$250 kV. If the mean ion energy is 250 keV, the power law would show vanishing flux above 1 MeV. In addition, even if there were to be $>$ 1-MeV ions in the pinch, at density $< 10^{20}$ cm^3, such ions would not give up much of their energy to the slower ions. The runaway ions that are useful for fusion are hence in the range of 50–400 keV, with lower current pinches producing mostly 50-keV ions and the higher current machines trapping more ions (higher density) out toward 400 keV. The (d,d) fusion cross section [161] may be approximated by a straight line fit (to $\pm 2\%$) over the range 50–400 keV as

$$\sigma(\text{barn}) \approx 0.34\varepsilon(\text{MeV}). \tag{26}$$

Equation (21) is rewritten using (24) and (25) as

$$\frac{R_2}{R_1} = \left(\frac{I_2}{I_1}\right)^2 \left(\frac{I_{b2}}{I_{b1}}\right) \left(\frac{I_{p2}}{I_{p1}}\right) \left(\frac{r_1}{r_2}\right)^3. \tag{27}$$

In general, the ratio of pinch currents is equivalent to the ratio of peak currents to within a factor of 2 for practical pinches. This is because the pinch current is mostly within the range of 0.8–0.4 of the peak current. A much lower value will cause neutron emission to die because there is no confining current to hold the pinch at an adequate density. A much higher value will render the voltage generated too low to be useful. If the

ratio of beam currents is similarly constrained (this is unknown at present) to a factor of 2, I^4 scaling will hold only in the special case that $r_1 \approx r_2$. The crux of the problem of scaling DPFs to higher currents is in this requirement. There are only two ways to meet this requirement: either the pressure must be quadratically increased with current (for a fixed compression ratio) or the compression ratio must be linearly increased with current. A glance at the literature reveals that this has not been the case in experiments conducted thus far. For example, a 300-kA DPF operates well at about 10 torr. A 1-MA DPF would demand about 111 torr with a fixed compression ratio to use the same anode radius and, hence, give the same pinch radius and satisfy I^4 scaling. However, at the same pressure, the higher current DPF would demand an anode radius that is three times larger and, hence (for a fixed compression ratio), would reduce the neutron rate by a factor of 81. Depending upon the beam current and pinch current ratios, this factor of 81 could be reduced or increased. The PF-1000 experiments ($\sim$1-MA pinch current) were conducted at pressures of $\sim$few torr and a large anode 23 cm in diameter (versus typical 3-cm diameter) for 300-kA DPFs such as NX2 [148] or DPF-3 [159]. It is easy to see why the neutron outputs measured on PF-1000 deviated from the higher scaling line in the figure and rolled off toward the lower one that is 100$\times$ weaker. The recent work of Lerner *et al.* [24] used a smaller anode at much higher pressure, and so, it is no surprise that his neutron outputs are higher than those measured on PF-1000. Lerner *et al.* (22) reported 4.6×10^{10} neutrons/cm at 675 kA, whereas Klir *et al.* [72] reported 1×10^{10} neutrons/cm at 2 MA. I^4 scaling would have predicted 8×10^{11} neutrons/cm at 2 MA, which is a factor of 80 higher than the Klir measurement. This is not intended as a criticism of the excellent work of Klir *et al.* Their measurements and interpretations are a valuable addition to the DPF lore. Their intention was not to maximize neutron output (to fall on the I^4 scaling line) but rather to configure their anode and working conditions on PF-1000 to obtain the best interferometric data for their experiments. Should they have desired to maximize neutron output at $\sim$1 MA, they would have, no doubt, used smaller anodes and tried to operate at higher pressures, as suggested by the scaling laws.

The path out of the dilemma posed by the two scaling lines in [14] is clear: We must find a way to make the higher current pinches denser by increasing their compression ratio if we use larger anodes, or else, we must find a way to use smaller anodes at much higher pressures. One strategy might be to dope the D_2 with a high-Z dopant such as Kr or Xe. Work by Bures *et al.* [152] and others [151], [153] has shown that small fractions $\sim$few $\%$ of high-Z dopants increase the neutron output in DPFs. It is likely that they do this by creating denser plasma zones (driven by radiative compression of pinch spots) that are better at stopping fast ions and also give higher fusion rates. For a 10–30-MA machine, the high-Z dopant might be puffed onto the axis via a fast gas valve.

There are material limits to the use of smaller anodes at higher currents. Equally challenging are the pressure limits. No one has demonstrated coherent DPF implosions at pressures of 100–200 torr, which would be needed for $\sim$10-MA currents. However, that is what makes research challenging.

The payoff for breakthroughs in higher pressure operation (with smaller anodes) or for making tighter pinches from larger anodes is that a DPF might be scaled toward ignition. Vikhrev and Korolev [165] considered the problem of achieving a thermonuclear burn wave (a breakeven condition) in a pinch. They distinguished such a breakeven from the classical Lawson criterion, as here, we deal with nonthermal ion distributions. A plasma in which the Lawson criterion is satisfied will ignite a thermonuclear chain reaction in the system. However, thermonuclear ignition can be achieved without producing a thermal plasma that could substantially facilitate the ignition problem, according to Vikhrev. A nonthermal plasma is easier to ignite because fast ions are produced in the igniting plasma not only due to collisional heating but also by accelerating the deuterium and tritium ions to high energies in electric fields. Their distribution is inherently nonthermal. It is hence possible to produce such an ion energy distribution at which fusion reactions will proceed more intensely than in the case of a thermal ion distribution, as we saw for the 300-kA case examined earlier. Vikhrev and Korolev presented a different version of the graph reprinted from [14]. The straight line 1 of their graph is based on measured data (similar to [14]). Line 2 is an extrapolation of line 1 out to 100-MA currents. The authors scaled the d.t reaction rates required for ignition to the d.d domain and plotted a straight line 3 that corresponds to the ignition criterion in a hypothetical d.t reactor. They suggested that 10^{16} neutrons/cm (d,d) at about 30 MA might suffice. This is also the neutron output of the higher (red) line shown in the graph of Bures and Krishnan (see Fig. 31). The calculations and projections by Vikhrev and Korolev provide a strong motivation for further research to be conducted on dense Z-pinches to determine whether a 30-MA design might push ignition in DT. Z at SNL is already at 20 MA, but as a major Marx-bank-driven pulsed power facility, its shot rate is limited, and there are competing priorities for its use in research.

Dense Z-pinches are initial value problems in which the final pinch physics are sensitive to conditions at the start of the dynamical implosion. The nonlinear nature of the dynamics makes modeling challenging. To compound the difficulty, such pinches quite often exhibit 3-D structures. Most of the data displayed in Fig. 31 are reported from a few shots or, in the case of the higher current data, *a single shot*. Repeatability and reproducibility are at the heart of experimental science, but practical limitations such as experimental priority and cost force all $>$ 1-MA experiments to contend with limited data sets for comparison with models. Therefore, a system that can produce larger data sets is valuable to better understand the statistical variation in the neutron yield and the causes of this statistical variation. A $\sim$0.5-MA PF source has been operated at 0.1 Hz while producing neutrons [159]. The plasma conditions in this DPF are similar in many respects to those in higher current pinches. Yet, this source can be (and is routinely) fired about 1000 times/day. A 3-D simulation of selected shots over a wide range of operating parameters, including electrode geometry, load mass, and external magnetic fields, could be benchmarked using such a high data rate. The simulation could be subsequently used to better predict an optimal load for Z and other high-current Z-pinch devices. A DPF could be also scaled to

the 5–10-MA level at a lower cost and a higher shot rate. The energy density similarity between DPF and gas puff Z-pinches, as well as the common physics in these plasmas, makes a strong case for conducting detailed research on a DPF testbed, to point to high value experiments of a facility such as Z.

ACKNOWLEDGMENT

The author would like to thank fellow colleagues B. Bures, V. Gribkov, M. Haines, D. Klir, P. Kubes, S. Lee, D. Parks, R. Rawat, and V. Vikhrev for meaningful discussions.

REFERENCES

[1] N. V. Fillipov, T. I. Fillipova, and V. P. Vinogradov, "Dense high-temperature plasma in a non-cylindrical Z-pinch compression," *Nucl. Fusion Suppl.*, vol. 2, pp. 577–587, Jan. 1962.

[2] J. W. Mather, "Investigation of the high-energy acceleration mode in the coaxial gun," *Phys. Fluids Suppl.*, vol. 7, no. 11, pp. S28–S34, Nov. 1964.

[3] A. Bernard, P. Cloth, H. Conrads, A. Coudeville, G. Gourlain, A. Jolas, C. H. Maisonnier, and J. P. Rager, *Nuclear Instruments and Methods*. Amsterdam, The Netherlands: North Holland, 1977, pp. 191–218.

[4] G. Decker, L. Flemming, H. J. Kaeppeler, T. Oppenlander, G. Pross, P. Schilling, H. Schmidt, M. Shakatre, and M. Trunk, *Plasma Physics*. Northern Ireland, U.K.: Pergamon, 1980, pp. 245–260.

[5] A. Bernard, H. Bruzzone, P. Choi, H. Chuaqui, V. Gribkov, J. Herrera, K. Hirano, A. Krejei, S. Lee, C. Luo, F. Mezzetti, M. Sadowski, H. Schmidt, K. Ware, C. S. Wong, and V. Zoita, "Scientic status of plasma focus research," *J. Moscow Phys. Soc.*, vol. 8, no. 2, pp. 93–170, 1998.

[6] V. A. Gribkov, "Plasma and fusion science," in *Proc. 17th IAEA Tech. Meet. Res. Using Small Fusion Devices*, C. Varandas and C. Silva, Eds., Lisbon, Portugal, Oct. 22–24, 2007, pp. 51–64.

[7] L. Soto, "New trends and future perspectives on plasma focus research," *Plasma Phys. Control. Fusion*, vol. 47, no. 5A, pp. A361–A381, May 2005.

[8] S. Lee, "Current and neutron scaling for megajoule plasma focus machines," *Plasma Phys. Control. Fusion*, vol. 50, no. 10, pp. 105005-1–105005-14, Oct. 2008.

[9] J. Tendys, "Internal report of Australian Atomic energy commission," Res. Establishment, Lucas Heights, Australia, Rep. AAEC/E334, Jan. 1976.

[10] M. Haines, "A review of the dense Z-pinch," *Plasma Phys. Control. Fusion*, vol. 53, no. 9, pp. 093001-1–093001-168, Sep. 2011.

[11] C. Coverdale, C. Deeney, A. L. Velikovich, J. Davis, R. W. Clark, Y. K. Chong, J. Chittenden, S. Chantrenne, C. L. Ruiz, G. W. Cooper, A. J. Nelson, J. Franklin, P. D. LePell, J. P. Apruzese, J. Levine, and J. Banister, "Deuterium gas-puff Z-pinch implosions on the Z accelerator," *Phys. Plasmas*, vol. 14, no. 5, pp. 056309-1–056309-7, May 2007.

[12] R. Welch, D. V. Rose, C. Thoma, R. E. Clark, C. B. Mostrom, W. A. Stygar, and R. J. Leeper, "Kinetic simulation of thermonuclear-neutron production by a 10^7-A deuterium Z pinch," *Phys. Plasmas*, vol. 17, no. 7, pp. 072702-1–072702-11, Jul. 2010.

[13] S. A. Slutz, M. C. Herrmann, R. A. Vesey, A. B. Sefkow, D. B. Sinars, D. C. Rovang, K. J. Peterson, and M. E. Cuneo, "Pulsed-power-driven cylindrical liner implosions of laser preheated fuel magnetized with an axial field," *Phys. Plasmas*, vol. 17, no. 5, pp. 056303-1–056303-15, May 2010.

[14] B. Bures and M. Krishnan, "An alternative scaling model for neutron production in Z-pinch devices," *Phys. Plasmas*, Dec. 2012, to be published.

[15] Courtesy of D. Klir who gathered these data from the ISI Web of Knowledge database.

[16] N. V. Filippov, *Fiz. Plazmy*, vol. 9, no. 25, 1983.

[17] N. V. Filippov, *Sov. J. Plasma Phys.*, vol. 9, no. 14, 1983.

[18] J. P. Rager, L. E. Bilbao, H. A. Bruzzone, C. Gourlan, U. Guidoni, H. Kroegler, S. Podda, B. V. Robouch, and K. Steinmetz, "Experiments on neutron production phase of Frascati 1-Mj plasma focus," in *Proc. 8th Int. Conf. Plasma Phys. Control. Nucl. Fusion Res.*, Brussels, Belgium, 1980, vol. 2, pp. 209–222, Then within this link click on "past fusion energy conferences" and select STIPUB563.pdf _VOL2.pdf. [Online]. Available: http://www-naweb.iaea.org/napc/physics/FEC/FEC2008/html/index.htm

[19] M. Scholz, B. Bienkowska, I. M. Ivanova-Stanik, L. Karpinski, M. Paduch, E. Zielinska, J. Kravarik, P. Kubes, M. J. Sadowski, A. Szydlowski, and H. Schmidt, "General characteristics of fusion-neutron emission from megajoule plasma-focus facility," *Chech. J. Phys.*, vol. 56, no. Suppl. B, p. 243, 2006.

[20] M. Sholz and B. Bienkowska, *Czech. J. Phys.*, vol. 56, no. Suppl. B, p. 243, 2006.

[21] P. Kubes, D. Klir, M. Paduch, T. Pisarczyk, M. Scholz, T. Chodukowski, Z. Kalinowska, K. Rezac, J. Kravarik, J. Hitschfel, J. Kortanek, B. Bienkowska, I. Ivanova-Stanik, L. Karpinski, M. J. Sadowski, K. Tomaszewski, and E. Zielinska, "Characterization of the neutron production in the modified MA plasma focus," *IEEE Trans. Plasma Sci.*, vol. 40, no. 4, pp. 1075–1081, Apr. 2012.

[22] M. J. Sadowski and M. Scholz, *Nucleonica*, vol. 47, p. 31, 2004.

[23] S. V. Trusilo, B. Y. Guzhovski, N. G. Makeev, and V. A. Zuckerman, "Determination of neutron generation in the cells with plasma focus," *Pis'ma Zh. Éksp. Teor. Fiz.*, vol. 33, no. 3, p. 148, Feb. 1981.

[24] E. J. Lerner, S. K. Murali, and A. Haboub, "Theory and experimental program for p-B^{11} fusion with the dense plasma focus," *J. Fusion Energy*, vol. 30, no. 5, pp. 367–376, Oct. 2011.

[25] M. A. Tafreshi1, M. Farrahi, M. Lamchi, S. Goudarzi, H. Habibi, M. Memarzadeh, V. Siahpoush, E. Saeedzadeh, V. P. Vinogradov, V. I. Krauz, V. A. Krivtsov, M. A. Karakin, V. V. Myalton, and V. P. Tykshaev, "Dena, a new PF device," in *Nukleonika*, 2001, vol. 46, no. 1, pp. S85–S87.

[26] P. Cloth, H. Conrads, B. Giesen, and F. Schongen, in *Proc. 9th Symp. Fusion Technol.*, Garmisch-Partenkirchen, Germany, 1976.

[27] J. M. Koh, R. S. Rawat, A. Patran, T. Zhang, D. Wong, S. V. Springham, T. L. Tan, S. Lee, and P. Lee, "Optimization of the high pressure operation regime for enhanced neutron yield in a plasma focus device," *Plasma Sources Sci. Technol.*, vol. 14, no. 1, pp. 12–18, Feb. 2005.

[28] B. L. Bures, M. Krishnan, and R. E. Madden, "Relationship between neutron yield and macroscale pinch dynamics of a 1.4-kJ plasma focus over hundreds of pulses," *IEEE Trans. Plasma Sci.*, vol. 39, no. 12, pp. 3351–3357, Dec. 2011.

[29] B. L. Bures, C. James, M. Krishnan, and R. Adler, "Application of an impedance matching transformer to a plasma focus," *Rev. Sci. Instrum.*, vol. 82, no. 10, pp. 103506-1–103506-5, Oct. 2011.

[30] N. J. Peacock, P. D. Wilcock, R. J. Speer, and P. D. Morgan, "Properties of the dense plasma produced in plasma focus," in *Proc. Phys. Contol. Nucl. Fusion Res.*, 1968, pp. 51–66.

[31] L. Bertalot, R. Deutsch, H. Herold, U. Jaeger, H. J. Kaeppeler, A. Mozer, T. Oppenlander, B. Ruckle, M. Sadowski, P. Schilling, and H. Schmidt, "Experiments on plasma focus dynamics, neutron production and ion emission," in *Proc. Plasma Phys. Control. Nucl. Fusion Res.*, 1980, pp. 177–186.

[32] K. D. Ware, "Field distortion switch for electrically driven flying plate experiments," Sci. Lab., Univ. California, Los Alamos, NM, LA-641 7-MS, 1976.

[33] K. Ware, "Initial start up conditions for DPF 6-1/2 and tuning to 50 KV–500 KJ operation with over 10^{12} neutrons/discharge in deuterium," personal communication.

[34] C. Maisonnier, F. Pecorella, J. P. Rager, M. Samuelli, C. Strangio, and A. Messina, "Comparative studies of plasma focus devices," presented at the 5th Conf. Plasma Physics Controlled Nuclear Fusion Research, IAEA, Tokyo, Japan, 1974, CN-33/E 6-2.

[35] J. S. Brzosko, B. V. Robouch, and J. Klobukowska, "A macroscopic study of the neutron, gamma- and X-ray emissivity in the Frascati plasma focus," *Fusion Technol.*, vol. 12, no. 1, pp. 71–92, 1987.

[36] H. Herold, A. Jerzykiewicz, M. Sadowski, and H. Schmidt, "Comparative analysis of large plasma focus experiments performed at IPF, Stuttgart, and IPJ, Œwierk," *Nucl. Fusion*, vol. 29, no. 8, pp. 1255–1269, Aug. 1989.

[37] S. Lee, T. Y. Tou, S. P. Moo, M. A. Elissa, A. V. Gholap, K. H. Kwek, S. Mulyodrono, A. J. Smith, Suryadi, W. Usala, and M. Zakaullah, "A simple facility for the teaching of plasma dynamics and plasma nuclear fusion," *Amer. J. Phys.*, vol. 56, no. 1, pp. 62–68, Jan. 1988.

[38] S. Lee and A. Serban, "Dimensions and lifetime of the plasma focus pinch," *IEEE Trans. Plasma Sci.*, vol. 24, no. 3, pp. 1101–1105, Jun. 1996.

[39] S. Lee, P. Lee, G. Zhang, X. Feng, V. A. Gribkov, M. Liu, A. Serban, and T. K. S. Wong, "High rep rate high performance plasma focus as

a powerful radiation source," *IEEE Trans. Plasma Sci.*, vol. 26, no. 4, pp. 1119–1126, Aug. 1998.
[40] P. Cloth and H. Conrads, "Neutronics of a dense plasma focus-an investigation of a fusion plasma," *Nucl. Sci. Eng.*, vol. 62, p. 591, 1977.
[41] M. Trunk, "Numerical parameter studies for the dense plasma focus," *Plasma Phys.*, vol. 17, no. 4, pp. 237–248, Apr. 1975.
[42] S. Lee, "Neutron yield saturation in plasma focus: A fundamental cause," *Appl. Phys. Lett.*, vol. 95, no. 15, pp. 151503-1–151503-3, Oct. 2009.
[43] S. Lee and S. H. Saw, "Neutron scaling laws from numerical experiments," *J. Fusion Energy*, vol. 27, no. 4, pp. 292–295, Dec. 2008.
[44] S. H. Saw and S. Lee. (2011, Feb.). Scaling the plasma focus for fusion energy considerations. *Int. J. Energy Res.* [Online]. *35(2)*, pp. 81–88. Available: wileyonlinelibrary.com
[45] S. V. Lebedev, D. J. Ampleford, S. N. Bland, S. C. Bott, J. P. Chittenden, J. Goyer, C. Jennings, M. G. Haines, G. N. Hall, D. A. Hammer, B. A. Palmer, S. A. Pikuz, T. A. Shelkovenko, and T. Christoudias, "Physics of wire array Z-pinch implosions: Experiments at Imperial College," *Plasma Phys. Control. Fusion*, vol. 47, no. 5A, pp. A91–A108, May 2005.
[46] S. V. Lebedev, R. Aliaga-Rossel, S. N. Bland, J. P. Chittenden, A. E. Dangor, M. G. Haines, and M. Zakaullah, "Two different modes of nested wire array Z-pinch implosions," *Phys. Rev. Lett.*, vol. 84, no. 8, pp. 1708–1711, Feb. 2000.
[47] J. Chittenden, S. V. Lebedev, C. A. Jennings, S. N. Bland, and A. Ciardi, "X-ray generation mechanisms in three-dimensional simulations of wire array Z-pinches," *Plasma Phys. Control. Fusion*, vol. 46, no. 12B, pp. B457–B476, Dec. 2004.
[48] P. Coleman, J. Thompson, M. Krishnan, and B. Bures, "An alternative concept for the structure of an x-ray emitting Z-pinch," *IEEE Trans. Plasma Sci.*, vol. 38, no. 4, p. 626, Apr. 2010.
[49] P. L. Coleman, M. Krishnan, J. R. Thompson, J. W. Banister, B. H. Failor, J. S. Levine, N. Qi, H. M. Sze, J. P. Apruzese, J. Davis, J. W. Thornhill, A. L. Velikovich, R. J. Commisso, and A. Verma, "Recent results for large diameter (12 cm) gas puff Z-pinches at peak currents of > 3 to < 6 MA," in *Proc. AIP 6th Int. Conf. Dense Z-Pinches*, J. Chittenden, Ed., Oxford, U.K., Jul. 25-28, 2005, vol. 808, pp. 163–168.
[50] J. S. Levine, J. W. Banister, B. H. Failor, N. Qi, H. M. Sze, A. L. Velikovich, R. J. Commisso, J. Davis, and D. Lojewski, "Implosion dynamics and radiative characteristics of a high yield structured gas puff load," *Phys. Plasmas*, vol. 13, no. 8, p. 082702, Aug. 2006.
[51] N. Qi, H. Sze, B. H. Failor, J. Banister, J. S. Levine, J. C. Riordan, P. Steen, P. Sincerny, and D. Lojewski, "Magnetic Rayleigh–Taylor instability mitigation in large-diameter gas puff Z-pinch implosions," *Phys. Plasmas*, vol. 15, no. 2, p. 022703, Feb. 2008.
[52] H. Sze, J. Banister, B. H. Failor, J. S. Levine, N. Qi, A. L. Velikovich, J. Davis, D. Lojewski, and P. Sincerny, "Efficient radiation production in long implosions of structured gas-puff Z pinch loads from large initial radius," *Phys. Rev. Lett.*, vol. 95, no. 10, p. 105001, Sep. 2005.
[53] K. Ware lab notes (personal communication).
[54] P. Simonen, N. M. Ghoniem, and N. H. Packan, "Pulsed flux effects on radiation damage," *J. Nucl. Mater.*, vol. 122, no. 1-3, pp. 391–401, May 1984.
[55] D. E. Potter. (1971, Sep.). Numerical studies of the plasma focus. *Phys. Fluids* [Online]. *14(9)*, pp. 1911–1925. Available: http://dx.doi.org/10.1063/1.1693700
[56] D. E. Potter, "The formation of high-density z-pinches," *Nucl. Fusion*, vol. 18, no. 6, pp. 813–823, Jun. 1978.
[57] M. M. Milanese and R. L. Moroso, "The first stages of the discharge in a low-energy dense plasma focus," *IEEE Trans. Plasma Sci.*, vol. 33, no. 5, pp. 1658–1661, Oct. 2005.
[58] W. Kies, "Power limits for dynamical pinch discharges," *Plasma Phys. Control. Fusion*, vol. 28, no. 11, pp. 1645–1657, Nov. 1986.
[59] K. H. Kwek, T. Y. Tou, and S. Lee, "Current sheath structures of the plasma focus in the run-down phase," *IEEE Trans Plasma Sci.*, vol. 18, no. 5, pp. 826–830, Oct. 1990.
[60] A. Bernard, A. Coudeville, A. Jolas, J. Launspach, and J. de Mascureau, "Experimental studies of the plasma focus and evidence for nonthermal processes," *Phys. Fluids*, vol. 18, no. 2, pp. 180–195, Feb. 1975.
[61] E. L. Ruden, "The polarity dependent effect of gyroviscosity on the flow shear stabilized Rayleigh–Taylor instability and an application to the plasma focus," *Phys. Plasmas*, vol. 11, no. 2, pp. 713–723, Feb. 2004.
[62] P. Kubes, M. Paduch, T. Pisarczyk, M. Scholz, T. Chodukowski, D. Klir, J. Kravarik, K. Rezac, I. Ivanova-Stanik, L. Karpinski, K. Tomaszewski, and E. Zielinska, "Interferometric study of pinch phase in plasma-focus discharge at the time of neutron production," *IEEE Trans. Plasma Sci.*, vol. 37, no. 11, pp. 2191–2196, Nov. 2009.
[63] F. N. Beg, M. Zakaullah, M. Nisar, and G. Murtaza, "Role of anode length in a mather-type plasma focus," *Mod. Phys. Lett. B*, vol. 6, no. 10, pp. 593–597, Apr. 1992.
[64] W. Kies, B. Lucas, P. Rowekamp, F. Schmitz, G. Ziethen, and G. Decker, "Pinches and micropinches in the SPEED 2 plasma focus," *Plasma Sources Sci. Technol.*, vol. 7, no. 1, pp. 21–27, Feb. 1998.
[65] V. A. Gribkov, B. Bienkowska, M. Borowiecki, A. V. Dubrovsky, I. Ivanova-Stanik, L. Karpinski, R. A. Miklaszewski, M. Paduch, M. Scholz, and K. Tomaszewski, "Plasma dynamics in PF-1000 device under full-scale energy storage: I pinch dynamics, shock wave diffraction and inertial electrode," *J. Phys. D, Appl. Phys.*, vol. 40, no. 7, pp. 1977–1989, Apr. 2007.
[66] V. A. Gribkov, A. Banaszak, B. Bienkowska, A. V. Dubrovsky, I. Ivanova-Stanik, L. Jakubowski, L. Karpinski, R. A. Miklaszewski, M. Paduch, M. J. Sadowski, M. Scholz, A. Szydlowski, and K. Tomaszewski, "Plasma dynamics in the PF-1000 device under full-scale energy storage: II. Fast electron and ion characteristics versus neutron emission parameters and gun optimization perspectives," *J. Phys. D, Appl. Phys.*, vol. 40, no. 12, pp. 3592–3607, Jun. 2007.
[67] S. Al-Hawat, "Axial velocity measurement of current sheath in a plasma focus device using a magnetic probe," *IEEE Trans. Plasma Sci.*, vol. 32, no. 2, pp. 764–769, Apr. 2004.
[68] R. Aliaga-Rossel and P. Choi, "Experimental observations of the spatial anisotropy of the neutron emission in a medium energy plasma focus," *IEEE Trans. Plasma Sci.*, vol. 26, no. 4, pp. 1138–1145, Aug. 1998.
[69] H. Krompholz, L. Michel, K. H. Schonbach, and H. Fischer, "Neutron-, Ion-, and electron-energy spectra in a 1 kJ plasma focus," *Appl. Phys. A, Mater. Sci., Process.*, vol. 13, no. 1, pp. 29–35, May 1977.
[70] S. Czekaja, R. Kasperczuk, M. Miklaszewski, T. Paduch, T. Pisarczy, and Z. Wereszczyn, "Diagnostic method for the magnetic field measurement in the plasma focus device," *Plasma Phys. Control. Fusion*, vol. 31, no. 4, pp. 587–594, Apr. 1989.
[71] N. Qi, S. F. Fulghum, R. R. Prasad, and M. Krishnan, "Space and time resolved electron density and current measurements in a dense plasma focus Z-pinch," *IEEE Trans. Plasma Sci.*, vol. 26, no. 4, pp. 1127–1137, Aug. 1998.
[72] D. Klir, P. Kubes, M. Paduch, T. Pisarczyk, T. Chodukowski, M. Scholz, Z. Kalinowska, B. Bienkowska, L. Karpinski, J. Kortanek, J. Kravarik, K. Rezac, I. Ivanova-Stanik, K. Tomaszewski, and E. Zielinska, "Search for thermonuclear neutrons in a mega-ampere plasma focus," *Plasma Phys. Control. Fusion*, vol. 54, no. 1, pp. 015001-1–015001-11, Jan. 2012.
[73] V. I. Krauz, K. N. Mitrofanov, V. V. Myalton, E. V. Grabovski, V. S. Koidan, V. P. Vinogradov, Y. V. Vinogradova, and G. G. Zukakishvili, "Dynamics of the current distribution in a discharge of the pf-3 plasma focus facility," *IEEE Trans. Plasma Sci.*, vol. 38, no. 2, pp. 92–99, Feb. 2010.
[74] K. Steinmetz, K. Hubner, J. P. Rager, and B. V. Robouch, "Neutron pinhole camera investigations on temporal and spatial structures of plasma focus neutron source," *Nucl. Fusion*, vol. 22, no. 1, pp. 30–32, Jan. 1982.
[75] M. V. Roshan, P. Lee, Z. Pan, R. Verma, R. S. Rawat, and S. V. Springham, "Correlation analysis of intense and high-energy deuteron beam, pinch images, and neutron yield," *IEEE Trans. Plasma Sci.*, vol. 38, no. 9, pp. 2434–2438, Sep. 2010.
[76] U. Jager and H. Herold, "Fast ion kinetics and fusion reaction mechanism in the plasma focus," *Nucl. Fusion*, vol. 27, no. 3, pp. 407–424, Mar. 1987.
[77] H. Schmidt, P. Kubes, M. J. Sadowski, and M. Scholz, "Neutron emission characteristics of pinched dense magnetized plasmas," *IEEE Trans. Plasma Sci.*, vol. 34, no. 5, pp. 2363–2367, Oct. 2006.
[78] A. Sestero, B. V. Robouch, and S. Podda, "Suggested relaxation of plasma focus discharges to helical force-free configurations," *Plasma Phys.*, vol. 22, no. 10/11, p. 1039, Oct. 1980.
[79] J. B. Taylor, "Relaxation of toroidal plasma and generation of reverse magnetic fields," *Phys. Rev. Lett.*, vol. 33, no. 19, pp. 1139–1141, Nov. 1974.
[80] W. Kies, G. Decker, U. Berntien, Y. V. Sidelnikov, D. A. Glushkov, K. N. Koshelev, D. M. Simanovskii, and S. V. Bobashev, "Pinch modes produces in the SPEED2 plasma focus," *Plasma Sources Sci. Technol.*, vol. 9, no. 3, pp. 279–287, Aug. 2000.
[81] M. M. Milanese, R. L. Moroso, and J. O. Pouzo, "Dynamics of the ionizing and magnetic fronts in the radial compression stage of a DPF

current sheath," *IEEE Trans. Plasma Sci.*, vol. 21, no. 4, pp. 373–377, Aug. 1993.
[82] K. V. Roberts and D. E. Potter, *Methods of Computational Physics*. New York: Academic, 1970.
[83] P. Morgan, N. J. Peacock, and D. E. Potter, in *Proc. 3rd Eur. Conf. Control. Fusion Plasma Phys.*, Utrecht, Holland, Jun. 23-27, 1969.
[84] S. Lee, S. H. Saw, A. E. Abdou, and H. Torreblanca, "Characterizing plasma focus devices—role of the static inductance—instability phase fitted by anomalous resistances," *J Fusion Energy*, vol. 30, no. 4, pp. 277–282, Aug. 2011.
[85] S. Lee, *Radiative Dense Plasma Focus Computation Package: RADPF*. [Online]. Available: http://www.plasmafocus.net; http://www.intimal.edu.my/school/fas/UFLF/
[86] M. Haines, "Kinetic effects in Z pinches," *Laser Part. Beams*, vol. 19, no. 3, pp. 345–353, Jul. 2001.
[87] F. N. Beg, A. E. Dangor, P. Lee, M. Tatarakis, S. L. Niffikeer, and M. G. Haines, "Optical and x-ray observations of carbon and aluminium fibre Z-pinch plasmas," *Plasma Phys. Control. Fusion*, vol. 39, pp. 1–26, Jan. 1997.
[88] S. K. H. Auluck, "An apparent momentum balance anomaly in the plasma focus," *IEEE Trans. Plasma Sci.*, vol. 25, no. 1, pp. 37–41, Feb. 1997.
[89] M. Krishnan, M. Geva, and J. L. Hirshfield, "Plasma centrifuge," *Phys. Rev. Lett.*, vol. 46, no. 1, pp. 36–38, Jan. 1981.
[90] M. Krishnan and R. R. Prasad. (1985, Jun.). Parametric analysis of isotope enrichment in a vacuum arc centrifuge. *J. Appl. Phys.* [Online]. *57(11)*, pp. 4973–4981. Available: http://dx.doi.org/10.1063/1.335272
[91] A. Ciardi and P. Hennebelle, "Outflows and mass accretion in collapsing dense cores with misaligned rotation axis and magnetic field," *Mon. Not. R. Astron. Soc., Lett.*, vol. 409, no. 1, pp. L39–L43, Nov. 2010.
[92] M. J. Bernstein and F. Hai, "Evidence for nonthermonuclear neutron production in a plasma focus discharge," *Phys. Lett. A*, vol. 31, no. 3, pp. 317–318, Mar. 1970.
[93] M. J. Bernstein and G. G. Comisar, "Neutron energy and flux distributions from a crossed-field acceleration model of plasma focus and Z-pinch discharges," *Phys. Fluids*, vol. 15, no. 4, pp. 700–708, Apr. 1972.
[94] Y. Yamada, Y. Kitagawa, and M. Yokoyama, "High-energy deuteron beam generated by a plasma focus device," *J. Appl. Phys.*, vol. 58, no. 1, pp. 188–192, Jul. 1985.
[95] H. Conrads, P. Cloth, M. Demmeler, and R. Hecker, "Velocity distribution of the ions producing neutrons in a plasma focus," *Phys. Fluids*, vol. 13, no. 1, pp. 209–211, Jan. 1972.
[96] M. Sadowski, H. Schmidt, and H. Herold, "Time-resolved studies of deuteron beams emitted from a plasma focus," *Phys. Lett. A*, vol. 83, no. 9, pp. 435–439, Jun. 1981.
[97] W. H. Bostick, H. Kilic, V. Nardi, and C. W. Powell, "Time resolved energy spectrum of the axial ion beam generated in plasma focus discharges," *Nucl. Fusion*, vol. 33, no. 3, pp. 413–420, Mar. 1993.
[98] J. H. Lee, L. P. Shomo, M. D. Williams, and H. Hermansdorfer, "Neutron production mechanism in a plasma focus," *Phys. Fluids*, vol. 14, no. 10, pp. 2217–2223, Oct. 1971.
[99] F. C. Mejia, M. Milanese, R. Moroso, and J. O. Pouzo, "Some experimental research on anisotropic effects in the neutron emission of dense plasma-focus devices," *J. Phys. D, Appl. Phys.*, vol. 30, no. 10, p. 1499, May 1997.
[100] S. V. Sringham, S. P. Moo, P. Lee, R. S. Rawat, A. Patran, and S. Lee, "Imaging of fusion protons from a 3 kJ deuterium plasma focus," *Jpn. J. Appl. Phys.*, vol. 44, no. 6A, p. 4117, 2005.
[101] F. Castillo, J. J. E. Herrera, I. Gamboa, J. Rangel, J. I. Golzarri, and G. Espinosa, "Angular distribution of fusion products and x rays emitted by a small dense plasma focus machine," *J. Appl. Phys.*, vol. 101, no. 1, p. 013303, Jan. 2007.
[102] C. Deeney, "Measurements of hot spots and electron beams in Z-pinch devices," Ph.D. dissertation, Imperial College, London, U.K., 1988.
[103] C. Deeney, H. Herold, and C. S. Wong, "Characterization of self-generated intense electron beams in a plasma focus," *Laser Part. Beams*, vol. 8, no. 3, pp. 469–476, Sep. 1990.
[104] P. Choi, C. Deeney, and C. S Wong, "Absolute timing of a relativistic electron beam in a plasma focus," *Phys. Lett. A*, vol. 128, no. 1/2, pp. 80–83, Mar. 21, 1988.
[105] M. Favre, P. Silva, P. Choi, H. Chuaqui, C. Dumitrescu-Zoita, and E. S. Wyndham, "Experimental investigations of hotspots in a low energy plasma focus operating in hydrogen-argon mixtures," *IEEE Trans. Plasma Sci.*, vol. 26, no. 4, pp. 1154–1161, Aug. 1998.
[106] P. Silva and M. Favre, "Properties of hotspots in plasma focus discharges operating in hydrogen-argon mixtures," *J. Phys. D, Appl. Phys.*, vol. 35, no. 20, pp. 2543–2550, Oct. 2002.
[107] R. Deutch and W. Kies, "Ion acceleration and runaway in dynamical pinches," *Plasma Phys. Control. Fusion*, vol. 30, no. 3, pp. 263–276, Mar. 1988.
[108] Y. Kato and S. H. Be, "Generation of soft x rays using a rare gas-hydrogen plasma focus and its application to x-ray lithography," *Appl. Phys. Lett.*, vol. 48, no. 11, p. 686, Mar. 1986.
[109] R. R. Prasad, M. Krishnan, J. Mangano, P. Greene, and N. Qi, "Dense plasma focus x-ray source for sub-micron lithography," in *Proc. 20th IEEE Int. Conf. Plasma Sci.*, Vancouver, BC, Canada, 1993, p. 185.
[110] R. Petr, A. Bykanov, J. Freshman, D. Reilly, and J. Mangano, "Performance summary on high power dense plasma focus x-ray lithography point source producing 70 nm line features in AlGaAs microcircuits," *Rev. Sci. Instrum.*, vol. 75, no. 8, pp. 2551–2559, Aug. 2004.
[111] F. N. Beg, I. Ross, A. Lorenz, J. F. Worley, A. E. Dangor, and M. G. Haines. (2000, Sep.). Study of x-ray emission from a table top plasma focus and its application as an x-ray backlighter. *J. Appl. Phys.* [Online]. *88(6)*, pp. 3225–3230. Available: http://dx.doi.org/10.1063/1.1287220
[112] D. Wong, A. Patran, T. L. Tan, R. S. Rawat, and P. Lee, "Soft x-ray optimization studies on a dense plasma focus device operated in neon and argon in repetitive mode," *IEEE Trans. Plasma Sci.*, vol. 32, no. 6, pp. 2227–2235, Dec. 2004.
[113] R. Verma, R. S. Rawat, P. Lee, M. Krishnan, S. V. Springham, and T. L. Tan, "Miniature plasma focus device as a compact hard x-ray source for fast radiography applications," *IEEE Trans. Plasma Sci.*, vol. 38, no. 4, pp. 652–657, Apr. 2010.
[114] V. A. Gribkov, A. Srivastava, P. L. C. Keat, V. Kudryashov, and S. Lee, "Operation of NX2 dense plasma focus device with argon filling as a possible radiation source for micro-machining," *IEEE Trans. Plasma Sci.*, vol. 30, no. 3, pp. 1331–1338, Jun. 2002.
[115] Y. B. Zel'dovich and Y. P. Raizer, *Physics of Shock Waves and High Temperature Hydrodynamics Phenomena*, W. Hayes and R. Probstein, Eds. New York: Dover, 1966.
[116] H. Bhuyan, M. Favre, E. Valderrama, G. Avaria, H. Chuaqui, I. Mitchell, E. Wyndham, R. Saavedra, and M. Paulraj, "Formation of hexagonal silicon carbide by high energy ion beam irradiation on Si (100) substrate," *J. Phys. D, Appl. Phys.*, vol. 40, no. 1, pp. 127–131, Jan. 2007.
[117] H. Bhuyan, M. Favre, A. Henriquez, G. Vogel, E. Valderrama, E. Wyndham, and H. Chuaqui, "Production of sub-micron size carbon composites by high energy carbon ion beams irradiation of solid targets," *Surf. Coat. Technol.*, vol. 204, no. 18/19, pp. 2950–2953, Jun. 2010.
[118] R. S. Rawat, "High energy density pulsed plasmas in plasma focus: Novel plasma processing tool for nanophase hard magnetic material synthesis," *Nanosci. Nanotechnol. Lett.*, vol. 4, no. 3, pp. 251–274, Mar. 2012.
[119] A. Anders, *Cathodic Arcs: From Fractal Spots to Energetic Condensation*. New York: Springer-Verlag, 2008, ser. Atomic, Optical, and Plasma Physics Series, #50.
[120] M. Krishnan, E. Valderrama, B. Bures, K. Wilson-Elliott, X. Zhao, L. Phillips, A.-M. Valente-Feliciano, J. Spradlin, C. Reece, and K. Seo, "Very high residual resistivity ratios of heteroepitaxial superconducting niobium films on MgO substrates," *Supercond. Sci. Technol.*, vol. 24, no. 11, p. 115002, Nov. 2011.
[121] W. Stygar, "Particle beams generated by a 6–12.5 kJ dense plasma focus," *Nucl. Fusion*, vol. 22, no. 9, p. 1161, Sep. 1982.
[122] F. Hohl and S. P. Gary, "Electron kinematics in a plasma focus," *Phys. Fluids*, vol. 20, no. 4, p. 683, Apr. 1977.
[123] H. Bhuyan, H. Chuaqui, M. Favre, I. Mitchell, and E. Wyndham, "Ion beam emission in a low energy plasma focus device operating with methane," *J. Phys. D, Appl. Phys.*, vol. 38, no. 8, pp. 1164–1169, Apr. 2005.
[124] H. Bhuyan, M. Favre, E. Valderrama, H. Chuaqui, and E. Wyndham, "Experimental studies of ion beam anisotropy in a low energy plasma focus operating with methane," *J. Phys. D, Appl. Phys.*, vol. 39, no. 16, pp. 3596–3602, Aug. 2006.
[125] V. Tang, M. L. Adams, and B. Rusnak, "Dense plasma focus Z-pinches for high-gradient particle acceleration," *IEEE Trans. Plasma Sci.*, vol. 38, no. 4, pp. 719–727, Apr. 2010.
[126] W. P. Leemans, B. Nagler, A. J. Gonsalves, C. Toth, K. Nakamura, C. G. R. Geddes, E. Esarey, C. B. Schroeder, and S. M. Hooker, "GeV electron beams from a centimetre-scale accelerator," *Nat. Phys.*, vol. 2, no. 10, pp. 696–699, Oct. 2006.
[127] V. S. Imshennik, N. V. Fillipov, and T. I. Fillipova, "Similarity theory and increased neutron yield in a plasma focus," *Nucl. Fusion*, vol. 13, no. 6, pp. 929–934, Dec. 1973.

[128] V. Vikhrev and V. D. Korolev, "Neutron generation from Z-pinches," *Plasma Phys. Rep.*, vol. 33, no. 5, pp. 356–380, May 2007, Pleiades Publ., Ltd.
[129] J. H. Lee, D. R. McFarland, and F. Hohl, "Dense plasma focus production in a hypocycloidal pinch," NASA Langley Res. Center, Hampton, VA, NASA Tech. Note TN D-8116, Dec. 1975.
[130] P. Silva, L. Soto, J. Moreno, G. Sylvester, M. Zambra, L. Altamirano, H. Bruzzone, A. Clausse, and C. Moreno, "A plasma focus driven by a capacitor bank of tens of joules," *Rev. Sci. Instrum.*, vol. 73, no. 7, pp. 2583–2587, Jul. 2002.
[131] P. Silva, J. Moreno, L. Soto, L. Birstein, R. Mayer, and W. Kies, "Neutron emission from a fast plasma focus of 400 joules," *Appl. Phys. Lett.*, vol. 83, no. 16, pp. 3269–3271, Oct. 2003.
[132] P. Silva, L. Soto, W. Kies, and J. Moreno, "Pinch evidence in a fast and small plasma focus of only tens of joules," *Plasma Sources Sci. Technol.*, vol. 13, no. 2, p. 329, May 2004.
[133] L. Soto, P. Silva, J. Moreno, M. Zambra, W. Kies, R. E. Mayer, A. Clausse, L. Altamirano, C. Pavez, and L. Huerta, "Demonstration of neutron production in a table-top pinch plasma focus device operating at only tens of joules," *J. Phys. D, App. Phys.*, vol. 41, no. 20, p. 205215, Oct. 2008.
[134] L. Soto, C. Pavez, J. Moreno, M. Barbaglia, and A. Clausse, "Nanofocus: An ultra-miniature dense pinch plasma focus device with submillimetric anode operating at 0.1 J," *Plasma Sources Sci. Technol.*, vol. 18, no. 1, p. 015007, Feb. 2009.
[135] C. Pavez and L. Soto, "Demonstration of x-ray emission from an ultra-miniature pinch plasma focus discharge operating at 0.1 J nanofocus," *IEEE Trans. Plasma Sci.*, vol. 38, no. 5, pp. 1132–1135, May 2010.
[136] A. Tarifeño, C. Pavez, J. Moreno, and L. Soto, "Dynamics and density measurements in a small plasma focus of tens-of-joules-emitting neutrons," *IEEE Trans. Plasma Sci.*, vol. 39, no. 2, pp. 756–760, Feb. 2011.
[137] A. Marquez, J. Gonzalez, A. Tarifeño-Saldivia, C. Pavez, L. Soto, and A. Clausse, "Modelling of the internal dynamics and density in a tens of joules plasma focus device," *Phys. Plasmas*, vol. 19, no. 1, p. 012703, Jan. 2012.
[138] R. Verma, M. V. Roshan, F. Malik, P. Lee, S. Lee, S. V. Springham, T. L. Tan, M. Krishnan, and R. S. Rawat, "Compact sub-kilojoule range fast miniature plasma focus as portable neutron source," *Plasma Sources Sci. Technol.*, vol. 17, no. 4, pp. 045020-1–045020-11, Nov. 2008.
[139] R. Verma, R. S. Rawat, P. Lee, M. Krishnan, S. V. Springham, and T. L. Tan, "Experimental study of neutron emission characteristics in a compact sub-kilojoule range miniature plasma focus device," *Plasma Phys. Control. Fusion*, vol. 51, no. 7, pp. 075008-1–075008-16, Jul. 2009.
[140] R. Verma, R. S. Rawat, P. Lee, S. Lee, S. V. Springham, T. L. Tan, and M. Krishnan, "Effect of cathode structure on neutron yield performance of a miniature plasma focus device," *Phys. Lett. A*, vol. 373, no. 60, pp. 2568–2571, Jul. 2009.
[141] A. Serban and S. Lee, "The effect of high axial sheath velocity on neutron yield in plasma focus," *Fusion Sci. Technol.*, vol. 35, no. 1, pp. 54–61, Jan. 1999.
[142] S. Lee and A. Serban, "Dimensions and lifetime of the plasma focus pinch," *IEEE Trans. Plasma Sci.*, vol. 24, no. 3, pp. 1101–1105, Jun. 1996.
[143] M. Favre, S. Lee, S. P. Moo, and C. S. Wong, "X-ray emission in a small plasma focus operating with H_2–Ar mixtures," *Plasma Sources Sci. Technol.*, vol. 1, no. 2, p. 122, May 1992.
[144] M. Zakaullah, "Study of neutron emission in a low-energy plasma focus with â-source-assisted breakdown," *Plasma Sources Sci. Technol.*, vol. 12, no. 3, pp. 443–448, Aug. 2003.
[145] S. Ahmad, S. S. Hussain, M. Sadiq, M. Shafiq, A. Waheed, and M. Zakaullah, "Enhanced and reproducible neutron emission from a plasma focus with pre-ionization induced by depleted uranium (U238)," *Plasma Phys. Control. Fusion*, vol. 48, no. 6, pp. 745–755, Jun. 2006.
[146] V. Nardi, A. Bortolotti, J. S. Brzosko, M. Esper, C. M. Luo, F. Pedrielli, C. Powell, and D. Zeng, "Stimulated acceleration and confinement of deuterons in focused discharges. I," *IEEE Trans. Plasma Sci.*, vol. 16, no. 3, pp. 368–373, Jun. 1988.
[147] M. Lu, M. Han, T. Yang, C. Luo, and T. Miyamoto, "A simple knife-edge design for initial phase optimization in plasma focus," *IEEE Trans. Plasma Sci.*, vol. 29, no. 6, pp. 973–976, Dec. 2001.
[148] R. Verma, R. S. Rawat, P. Lee, S. V. Springham, T. L. Tan, and M. Krishnan, "Realization of enhancement in time averaged neutron yield by using repetitive miniature plasma focus device as pulsed neutron source," *J. Phys. D, Appl. Phys.*, vol. 42, no. 23, p. 235203, Dec. 2009.
[149] M. Krishnan, B. Bures, R. Madden, F. Blobner, and K. Wilson Elliott, "A fast pulse, high intensity neutron source based upon the dense plasma focus," in *Proc. 10th Int. Conf. Appl. Nucl. Tech./AIP Conf. Proc.*, 2009, pp. 56–68.
[150] B. L. Bures, C. James, M. Krishnan, and R. Adler, "Application of an impedance matching transformer to a plasma focus," *Rev. Sci. Instrum.*, vol. 82, no. 10, p. 103506, Oct. 2011.
[151] R. Verma, R. S. Rawat, P. Lee, M. Krishnan, S. V. Springham, and T. L. Tan, "Experimental study of neutron emission characteristics in a compact sub-kilojoule range miniature plasma focus device," *Plasma Phys. Control. Fusion*, vol. 51, no. 7, p. 075008, Jul. 2009.
[152] B. L. Bures, M. Krishnan, R. E. Madden, and F. Blobner, "Enhancing neutron emission from a 500J plasma focus by altering the anode geometry and gas composition," *IEEE Trans. Plasma Sci.*, vol. 39, no. 4, pp. 667–671, Apr. 2010.
[153] R. Verma, P. Lee, S. Lee, S. V. Springham, T. L. Tan, R. S. Rawat, and M. Krishnan, "Order of magnitude enhancement in neutron emission with deuterium-krypton admixture operation in miniature plasma focus device," *Appl. Phys. Lett.*, vol. 93, no. 10, p. 101501, Sep. 2008.
[154] E. J. T. Burns, S. M. Falacy, R. A. Hill, P. D. Thacher, H. A. Koehler, B. Davis, and R. E. Shafer, "A high-neutron-output dense plasma focus," *Phys. Lett. A*, vol. 133, no. 3, pp. 144–148, Nov. 1988.
[155] B. L. Bures, M. Krishnan, and C. James, "A plasma focus electronic neutron generator," *IEEE Trans. Plasma Sci.*, vol. 40, no. 4, pp. 1082–1088, Apr. 2012.
[156] M. Krishnan, B. Bures, C. James, R. Madden, W. Hennig, D. Breus, S. Asztalos, K. Sabourov, and S. Lane, "A fast pulsed neutron source for time-of-flight detection of nuclear materials and explosives," in *Proc. 11th Int. Conf. Appl. Nucl. Tech., AIP Conf.*, vol. 1412, pp. 47–54.
[157] F. D. Brooks, A. Buffler, M. S. Allie, K. Bharuth-Ram, M. R. Nchodu, and B. R. Simpson, "Determination of HCNO concentrations by fast neutron scattering analysis," *Nucl. Instrum. Methods Phys. Res. A, Accel. Spectrom. Detect. Assoc. Equip.*, vol. 410, no. 2, pp. 319–328, 1998.
[158] V. A. Gribkov and R. Miklaszewski, "On a possibility of the single-shot detection of hidden objects by using nanosecond impulse neutron inspection system," *Acta Phys. Chim. Debr.*, vol. 38/39, pp. 185–193, 2005.
[159] B. L. Bures, M. Krishnan, and R. E. Madden, "Relationship between neutron yield and macroscale pinch dynamics of a 1.4-kJ plasma focus over hundreds of pulses," *IEEE Trans. Plasma Sci.*, vol. 39, no. 12, pp. 3351–3357, Dec. 2011.
[160] G. Decker, W. Kies, M. Malzig, C. van Calker, and G. Ziethen, "High performance 300 kV driver speed 2 for MA pinch discharges," *Nucl. Instrum. Methods Phys. Res. A, Accel. Spectrom. Detect. Assoc. Equip.*, vol. 249, pp. 477–483, 1986.
[161] J. D. Huba. (2006). *Plasma Formulary* [Online]., p. 44. Available: www.ppd.nrl.navy.mil/nrlformulary/NRLFORMULARY07.pdf
[162] G. Decker, L. Flemming, H. J. Kaeppeler, T. Oppenlander, G. Pross, P. Schilling, H. Schmidt, M. Shakhatre, and M. Trunk, "Current and neutron yield scaling of fast high voltage plasma focus," *Plasma Phys.*, vol. 22, no. 3, pp. 245–260, Mar. 1980.
[163] R. L. Gullickson and H. L. Sahlin, "Measurements of high-energy deuterons in the plasma-focus device," *J. Appl. Phys.*, vol. 49, no. 3, pp. 1099–1105, Mar. 1978.
[164] K. H. Beckurts and K. Wirtz, *Neutron Physics*. Berlin, Germany: Springer-Verlag, 1964.
[165] V. V. Vikhrev and V. D. Korolev, "Neutron generation from Z-pinches," *Plasma Phys. Rep.*, vol. 33, no. 5, pp. 356–380, May 2007.
[166] V. V. Vikhrev and V. D. Korolev, "Neutron generation from Z-pinches," *Fizika Plazmy*, vol. 33, no. 5, pp. 397–423, 2007.

Mahadevan Krishnan (M'90) was born in Chennai, India, in 1950. He received the B.Sc. (Hons, ext.) degree in mechanical engineering from the University of London, London, U.K., in 1971 and the Ph.D. degree in aerospace sciences from Princeton University, Princeton, NJ, in 1976.

He was a Principal Scientist with Science Research Laboratories, Alameda, CA; the Deputy Director of Pulsed Power and Chief Scientist with Physics International Company; and an Associate Professor of applied physics and mechanical engineering with Yale University, New Haven, CT. He is the President of Alameda Applied Sciences Corporation, San Leandro, CA.